Doctoral Thesis

Dynamic Behavior of Simple Molecules Adsorbed in Mordenite as Studied by Nuclear Magnetic Relaxation

by

Qiang XU

The Graduate School of Faculty of Science

Osaka University

1994

Doctoral Committee

Professor Nobuo NAKAMURA

Professor Shichio KAWAI

Professor Takeshi OHNO

Professor Shinnichiro SUZUKI

Associate Professor Taro EGUCHI

ACKNOWLEDGMENTS

I would like to express my sincere thanks to Professor Nobuo Nakamura for his fruitful instruction, stimulative discussions filled with his deep insight into science and kind encouragements, and for critical reading of this manuscript.

I was very fortunate to be able to work under the guidance of Associate Professor Taro Eguchi. Since we met at Osaka airport on my first day in Japan, we have worked together almost every day for about seven years. I am most indebted to him for his intellectual support. He introduced me so much knowledge that ranges from the ABC of Japanese Language to NMR techniques and theories, from thinking about experiment to philosophy of science, and so on. He provided me with discussions full of inspiring ideas, appropriate advice, continuing collaboration and timely encouragements, which led my present work to success.

I have enjoyed working together with Dr. Hirokazu Nakayama since my first day in the university campus. This thesis has benefited from his constructive suggestions, generous cooperation and kind encouragements. The most grateful thanks are due to him.

The author is also deeply indebted to Emeritus Professor Michihiko Kishita and Professor Takeshi Ohno for their fruitful instruction and kind encouragements.

I also wish to thank Assistant Professor Satoru Ueda (Institute of Scientific and Industrial Research) for his kind guidance to the technique for synthesizing mordenite, and Assistant Professor Akira Inaba and Dr. Sadamu Takeda (Faculty of Science) for their valuable discussions and support. Ms. K. Tasaki (Central Research Institute, Nissan Chemical Industries, Ltd.) kindly provided high-purity silica sol and Mr. A. Harada (Tosoh Co. Ltd.) kindly carried out the chemical analysis of mordenite. Deep thanks are due to them.

The author wishes also to thank Dr. Keisuke Miyakubo and Mr. Tetsuya Kawai and all the members of Solid State Chemistry laboratory for their generous assistance. I am deeply indebted to Associate Professor Seiko Komorita and all the people in Chemistry Department, College of General Education, for their helps and kindness. I am grateful to Professor Toshikazu

Ibata, a member of the committee for foreign students of Osaka University, for his kindness and encouragement.

I thank Professors Shichio Kawai and Shinnichiro Suzuki for critical reading of this manuscript and for their kind encouragements.

I am also grateful for the heartwarming kindness by many Japanese people during my seven-year stay in Japan. I would like to thank Okumura Foundation, Association of International Education of Japan and Japanese Government for the financial supports.

Finally, I am indebted to all the members of my family for their encouragements. I am so sorry I had no time to come home to see my parents during my study in the Doctor course in Osaka University. Brother Gang Xu provided me the opportunity to come to Japan and financially and mentally supported me to study here. My wife Daifei Fang made my favorite dishes for me every day although she had to learn many subjects in her own major course (Pharmaceutical Science).

February, 1994

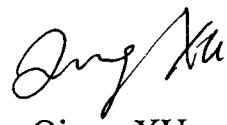

Qiang XU

ABSTRACT

The dynamic properties and the interaction between adsorbed molecules and the guest-host interaction in the system of small paraffins C_nH_{2n+2} (n = 1-4) adsorbed in mordenite were studied by NMR relaxation measurements at *low temperatures*.

Chapter 1 gives general introductory remarks on zeolites, particularly mordenite, and the subject admolecules for the present work.

Chapter 2 presents a brief description of the theoretical concepts of the proton magnetic relaxation which are relevant to the analysis of the NMR relaxation data for admolecules.

Chapter 3 describes the methods of spin-lattice relaxation time (T_1) measurements. The design and construction of a new NMR cryostat for adsorbed gas and the handling system for the adsorption experiments are described. The new NMR cryostat proved to be highly efficient in measuring the relaxation time *in situ* at low temperatures and convenient for pre-treating the adsorbent and filling gas samples. The details of synthesis of high-purity mordenite sample are also given. The synthesized sample was found to be iron-free, which enabled us to determine the reliable values of T_1.

Chapter 4 presents the results of the measurements of the spin-relaxation times T_1 for methane, ethane, propane and butane adsorbed in mordenite in the low temperature region at various coverages. A single T_1 minimum was observed for each of ethane, propane and butane at 28, 75, and 115-125 K, respectively, whereas two T_1 minima appeared at low loadings for methane, one locating at 15 K, and the other at 50 K. Numerical estimation of the relaxation rate indicated that translational diffusion of admolecules can not interpret the T_1 minima in all adsorption systems and all the T_1 minima must be attributed to molecular reorientational motion.

The T_1 minimum for ethane is due to the reorientation about its C-C axis in the main-channel, and at low temperatures the rotational tunneling about the C-C axis affects the relaxation process. The excitation energy to the first torsional level, E_{01}, and E_a, the activation energy for the molecular rotation, were determined to be 0.12 and 1.0 kJ mol^{-1}, respectively.

For propane adsorbed in mordenite, the single T_1 minimum is also due to the reorientation of the admolecules in the main-channel. On the low temperature side of the T_1 minimum the intramolecular reorientation of the CH_3 group about the C-C axis together with its tunneling rotation dominates the relaxation. The E_{01} was estimated to be 0.5 kJ mol^{-1}, and the barrier for internal rotation to be about 6 kJ mol^{-1}. T_1 in the high-temperature side of the T_1 minimum is attributed to the reorientation about the long axis of a whole-molecule, the activation energy for which was estimated to be 3.5 kJ mol^{-1}.

Butane exhibits similar T_1 behavior to that for propane, but has significant loading dependence. The barrier for internal rotation of the CH_3 group about the C-C axis was estimated to be 6 kJ mol^{-1} and E_{01} for the tunneling rotation to be 0.6 kJ mol^{-1} whereas the E_a for the molecular axial rotation is 5.0-5.5 kJ mol^{-1}. The loading dependence of T_1 in butane is discussed.

Methane shows relaxation behavior very different from the other three do. By analyzing the T_1 data, it was found that such difference originates from the presence of the side-pocket in the channel of mordenite. Methane molecules locating and reorienting in the main-channel give rise to the T_1 minimum at 15 K and those in the side-pocket lead to the minimum at 50 K. By considering the Boltzmann distributions between the molecules in the main-channel and those in the side-pocket, the loading dependence and the temperature dependence in the low-temperature region are well interpreted. The methane molecule in the side-pocket experiences the lower potential energies than in the main-channel by about 70 J mol^{-1} ($\approx$ 8.4 K). The activation energies for the reorientation of methane are 1.0 and 2.0 kJ mol^{-1} in the main-channel and in the side-pocket, respectively.

It is noted that the activation energy E_a for the reorientation in the main-channel varies systematically in the order of carbon number, satisfying that a kind of the law of corresponding state holds. The law holds also for the temperature that the T_1 minimum appears.

The co-adsorbed system of methane and argon in mordenite is also investigated by the proton T_1 measurements. The dependence of T_1 on the gas composition is attributed to a preferential adsorption of CH_4 in the side-pocket.

Chapter 5 investigates the behavior of methane molecules adsorbed in mordenite in the high temperature region above about 100 K. The adsorption isotherm was measured between 150 and 320 K. It was found that the adsorption is of the Langmuir-type at low coverages above 250 K and the monolayer capacity was estimated to be 55 ml/g. The differential isosteric heat of adsorption was estimated to be 26 kJ mol^{-1}, which is almost independent of the coverage at the lower coverage than 0.4. The adsorbed phase was found to be well described by a model of the one-dimensional van der Waals gas.

T_1 for methane decreases with increasing temperature in the high temperature region. Comparison of it with T_1 in the neat gas of methane suggested that the spin-rotation interaction may affect the relaxation.

Chapter 6 gives a general conclusion. The present study indicates that both the temperature and the coverage dependence of the spin-relaxation time can provide a powerful clue to investigate the reorientational motion of the admolecule at low temperatures quantitatively and to obtain detailed information on the dynamics and the distributions of adsorbed molecules in various adsorption sites in zeolite pores.

CONTENTS

Chapter 1

INTRODUCTION

1.1 General Remarks

Zeolite is the generic name of the crystalline aluminosilicates which are represented chemically by the formula:

$$M_{2/n}O{\cdot}Al_2O_3{\cdot}y\,SiO_2{\cdot}w\,H_2O$$

where n is the cation valence, and w represents the water content in the voids of the zeolite. Structurally, zeolites belong to crystalline inorganic giant molecule consisting of infinitely extending three-dimensional, four-connected frameworks of AlO_4 and SiO_4 tetrahedra which are linked to each other by sharing the oxygen atoms. The framework structure contains channels or interconnected voids (cages) depending on the species of zeolites. The interior spaces are occupied by cations, and in fresh crystals by water molecules which are called "zeolitic water". The cations are mobile and ordinarily undergo ion exchange. The water can be removed reversibly, generally by heating and/or evacuation, which leaves intact a crystalline host framework unchanged.[1-4]

Zeolites have attracted much attention particularly from industrial viewpoints,[1-9] because of their special structure-related properties as follows:

1) Microporous character with uniform pore dimensions, allowing some hydrocarbon molecules to enter the pores while prohibiting others with large molecular size from penetrating into the pore. This property is applied practically to "molecular sieve".
2) Ion-exchange property which allows various sorts of ion exchange reactions to proceed.
3) Ability to catalyze organic reactions with high thermal stability.

Zeolites have long been utilized in industry, for example, to cracking of crude oil to gasoline. Zeolites are also good substrates for studying the adsorption process because of remarkably large specific surface area compared with other adsorbents such as graphite, and because they provide well-defined surface for physi-adsorption of light gases.

So far numerous experimental studies on zeolites for applicative purposes have extensively been done. In two major industrial applications of them, that is, (shape selective) catalysis and selective adsorption processes, it has been recognized that migration or diffusion of sorbed molecules through the pores and cages plays a very important role. And hence various methods were developed to study the intracrystalline diffusion.[10-12] Among them, the nuclear magnetic resonance pulsed field gradient (PFG) is a powerful tool for measuring the self-diffusion[10,13-18] and the measurements of nuclear magnetic relaxation times

provided useful information on the variety of molecular mobilities[16,18-21] at high temperatures.

However, in spite of rapid development of the applicative researches, many problems remain unsolved in the fundamental sense. Only a few measurements have been done on dynamical properties of adsorbed molecules in low temperature region, guest-host interaction in the pore, specification of adsorption sites, the potential energies at these adsorption sites and molecular distributions in the void space, etc. Very recently a few MD (molecular dynamics) simulation studies have been done to clarify these points but these works have not yet provided very reliable information on details of structure and properties of adsorption systems.

In order to obtain some clue to elucidate the excitation process of molecular motion, particularly, the rotation or reorientation of the guest molecules, to obtain information on the potential energies at adsorption centers and molecular distributions in the pores, and to reveal possible existence of specific or preferential adsorption sites, we measured the proton spin-lattice relaxation times (T_1) for a series of guest paraffin molecules (methane, ethane, propane and butane) in mordenite at various coverage and over a wide temperature range of 4.2-400 K.

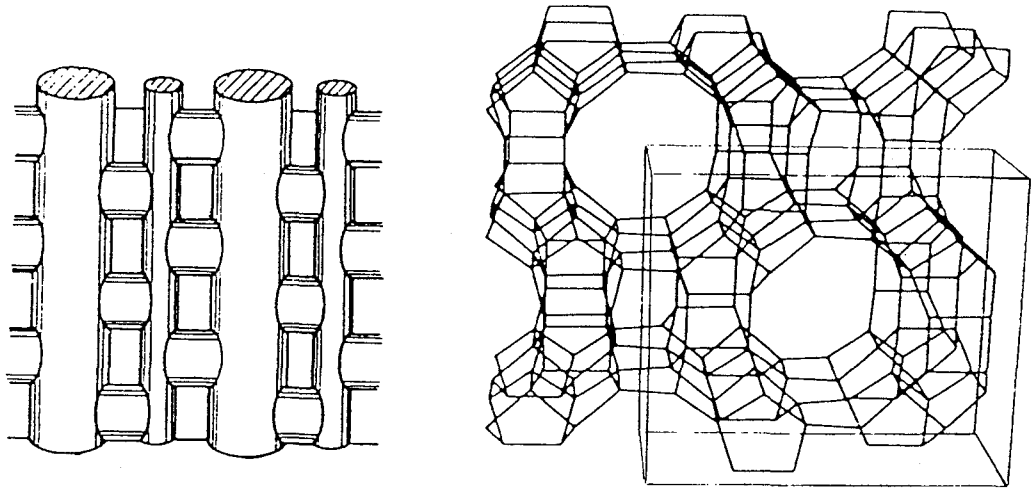

Fig. 1-1 Structure of mordenite. (Figures taken from Ref. 4)

1.2 Mordenite and Admolecules*

Mordenite is a material belonging to zeolite compound, which has straight channels (0.67 × 0.70 nm^2). The channels are running parallel to the c axis as shown in Fig. 1-1.[3,4,22] The wall of channel caves in at several places and forms side-pockets the opening of which consists of an eight-membered oxygen ring with a free aperture of 0.29 × 0.57 nm^2. (X-ray crystallographic data: CmCm, a=1.833, b=2.072, c=0.76 nm)[22]

Barrer[23] first measured the adsorption of various gases in H- and Na-mordenites and obtained many useful results. Takaishi *et al.*[24-26] measured the physisorption of Ar, O_2, and N_2 by Na- mordenite and reached the conclusion that the sorbed molecules behave like one-dimensional (1-D) gas. Furuyama[27,28] and Tyburce[29] investigated the effects of substitution of Na^+ by various cations on the adsorption properties of Na-mordenite. Itabashi[30] showed that Na^+ ions are located at the channel wall only when the unit cell contains more than 5.2 Na^+ ions. They found also that the side-pockets would not be blocked by the Na^+ ions when the unit cell contains less than 5.2 Na^+ ions. Ripmeester[31] measured the ^{129}Xe NMR spectrum of xenon adsorbed on ion-exchanged and chemically modified mordenites and revealed that the side-pocket space is available for xenon adsorption in the Na^+, K^+ and NH_4^+ mordenites but is not in the Cs^+ mordenite. Recently Ohgushi[32] reported that the state of the molecules of Ar, Kr and Xe adsorbed in Na-mordenite can be described by a model of mobile 1-D gas at high temperatures but adsorbed molecules may be immobile at very low temperatures because admolecules may be trapped in the shallow adsorption potential valley at the entrance window to the side-pocket. Using *Monte Carlo* Simulations Smit[33] showed that methane can be preferentially adsorbed in and interact strongly with the side-pockets of Na-mordenite at high Si/Al ratio (>7).

The previous works described above presented valuable information on structure of mordenite as well as admolecules such as N_2, O_2 and the rare gases. Information is, however, still required on states and properties of small paraffins adsorbed in mordenite. As shown in Table 1-1, methane and ethane have diameters almost the same as that of Ar, Kr, Xe, N_2 and O_2.[3] The 1-D gas behavior is also expected for small paraffins. On the other hand, propane and butane have slightly larger diameters, and have shape of zigzag chain. The mobilities of them may be reduced in the pore of mordenite.

* Admolecule denotes adsorbed molecule.

Table 1-1. Dimensions for various molecules[3)]

	Lennard-Jones (6-12)	
	r_{min} / Å	σ / Å a)
Ar	3.84	3.40
O_2	4.02	3.46
N_2	4.09	3.64
Kr	3.96	3.60
Xe	4.45	3.96
CH_4	4.25	3.8
C_3H_8		4.3
n-C_4H_{10}		4.3

a) collision diameter, σ, calculated from the minimum equilibrium cross-sectional diameter, which corresponds to the minimum distance between two molecules at collisional state.[34)]

Compared with the rare gases, the rotational degrees of freedom that paraffin molecules possess will be another interesting aspect of the ad-paraffins. In low-temperature region where the translational diffusion is not activated, it is expected that the molecular rotational motion can be easily detected and, since its state is governed by potential energy by the local environment, it can be one of the best probes to examine the characteristics of pores of mordenite.

As described above, there exist side-pockets on the walls of channels of mordenite. If one finds a guest molecule which can enter the side-pocket and examines the feature of its rotation, some valuable information on the structure and energy relation of the side-pocket can be obtained. Similarly, by adsorbing a large molecule and examining its rotational characteristics other important information on the main-channel can be derived. The rotational degrees of freedom of molecules with various sizes can therefore be a good probe for the investigation of the detailed structure of the channels of mordenite.

Two-component gas adsorption system in zeolite is also another interesting aspect. The adsorbent-adsorbate interactions will play an important role, in addition to the adsorbate-adsorbate interactions in the real adsorption system. It is expected that the "phase diagram" will exhibit considerably different feature from that of the bulk mixture. The information on the adsorption states and the intermolecular interactions is perhaps contained in and can be experimentally extracted from such a "phase diagram". The system of argon and methane co-adsorbed in mordenite provides a clue to clarify these points.

1.3 Purpose of the Present Study

The purpose of the present study is to investigate the dynamic processes of small paraffins adsorbed in mordenite. To clarify whether the admolecules of methane behave as 1-D gases in the channel of mordenite at high temperatures, adsorption isotherm measurements were carried out. In order to investigate the excitation process of the rotational and the translational motions, ^1H spin-lattice relaxation times of the admolecules were measured over a wide temperature range of 4.2-400 K. Analyses of the results of the measurements will bring about the information on the rotational motions of the admolecules. Information on the potential energies at various adsorption sites and the distributions in the channels will also be exhibited. The question how many specific adsorption sites exist in the pores of mordenite will be answered. The mechanism of the excitation of the admolecular motion will be compared with that of the bulks. How the molecules in the gas phase at equilibrium with the adsorption phase affect the nuclear magnetic relaxation of admolecules will be clarified. By investigating the "phase diagram" of argon-methane co-adsorption system, an attempt will be made to extract any useful information on the adsorption states and the intermolecular interactions.

Accordingly, this thesis will be described as a following order:

Chapter 2 reviews the concept of nuclear magnetic relaxation and its relation to molecular motion. Experimental details are presented in Chapter 3. Chapter 4 gives the results and discussion of the NMR experiments on a series of adsorbed paraffins as well as Ar-CH_4 co-adsorption system in the low-temperature region. Chapter 5 analyzes and interprets the results of the adsorption isotherms and the relaxation experiments on adsorbed methane in high-temperature region. Chapter 6 will give general discussion and conclusion.

References to Chapter 1

1. 原伸宜, 高橋浩共編, *ゼオライト -- 基礎と応用*, 講談社サイエンティフィク (1975)
2. 富永博夫編, *ゼオライト -- 科学と応用*, 講談社サイエンティフィク (1987)
3. D.W. Breck, *Zeolite Molecular Sieves, Structure, Chemistry and Use*, JohnWiley & Sons, Inc., *New York*, (1974)
4. H. Van Bekkum, E. M. Flanigen, and J. C. Jansen, *Stud. Surf. Sci. Catal.*, **58** , Elsevier, (1991)
5. L. B. Young, S. A. Butter and W. W. Kaeding, *J. Catal.*, **76**, 418 (1982)
6. N. Y. Chen, R. L. Gorring, H. R. Ireland and T. R. Stein, *Oil Gas J.*, **75**, 165 (1977)
7. S. L. Meisel, J. P. McCullough, C. H. Lechthaler and P. B. Weisz, *Chem. Technol.*, **6**, 86 (1976)
8. E. M. Flanigen, J. M. benett, R. W. Grose, J. P. Cohen, R. L. Patton, R. M. Kirchner and J. V. Smith, *Nature (London)*, **271**, 512 (1978)
9. R. M. Dessau, *ACS Symp. Ser.*, **135**, 123 (1980)
10. J. Karger and D. M. Ruthven, *Diffusion in Zeolites*, JohnWiley & Sons, Inc., *New York*, (1991)
11. H-J. Doelle, J. Heering, L. Riekert and L. Marosi, *J. Catal.*, **71**, 27 (1981)
12. J. Wei, *J. Catal.*, **76**, 433 (1982)
13. H. Pfeifer, in *NMR - Basic Principles and Progress,* (ed. P. Diehl, E. Fluck and R. Kosfeld), Springer - Verlag, *Berlin*, **7**, 53 (1972)
14. H. Pfeifer, *Phys. Rep. C*, **26**, 293 (1976)
15. J. Karger and J. Caro, *J. Chem. Soc., Faraday Trans. 1*, **73**, 1363 (1977)
16. J. Karger, H. Pfeifer, M. Rauscher and A. Walter, *J. Chem. Soc., Faraday Trans. 1*, **76**, 717 (1980)
17. J. Karger and D. M. Ruthven, *J. Chem. Soc., Faraday Trans. 1*, **77**, 1485 (1980)
18. J. Caro, M. Bulow, W. Schirmer, J. Karger, W. Heink, H. Pfeifer and S. P. Zdanov, *J. Chem. Soc., Faraday Trans. 1*, **81**, 2541 (1985)
19. H. A. Resing and J. K. Thompson, *J. Chem. Phys.*, **46**, 2876 (1967)
20. H. A. Resing , *Advan. Mol. Relaxation Processes,* **1**, 109 (1968)
21. H. A. Resing , *Advan. Mol. Relaxation Processes,* **3**, 199 (1972)
22. W. M. Meier, *Z. Kristallogr.*, **115**, 439 (1961)
23. R. M. Barrer and D. L. Peterson, *Proc. R. Soc. London, Ser. A*, **280**, 466 (1964)
24. T. Takaishi, A. Yusa, and F. Amakasu, *Trans. Faraday Soc.*, **647**, 3565 (1971)
25. T. Takaishi, A. Yusa,Y. Ogino and S. Ozawa, *J. Chem. Soc., Faraday Trans. 1*, **70**, 671 (1974)
26. T. Takaishi, A. Yusa,Y. Ogino and S. Ozawa, *Jpn. J. Appl. Phys., Suppl., v2, pt2,* 279

(1974)
27. S. Furuyama and M. Nagato, *J. Phys. Chem.*, **88**, 1735 (1984)
28. S. Furuyama, M. Miyazaki and H. J. Inoue, *J. Phys. Chem.*, **88**, 1741 (1984)
29. B. Tyberce, C. Kappenstein, P. Cartraud and E. Garnier, *J. Chem. Soc., Faraday Trans. 1*, **87**, 2849 (1991)
30. K. Itabashi, T. Fukushima and K. Igawa, *Zeolites*, **6**, 30 (1986)
31. J. A. Ripmeester, *J. Magn. Reson.*, **56**, 247 (1984)
32. T. Ohgushi and H. Yokoyama, *J. Chem. Soc., Faraday Trans. 1*, **88**, 3095 (1992)
33. B. Smith and C. J. J. den Ouden, *J. Phys. Chem.*, **92**, 7169 (1988)
34. Jacob N Iaraelachvili, *Intermolecular and Surface Forces,* Academic Press Limited (1985)

Chapter 2

THEORETICAL BACKGROUND

The purpose of this chapter is to present a basic description of the theoretical concepts and backgrounds of the nuclear magnetic relaxation which are relevant in analyzing the NMR relaxation data for admolecules.

2.1 Molecular Motions and Relaxation Times of NMR

2.1.1 Phenomenological Description of Relaxation Times

In this section we describe general scheme of nuclear relaxation process by which the nuclear magnetization approaches thermal equilibrium in a constant magnetic field of strength H_0 from the macroscopic viewpoint.[1] At equilibrium the nuclear magnetization M_0 of a system consisting of nuclear spins I is given by Curie's law:

$$M_0 = N_0\gamma^2(h/2\pi)^2I(I+1)H_0/(3kT), \tag{2-1}$$

where h is the Planck constant, k the Boltzmann constant, γ the nuclear gyromagnetic ratio, and N_0 the number of nuclear spins in unit volume (cm^3). Suppose that the system is by some reason deviated from the equilibrium. The magnetic field exerts a torque upon the nuclear spin magnetic moment, the motion of which obeys the equation of motion,

$$d\boldsymbol{M}/dt = \gamma \boldsymbol{M} \times \boldsymbol{H}, \tag{2-2}$$

and, as a result, the magnetization undergoes the Larmor precession about the static field $\boldsymbol{H}_0$. Eq. (2-2) does not contain any mechanism for the system to return to thermal equilibrium and so the magnetization will continue to precess endlessly if any force to disturb the spin system is not exerted on it. However, we can observe the actual spin system to return to equilibrium. Bloch gave a phenomenological interpretation to this relaxation effect by introducing relaxation terms into Eq. (2-2).

Providing that $H_Z = H_0$, $H_{X,Y} = 0$ so-called Bloch equations are:

$$dM_Z/dt = -(M_Z-M_0)/T_1, \tag{2-3}$$

$$dM_X/dt = -M_X/T_2 + \gamma M_Y H_0, \tag{2-4}$$

$$dM_y/dt = -M_y/T_2 - \gamma M_x H_0, \tag{2-5}$$

where T_1 corresponds to "the longitudinal relaxation time" caused by the relaxation along the field H_0 and T_2 to "the transverse relaxation time" caused by the relaxation transverse to H_0.

Suppose that the spin system, initially at thermal equilibrium, is disturbed in such a way to realize the condition that $M_x = M_0$ and $M_{y,z} = 0$ (as is done by a $\pi/2$ pulse in practice). The solution of Eqs. (2-3~5) is

$$(M_0 - M_z)/M_0 = \exp[-t/T_1] \tag{2-6}$$

$$M_x = M_0 \cos(-\gamma H_0 t) \exp[-t/T_2] \tag{2-7}$$

$$M_y = M_0 \sin(-\gamma H_0 t) \exp[-t/T_2] \tag{2-8}$$

Thus equations give the individual components of M at time t after the disturbance ($\pi/2$ pulse). While M_z relaxes exponentially to M_0 in the H_0 direction, the transverse components rotate about H_0 at the frequency of $\omega = \gamma H_0$ and their amplitudes decrease exponentially in time to zero. This rotating magnetization induces an induction signal to the rf (radio frequency) coil wound around the sample. This signal is called "free induction signal" and can be measured with a suitable apparatus.

T_1 is also called "the spin lattice relaxation time"; during the period of the longitudinal relaxation process the spin system must transfer its energy to "lattice", i.e., the heat bath which consists of remaining degrees of freedom (electronic, rotational, translational, etc.) of the outer system. Likewise T_2 is usually called the spin-spin relaxation time because it refers to thermal equilibrium within the spin system itself.

We shall describe the experimental methods to determine T_1 and T_2 in Chapter 3.

2.1.2 Nuclear Magnetic Relaxation and Molecular Motions

Although T_1 and T_2 were defined by the Bloch equation as the spin-lattice and the spin-spin relaxation times, respectively, the entity responsible for the relaxation is still unknown. In this section we consider the relaxation process from the microscopic point of view, by relating it to the molecular motion.[1-3] For the sake of simplicity, we shall consider the simplest example of two protons ($I = 1/2$) interacting with each other through the magnetic dipole-dipole coupling.

When nuclear magnetic relaxation is observed in the laboratory-fixed coordinate system, i.e., in the laboratory frame, the total Hamiltonian is given by

$$H = H_Z + H_D(t), \tag{2-9}$$

where H_Z and H_D are the Zeeman and the Dipolar Hamiltonian, respectively. Taking the z axis in the direction of the static field H_0,

$$H_Z = -\gamma(h/2\pi)H_0(I_{1z} + I_{2z}). \tag{2-10}$$

The allowed transitions occur between the levels adjacent in energy according to the spin selection rule, giving

$$\Delta E = \gamma(h/2\pi)H_0 = (h/2\pi)\omega_0. \tag{2-11}$$

Since there are a great number of nuclei in our macroscopic sample, we shall specify the number of spins in the two states m = +1/2 and -1/2 by N_+ and N_-, respectively (Fig. 2-1), where m is the magnetic quantum number of proton spin specifying the spin energy state.

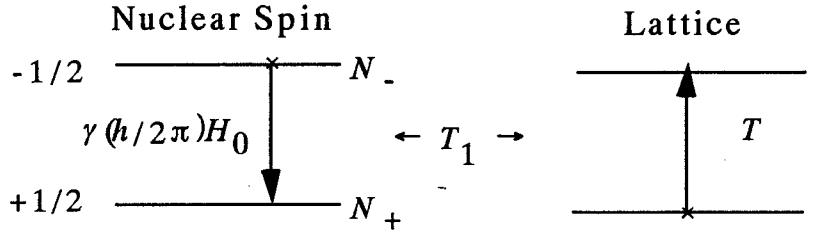

Fig. 2-1 Energy levels for I =1/2 and a possible transition

Furthermore, we consider a heat or energy reservoir, i.e., the lattice, which is able to exchange the energy with the spin system when a net number of transitions occur between two spin states. If the initial ratio of N_-/N_+ corresponds to non-equilibrium state, the heat (energy) flow from the spin system to the lattice takes place and it continues until the equilibrium of the spin system is attained. The final equilibrium populations, N_+^0 and N_-^0, are then given by

$$\frac{N_-^0}{N_+^0} = e^{-\gamma(h/2\pi)H_0/kT}. \tag{2-12}$$

Let us denote the probability per second that a coupling between the spin and the lattice will induce an upward transition of spin (+ → -) by $W\uparrow$ and the reverse by $W\downarrow$. Then we have a rate equation

$$\frac{dN_+}{dt} = N_-W\downarrow - N_+W\uparrow. \tag{2-13}$$

Now we put that $N = N_+ + N_-$ and $n = N_+ - N_-$. We then rewrite the rate equation by using the population difference n of two levels as

$$\frac{dn}{dt} = \frac{n_0 - n}{T_1}, \tag{2-14}$$

where

$$n_0 = N \frac{W_\downarrow - W_\uparrow}{W_\downarrow + W_\uparrow} \tag{2-15}$$

is the population difference at equilibrium and

$$\frac{1}{T_1} = W_\downarrow + W_\uparrow. \tag{2-16}$$

It is noted that the spin-lattice relaxation time T_1 introduced by Bloch is related to (microscopic) transition probabilities.

Next, we introduce the so-called "spin-temperature hypothesis" which states as follows.[4,5] A spin system isolated from the lattice and subjected to spin-spin interactions proceeds toward the state of internal equilibrium with a characteristic time constant T_2 (spin-spin relaxation time), and because the internal equilibrium is usually attained very quickly, i.e., T_2 is very short due to strong dipolar interaction, we can define a common temperature to within the closed spin system. Then the probability of finding the system in any of its energy levels is governed by the Boltzmann distribution $\exp(-E_m/k\theta_S)$, where θ_S is the "spin temperature" of the spin system. If a spin temperature is maintained within the system, T_1 is related to the transition probability per second, W_{mn}, between spin states $|m\rangle$ and $|n\rangle$ by[6]

$$\frac{1}{T_1} = \frac{1}{2} \sum_{n,m} W_{mn}(E_m - E_n)^2 / \sum_n E_n^2, \tag{2-17}$$

where E_m and E_n are the energies of states $|m\rangle$ and $|n\rangle$, respectively.

Now, it has been established that the dipolar Hamiltonian can be expanded into a series of the products of spin operators A_q and random time-dependent spatial function $F_q(t)$:

$$H_D(t) = \sum_q F_q(t) A_q. \qquad (q = 0, \pm 1, \pm 2) \tag{2-18}$$

Here only $\langle m|A_q|m+q\rangle$ becomes non-vanishing elements. The transition probabilities occurring in the summation depend not only on the magnitude of the spin part of the dipolar matrix elements $\langle m|A_q|n\rangle$, but also on the time dependent spatial part $F_q(t)$ of the dipolar

Hamiltonian. Then the assumption that fluctuations are represented by a stationary random process brings about the following expression for W_{mn},

$$W_{mn} = |\langle m|A_q|n\rangle|^2 J_q(\omega_{mn}), \tag{2-19}$$

where $J_q(\omega_{mn})$ is the spectral density of the time correlation function $G_q = F_q(t)F_q^*(t+\tau)$ of the spatial fluctuation at frequency ω_{mn}, which is given by

$$J_q(\omega_{mn}) = \int_{-\infty}^{\infty} \overline{F_q(t)F_q^*(t+\tau)}\, e^{-i\omega_{mn}\tau}\, d\tau. \tag{2-20}$$

Because the spin operators in the dipolar Hamiltonian are associated with the zero quantum (q = 0), the single quantum (q = ±1), and the double quantum (q = ±2) transitions of the coupled spin system, the spectral densities with the frequency components $\omega_{mn} = \omega_0$ and $\omega_{mn} = 2\omega_0$ contribute to the transition probabilities W_{mn}. Thus Eq. (2-17) becomes

$$\frac{1}{T_1} = \frac{9}{8}\gamma^4\left(\frac{h}{2\pi}\right)^2\{J_1(\omega_0) + J_2(2\omega_0)\}. \tag{2-21}$$

A spin temperature hypothesis described above is valid under the condition $\tau_c > T_2$, where τ_c is a characteristic correlation time representing the rate of the fluctuation. However, the same T_1 expression as Eq. (2-21) can be derived by the weak collision theory, first given by Bloembergen, Purcell, and Pound (BPP),[7] and established by Kubo and Tomita.[8] In the case $\tau_c < T_2$, the effective dipolar interaction responsible for the spin relaxation may be small and treated as a small perturbation. The spin-spin relaxation time T_2 is also given by

$$\frac{1}{T_2} = \frac{9}{8}\gamma^4\left(\frac{h}{2\pi}\right)^2\left\{\frac{1}{4}J_0(0) + \frac{5}{2}J_1(\omega_0) + \frac{1}{4}J_2(2\omega_0)\right\}. \tag{2-22}$$

Eqs. (2-21) and (2-22) hold in principle under the condition $\tau_c < T_2$, T_1, but Eq. (2-21) can usually be applied in the slow motion case of $\tau_c \geq T_2$. The calculation of the spectral densities is probably the most difficult part of the problem. The precise form of $J_q(\omega)$ will depend on the nature of the molecular and ionic motion. In the case of the dipolar relaxation in the weak collision limit, however, the ratio of the spectral densities is proved to be[9]

$$J_0(\omega) : J_1(\omega) : J_2(\omega) = 6 : 1 : 4 \tag{2-23}$$

independently of the modes of molecular motion. It is, therefore, sufficient to calculate only one spectral density.

When the fluctuation is approximated by an exponential time correlation function as usual, we can write the auto-correlation function as

$$G_q(\tau) = \langle f_q(t)^* f_q(t+\tau)\rangle = \langle |f_q(t)|^2\rangle \, e^{-|\tau|/\tau_c}, \tag{2-24}$$

where $f_q(t)$ is the time dependent random part of $F_q(t)$. Then Eq. (2-20) may be rewritten as

$$J_q(\omega) = \int_{-\infty}^{\infty} G_q(\tau)\, e^{i\omega\tau}\, d\tau. \tag{2-25}$$

Therefore, in the case of powdered crystal or liquid, the expressions of T_1 so far encountered in the literature are arranged in a complete form, [9,10]

$$T_1^{-1} = C \sum_i b_i B(\tau_{ci}), \tag{2-26}$$

where $B(\tau_c)$ is defined by

$$B(\tau_c) = [\tau_c/(1+\omega_0^2\tau_c^2)] + [4\tau_c/(1+4\omega_0^2\tau_c^2)], \tag{2-27}$$

and is independent of modes of molecular motion. The first and the second terms of Eq. (2-27) come from $J_1(\omega)$ and $J_2(2\omega)$, respectively. The constant factor (coupling constant) C in Eq. (2-26) represents the strength of the dipolar interaction, which depends on the modes of motion; b_i designates the contribution of i-th "normal mode to the spin relaxation" with the correlation time τ_{ci}.

An important point of Eqs. (2-26) and (2-27) is that, when only one mode of molecular motion contributes to the relaxation, T_1 assumes the minimum at $\omega_0\tau_c = 0.615$. For example, provide that we measure the T_1 at the Larmor frequency of about 10 MHz, then we can observe a minimum of the T_1 when the correlation time of the molecular motion reaches $\tau_c \approx 10^{-8}$ s. In addition, since the condition $\omega_0\tau_c = 0.615$ gives rise to a certain value of $B(\tau_c)$, we can determine the value of C. C can also be calculated theoretically by modeling the molecular motion and so by the comparison of the experimental C with the theoretical one we can determine the "mode" of the motion as well. Through the measurements of T_1, therefore, we can obtain useful information concerning molecular motions the correlation time of which lies between about 10^{-5} and 10^{-11} s.

2.2 Theoretical Expectations for Nuclear Magnetic Relaxation and Motions of Adsorbed Molecules

In the previous section we described how molecular motions affect nuclear magnetic relaxation by considering the simplest example of two-proton system interacting through magnetic dipole-dipole coupling. As in bulk phases, the protons in the adsorbed molecules undergo nuclear dipolar interaction with other protons within the molecule (intramolecular contribution to relaxation time) and with protons in other neighboring molecules (intermolecular contributions). The intramolecular dipolar interaction is modulated mainly by molecular rotation and the intermolecular one by molecular translational diffusion.

When the rate of translational diffusion and that of rotation differ largely from each other, these motions cause effective relaxation separately in different temperature regions. In such a case two separate T_1 minima due to translational diffusion and rotation will appear. Typical example showing such phenomenon is crystals consisting of spherical or nearby spherical molecules , so-called plastic crystal.[11,12] In the case of associated molecules (such as water[7,13]) translational and rotational jumps happen to occur at roughly equal frequencies, $\tau_T \approx \tau_d$. In such a case, it is not easy to distinguish the rotation and translation, i.e., the intermolecular and intramolecular contributions, since we can observe only one broad T_1 minimum.

For molecules which undergo anisotropic motions in the adsorbed or solid state, there are temperature regions where rotation about the unique axis causes effective relaxation. For example, for adsorbed benzene the rotation about the six-fold axis easy to occur, while rotations about other axes appear to take place only in a diffusion step.[14,15]

The rate of molecular motion is usually represented in terms of the correlation time and the temperature dependence of the correlation time is usually given by the Arrhenius activation process,

$$\tau_c = \tau_0 \exp(E_a/RT), \tag{2-28}$$

If the molecules are homogeneously adsorbed, we can consider that the molecular motions of individual molecules are excited to similar extent to each other, and so it may be described using a single correlation time. However, when the surface is considerably inhomogeneous, the rates of motion may distribute irregularly and such a situation is described by regarding that the correlation times distribute over some time domain. In the case of adsorption system, if there are various specific adsorption sites in the substrate, one needs to assume several correlation times to describe the motions of molecules at individual specific sites.

Until now we only considered the proton-proton dipolar interactions. However, electronic magnetic moment is about a thousand times larger than nuclear moments and hence if the system contains a trace of paramagnetic centers, their electronic spins may produce a local

magnetic field which governs predominantly the nuclear relaxation. It should be noted that commercial zeolites including mordenite contain usually paramagnetic iron impurities of about hundreds ppm. Paramagnetic impurities contained in adsorbent lattices may cause an efficient nuclear spin relaxation and make the analysis of the relaxation data for adsorbed molecules very complex. At high temperatures, molecular diffusion ($D_m \sim 10^{-6}$ cm^2/s) is much faster than the spin diffusion ($D_S \sim 10^{-12}$ cm^2/s).[16] In such a case, molecular diffusion brings the adsorbate molecules to the vicinity where the field of the electronic spin causes drastic nuclear relaxation. When the diffusion of adsorbate molecules is very fast but the intermolecular proton dipolar interaction is small the relaxation rate due to localized electron spins can be described by the theory of Torrey,[17,18] but in most experiments so far performed the relaxation rate are approximated by the normal BPP equation with the correlation time τ_d instead of τ_c, the life time between translational jumps. In some fortunate cases the T_1 measurements in the presence of paramagnetic impurities can be used to extract information on the translational motion.[12]

If the electron spins undergo rapid flip-flop motion because of strong exchange interaction between the electrons, this flipping gives effect on the nuclear spin relaxation. Providing that this electron motion is characterized by a relaxation time τ_e (~10^{-6} s), the effective correlation time for the nuclear T_1, τ_c, may be given by[7,12]

$$\tau_c^{-1} = \tau_d^{-1} + \tau_e^{-1} \qquad (2\text{-}29)$$

When τ_d becomes longer than τ_e, the nuclear relaxation is governed dominantly by paramagnetic relaxation and T_1 depends only weakly on temperature. When translational diffusion becomes slow enough so that the mean square molecular diffusion distance per step (per τ_d) is shorter than the distance between paramagnetic centers, R, the nuclear spin relaxation is governed by "spin diffusion" mechanism.[12] Let θ be the time taken for a molecule to travel the distance R; then

$$\theta = (R^2/r^2),\ \sim 100\tau_d \qquad (2\text{-}30)$$

where r is the elementary jump distance. At this time, non-exponential recovery of nuclear magnetization will be observed.[19]

Molecular reorientation may be highly excited in this low temperature region. If there exist a small amount of paramagnetic impurities, the relaxation may be governed by τ_e, and therefore, it is difficult or, in many cases almost impossible, to obtain information about the reorientation of adsorbed molecules. In order to observe molecular rotational motion by T_1 measurement, we have to remove the impurities completely or to prepare highly pure adsorbents, as will be described in Chapter 3.

References to Chapter 2

1. C. P. Slichter, *Principles of Magnetic Resonance*, Harper and Row, New York, (1963)
2. A. Abragam, *The Principles of Nuclear Magnetism*, Oxford Univ. Press, London/New York, (1961)
3. P. S. Alen, *MTP International Review of Science: Magnetic Resonance*, Physical Chemistry Series 1, Vol. 4, ed. by C. A. MaDowell, Butterworths, (1972)
4. D. Wolf, *Spin Temperature and Nuclear-Spin Relaxation Matter,* Oxford Univ. Press, (1979)
5. M. Goldman, *Spin Temperature and Nuclear Magnetic Resonance in Solid*, Oxford Univ. Press, (1970)
6. L. C. Hebel and C. P. Slichter, *Phys. Rev.*, **113**, 1504 (1959)
7. N. Bloembergen, E. M. Purcell, and R. V. Pound, *Phys. Rev.*, **73**, 679 (1948)
8. R. Kubo and K. Tomita, *J. Phys. Soc. Jpn.*, **9**, 888 (1954)
9. G. Soda and H. Chihara, *J. Phys. Soc. Jpn.*, **36**, 954 (1974)
10. D. E. Woessner, *J. Chem. Phys.*, **42**, 1855 (1965)
11. H. A. Resing, *Mol. Cryst.*, **9**, 101 (1969)
12. H. A. Resing and J. K. Thompson, *J. Chem. Phys.*, **46**, 2876 (1967)
13. H. A. Resing, *Advan. Mol. Relaxation Processes,* **1**, 109 (1968)
14. D. E. Woessner, *J. Phys. Chem.*, **70**, 1217 (1966)
15. J. K. Thompson, J. J. Krebs and H. A. Resing, *J. Chem. Phys.*, **43**, 3853 (1965)
16. W. B. Blumberg, *Phys. Rev.*, **119**, 79 (1960)
17. H. C. Torrey, *Phys. Rev.*, **92**, 962 (1953)
18. G. J. Kruger, *Z. Naturforsch. A*, **24**, 560 (1969)
19. H. A. Resing , *Advan. Mol. Relaxation Processes,* **3**, 199 (1972)

Chapter 3

EXPERIMENTAL

3.1 Synthesis and Characterization of Mordenite

3.1.1 Introductory Remarks

The first synthesis of mordenite was carried out by Barrer in 1948.[1] Thereafter many studies on its synthesis have been reported. The representative methods of synthesis were developed by Domine (1966),[2] Sand (1968),[3] and Whittemore(1972).[4] As in the cases of the synthesis of various zeolites in industrial plants and in laboratories,[5] hydrothermal synthesis in autoclaves was applied to mordenite. The crystallization occurs in hydrogels prepared by mixing aqueous solution of sodium silicate or silica sol and solution of sodium aluminate, under high pressure (>10 atm) and at high temperature (>200 °C). Since both amorphous substrate and aqueous liquid phase coexist, and the Si/Al ratio varies during reaction, it is difficult to obtain crystals with constant composition under such conditions. In addition, because the autoclaves are usually made of metals, it is difficult to avoid the contamination of the product by paramagnetic impurities such as iron which may prevent us from obtaining reliable relaxation data.

Ueda *et al.* developed a method to synthesize mordenite under a mild condition, that is, at 100 °C and at 1 atm in aqueous solutions without using any amorphous substrate.[6,7] They also revealed that the Si/Al ratio in the crystal can be kept constant throughout the reaction even though the Si/Al ratio increases in the solution as the reaction proceeds. They explained that some homogeneous *chemical species* are formed in the initial solution, which have the same compositions and structure as the mordenite crystal, and the crystallization corresponds to the precipitation of the *chemical species.*[6-8]

We, therefore, prepared the sample for the present work by a similar method to that developed by Ueda *et al.*

3.1.2 Details of Synthesis

The procedure of synthesis is illustrated in Fig. 3-1. We used Teflon wares in the all steps of the preparation so as to avoid the contamination of the product by paramagnetic species.

High-purity mordenite used in the present study was synthesized from aqueous clear solution at 100 °C under atmospheric pressure. The composition of starting material in the synthesis was $10Na_2O{\cdot}0.25Al_2O_3{\cdot}36SiO_2{\cdot}440H_2O$, which is the optimum composition for

high quality and high yield according to Ueda.[6] The procedure of synthesis is as follows: Calculated amount of aluminum metal foil (Koch Chemicals Ltd., 99.9995 %) was added to solution of sodium hydroxide (Wako Chemical Industry Ltd., special grade, Fe < 1ppm) in 1000 ml Teflon container. The mixture was heated in a water bath to dissolve aluminum metal and finally a fixed amount of aqueous colloidal silica sol (Central Research Institute of Nissan Chemical Industry Ltd., grain diameter (BET) = 12.7 nm, Fe < 1 ppm) was added dropwise to the solution under stirring. Viscous amorphous solid formed at the beginning of reaction dissolved perfectly within 30 minutes on heating with continuous stirring in boiling water bath. After the solution became transparent, ground mordenite seeds were added to it. The container was sealed and its temperature was kept at 100 °C for 1 week.

After the above procedure, fine solids produced were separated from the solution, washed repeatedly with hot water. To repeat washing is necessary for obtaining highly adsorptive mordenite. Finally the product was dried in an oven at 100 °C.

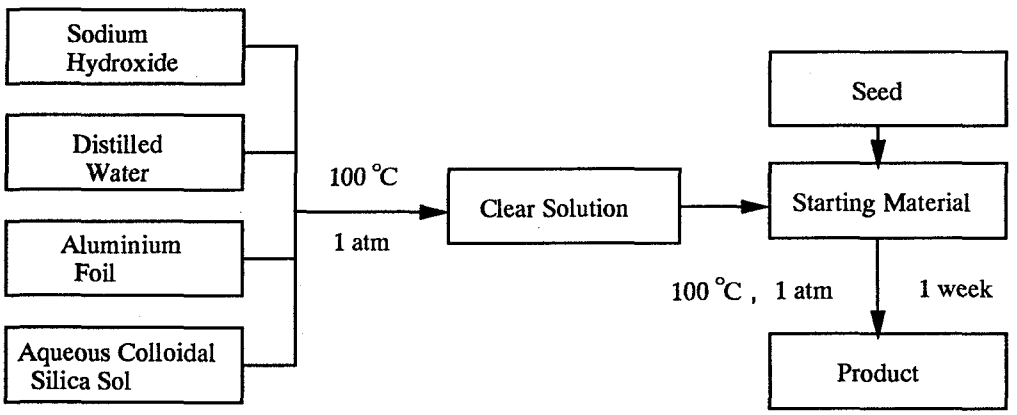

Fig. 3-1 Procedure of Synthesis of Mordenite

3.1.3 Analysis and Characterization

The identification of the product was made by X-ray diffractometry (CuKα radiation) at the X-ray Diffraction Service of Department of Chemistry, Faculty of Science and by scanning electron micrograph (SEM) at Department of Earth and Planetary Science, College of General Education. Compositions of the product were determined by the atomic absorption spectroscopy for Na, Al, and Si, and by the inductively coupled plasma spectrometry for Fe. The results are tabulated in Table 3-1.

The SEM photographs of the present product, and the mordenite seeds of commercial source are shown in Fig. 3-2. It is obvious that the crystals synthesized in the present work are larger in size and have better morphology than the commercial ones.

Table 3-1. Composition of the Synthesized Mordenite[a)]

SiO_2[b)]	84.6 wt%
Al_2O_3[b)]	9.6
Na_2O[b)]	5.8
Fe_2O_3[c)]	< 20 ppm[e)]
total	100.0
SiO_2/Al_2O_3[d)]	14.9
Na_2O/Al_2O_3[d)]	0.99

a): carried out in Tosoh Corporation Ltd.
b): by atomic absorption spectroscopy
c): by inductively coupled plasma spectrometry
d): molar ratio
e): lower than the limit of detection

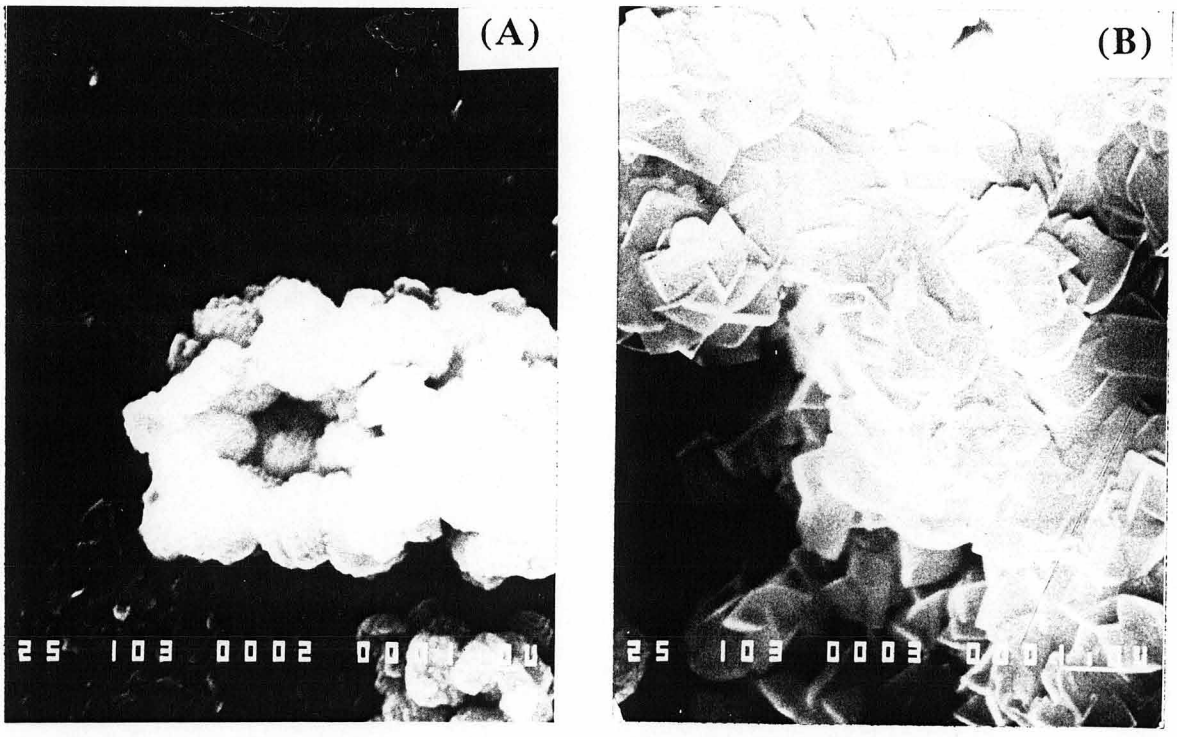

Fig. 3-2 SEM photographs for mordenites.
(A) commercial (B) synthesized

The X-ray powder diffraction patterns of the synthesized and the commercial mordenite are shown in Fig. 3-3. The positions of the reflections are almost the same, and the relative intensities are similar in two samples. These facts indicate that two samples of different sources have the same crystal structure. However, each reflection from the crystal synthesized here is sharper than that from commercial material, suggesting that the quality of the former crystal is higher than that of the latter.

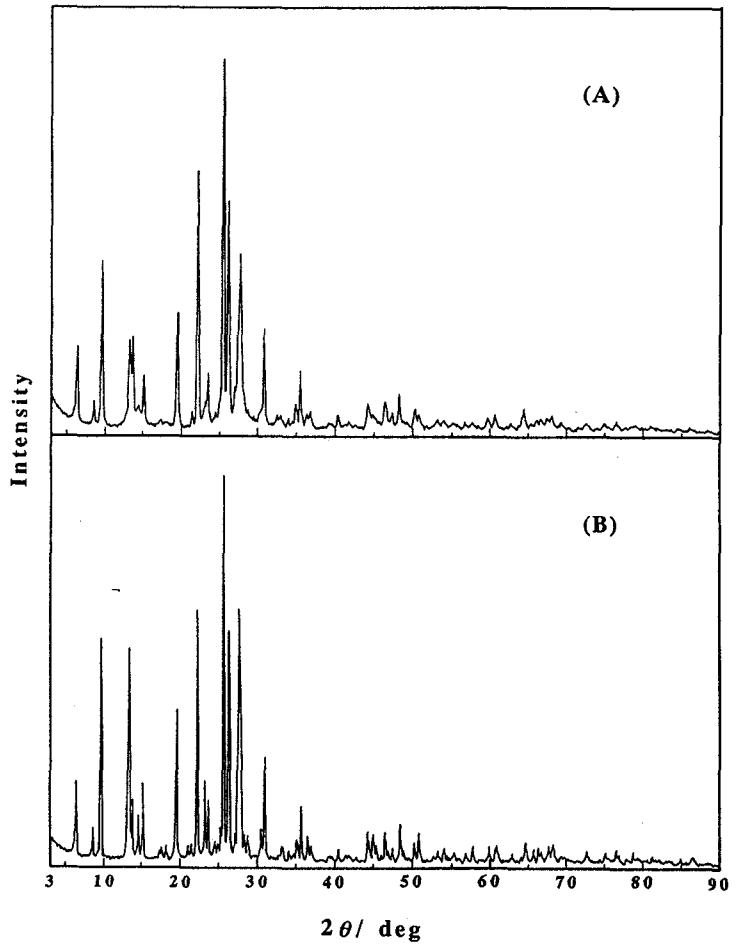

Fig. 3-3 X-ray powder diffraction patterns of mordenites.
(A) commercial (B) synthesized

The newly synthesized mordenite was revealed to have high ability of adsorption. It can adsorb benzene, toluene and xylene of at least 2 molecules per unit cell corresponding to 1 molecule per section of channel (One unit cell contains two sections of parallel channels.[9-11] See Fig. 1-1). This fact indicates that the product is *so-called* large-pore mordenite, the pores of which are almost perfectly open and penetrable.[12]

If paramagnetic impurities are contained in the zeolite frameworks, the local field experienced by a molecule will be influenced by the impurities and modulated through the translational diffusion.[13,14] Because the commercial sample is contaminated by about 200 ppm of iron, T_1 at high temperatures exhibits shorter values as shown in Fig. 3-4, and the recovery of the magnetization after 90° pulse shows nonexponential behavior. On the other hand, the synthesized mordenite contains no detectable iron impurity, and hence normal behavior of T_1 was observed at high temperatures. Therefore we can state that reliable values of T_1 of protons can be obtained by using the high-purity synthesized mordenite.

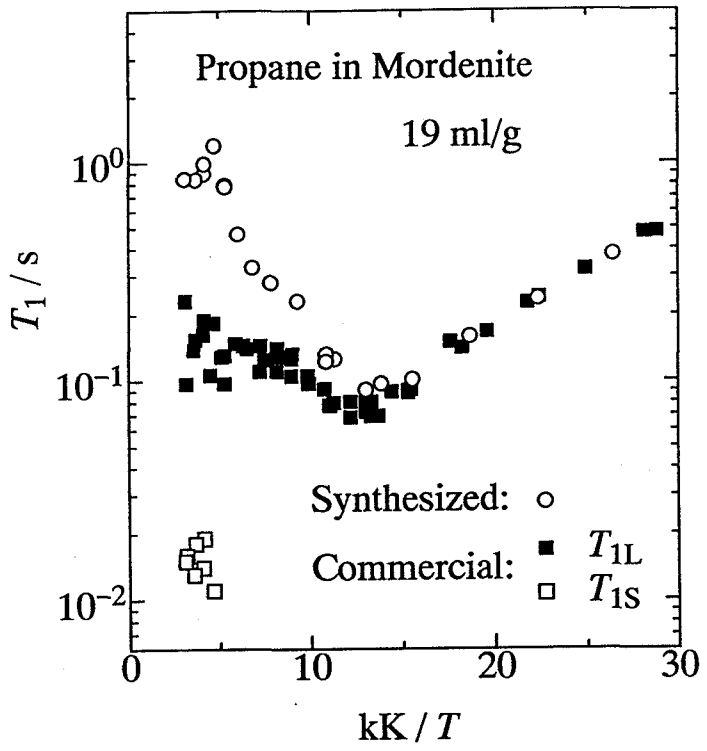

Fig. 3-4 Temperature dependence of T_1 for propane adsorbed in commercial and synthesized mordenites. (at 40.4 MHz)

3.2 Cryostat and Adsorption System

3.2.1 Introductory Remarks

Many NMR studies, including deuteron lineshape measurements,[15] measurements of diffusion constant by PFG[16] and relaxation measurements,[13, 14, 17] on molecules adsorbed in zeolites or on other adsorbents have been reported so far. Almost all of the studies have encounted difficulties in the sampling processes. Usual sampling procedure consists of the following steps: first to fill zeolite into glass cell and bake it at high temperature in vacuo, then to introduce gas into the cell (if the efficiency of adsorption is low, it is necessary to keep the cell at low temperature by using refrigerant such as liquid nitrogen) and soon to seal off the glass cell.[16] The most important point associated with this method is difficulty in controlling the amount of adsorption. If one wants to determine the coverage dependence of mobility of adsorbate by relaxation measurements, it is necessary to repeat the above procedure, and every time the excess adsorbate has to be consumed. In addition, in the case of the gas that is only poorly adsorbed, the pressure in the cell should be increased to realize sufficient adsorption at high temperature. Relative amount of free gas molecules then increases, which contribute to the NMR signal significantly, and causes uncertainty in the relaxation measurement.

As described later in detail, we found that the dead space of sample container can become almost vacuum when the specimen is kept at low temperatures. In such a case the heat exchange is attained by introducing helium gas into the sample cell. Because of above several difficulties it is inconvenient to use a sealed cell for low temperature experiment.

In the present study, a new NMR probe has been designed and constructed, which is directly connected to the gas adsorption system and the vacuum line so as to measure NMR signals *in situ* conditions. This system resembles a NMR cryostat constructed by Eguchi[18] for relaxation measurements on condensed gases. The present system has been designed under following conditions:

1) Because of the poor signal intensity of the adsorbed matter, sample cell should have as large volume as possible, but must simultaneously realize homogeneous magnetic field through the sample.

2) The sample cell should be easy to handle for baking under evacuation, and for mounting into the cryostat on keeping the vacuum condition.

3) The system should be easy to handle for introducing exact amount of gases into the sample cell.

4) It should be utilized for the measurement of the adsorption isotherm as well as NMR experiments.

5) NMR measurements can be carried out over a wide temperature range between liquid helium and room temperatures. The cryostat must maintain the sample temperature at 4.2 K for at least 5 hours on single charge of liq. He.

6) During the NMR measurements at low temperatures, it is necessary to introduce helium gas into sample cell for heat exchange.

The following paragraphs deal with detailed descriptions of the cryostat and the adsorption system as well as their performance.

3.2.2 Cryostat and Adsorption System

Fig. 3-5 shows the cryostat constructed. It consists of two main parts, one being the NMR probe, and the other the refrigerant container consisting of double glass Dewer vessels, **H** and **I**.

The probe unit **J** consists mainly of the sample cell **g**, the rf coil **h** and the shield can **b** . A KARMA wire heater (denoted as **i**; 100 Ω) is wound around the shielding can **b** (copper, 28 mm in outside diameter and 1 mm in wall thickness). The shielding can **b** serves also as an electrical shield. It has vents on its top and bottom to transfer the liquid He easily. The rf coil **h** (Teflon coated copper wire of 1.0 mm ϕ) is connected to the rf cable which is a stainless steel tubing (1 mm in outside diameter, silver plated) running through the center of the stainless tube **A**; the electrical insulation in the cable is insured by Teflon spacers. A BNC connector is soldered on the top of the co-axial cable and is sealed air-tightly with a rubber O-ring. The opposite end of the coil is grounded at the top of the shielding can **b**.

The sample cell **g** has an inner volume of about 4 cm^3 (a quartz tube of 12 mm in inside diameter, 14 mm in outside diameter and 40 mm long). Its temperature is measured by the thermocouples **j** (one pair of Cu - Constantan and one pair of Au+0.07%Fe - Chromel) attached at its bottom. The sample cell is fused to the Kovar tube **e** with Kovar seal, which is attached to a connector **d** (1/8 inch VCR, *Cajon* Company). Zeolite sample is filled through the opening of the connector. The connector is sealed with the copper O-ring **c** (Cu-2-VCR-2, *Cajon*, 2.3 mm inside diameter). The gland of VCR is connected to the gas filling tube (**G**), which assumes a double-tube structure to prevent the gases from condensing in the path. The nozzle for evacuating the double tube space is **C**. The gas filling tube is connected to a stop-valve (denoted as **D**, Carp 6•35, Fuji Kin) the ends of which are terminated by flanges (denoted as E_1 , E_2, KF16) sealed with a rubber O-ring. The flange E_2 is connected to the flexible tube **F**, which is attached with Kovar seal to the Pyrex glass tube. Hereafter we call the glass-made vacuum line and the handling system of adsorbate gas jointly "adsorption system", which is schematically shown in Fig. 3-6.

The adsorption system is made of Pyrex glass and high vacuum greaseless Teflon stop-cocks. It consists of four glass flasks (1020.8, 1032.0, 1023.7, 1033.6 ml, respectively) and

A- electronical co-axial cable with a BNC connector
B - refrigerant vent
C - nozzle for evacuating the double-tube heat insulator
D - valve
E_1, E_2 - KF16 flange
F - flexible tube to vacuum system
G - gas filling tube (SUS)
H - inner Dewer vessel
I - outer Dewer vessel
J - NMR probe unit
K - electric resistor
a - Teflon spacer
b - shielding can
c - copper gasket
d - 1/8 inch VCR
e - Kovar tube
f - Kovar seal
g - sample cell (quartz)
h - rf coil
i - heater wire
j - thermocouples
k - vent

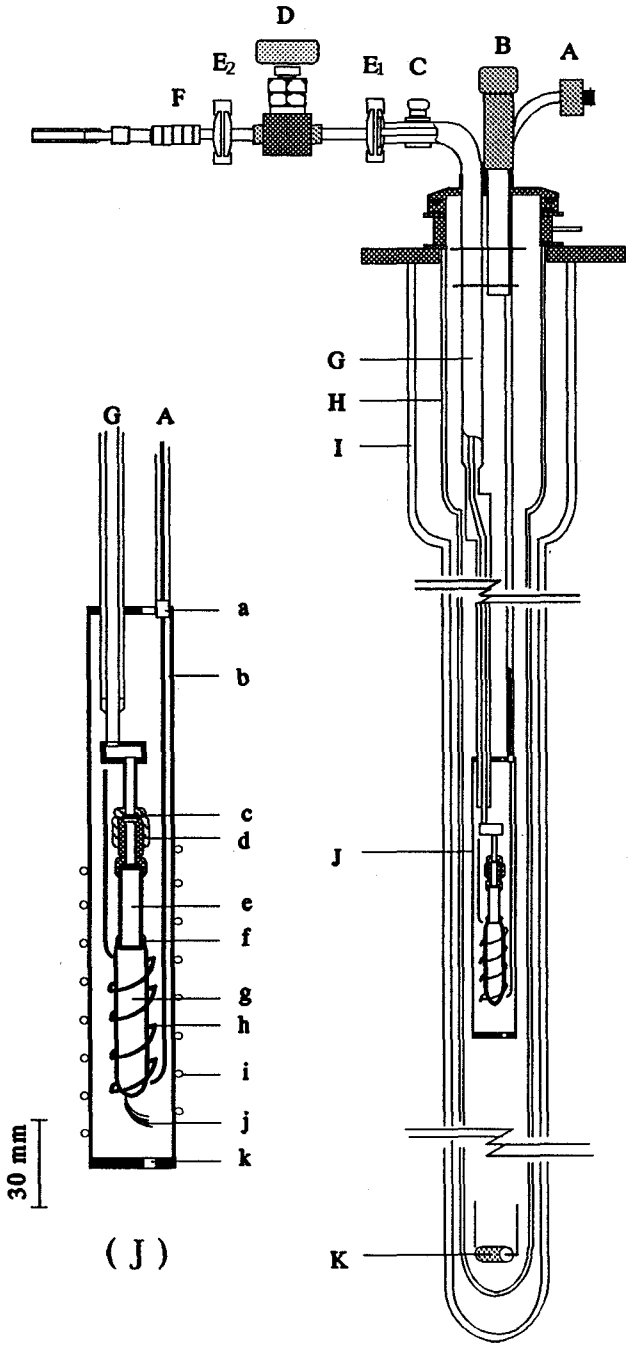

Fig. 3-5 Diagram of the cryostat constructed.

a pressure gauge (BARATRON 122A, PDR-C-1, MKS INSTRUMENTS, INC.) which works in the range from 10^{-1} to 10^{3} Torr.

The evacuation is done by, through a liquid nitrogen trap, an oil diffusion pump (YH-500A, 1200 l/min, ULVAC JAPAN Ltd.), and a mechanical rotary pump (D-330K, 320 l/min, ULVAC JAPAN Ltd.). An ion gauge (Model IG-11, Shimadzu) and a Geissler tube are used to measure the degree of the vacuum.

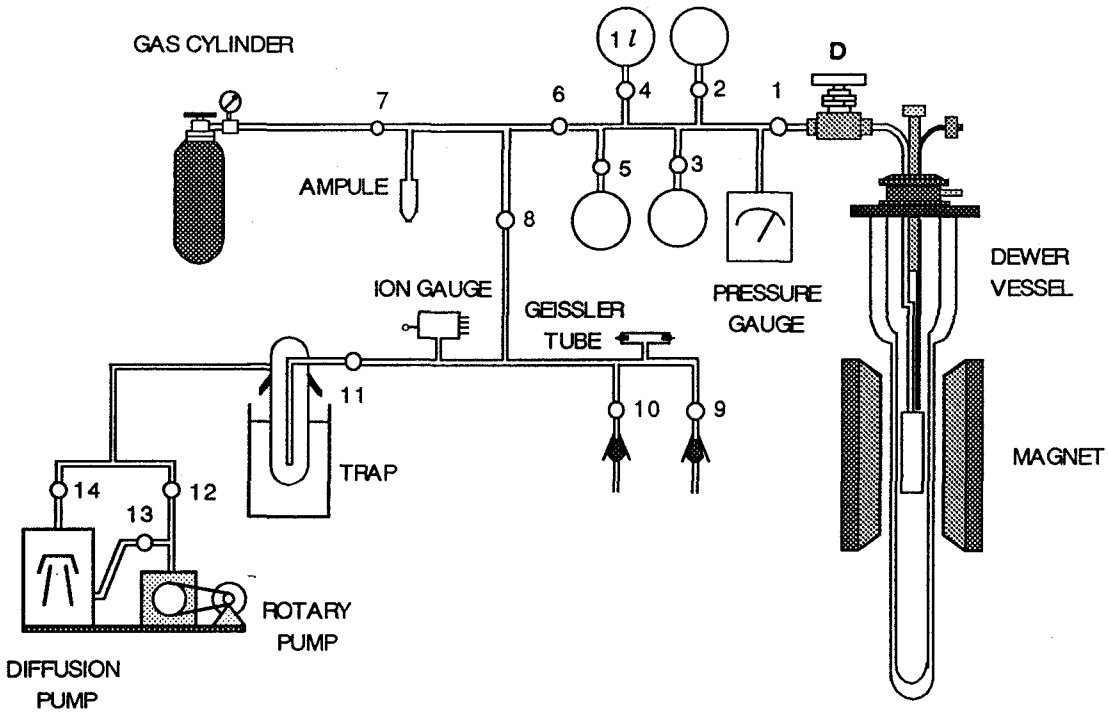

Fig. 3-6 Adsorption system

3.2.3 Operation

Calcination of zeolite

Zeolite sample is filled through the opening of the connector **d** (Fig. 3-5). The connector is sealed with the copper o-ring **c**. The volume of the sample cell is about 4 ml, and 2.1 g of dehydrated mordenite was used in the present experiments.

For baking the zeolite sample, we separate the probe from the gas line at **E2**, take it out of the Dewer vessel and set it into a calcinatory. The calcination is carried out by increasing the temperature of the sample cell to 673 K in 12 hours or more and keeping it at 673 K for 24-36 hours with evacuating until the pressure of the probe reaches 10^{-6} Torr.

After the calcination the valve **D** is closed to keep the inner of the sample cell vacuum and the cell is mounted into the NMR cryostat.

Filling the gas specimens

As shown in Fig. 3-6 the specimen gas is supplied from a gas cylinder. The sample gas is firstly stored in the flasks before being introduced into the NMR sample cell **g** in Fig. 3-5.

The dead volume is 78.7 ml between stopcocks **1** and **6** , is 42.1 ml between stopcock **1** and valve **D**, and is 17.2 ml between valve **D** and the sample cell. The gas sample is introduced into the sample cell at room temperature and the amount filled is monitored by the pressure gauge.

The system is also used to introduce the helium gas into the sample cell for heat-exchange in measurements at low temperatures, and to measure the adsorption isotherm.

Temperature measurement and controls

After closing the valve **D**, we cool the NMR probe to about 100 K by liquid nitrogen filled in the outside Dewer vessel. In order to cool the sample slowly, the cooling speed is controlled by passing an appropriate electric current through the heater **i** in Fig. 3-5. The average cooling rate is 20 K/h.

Sample temperature is measured by the thermocouples **j** at the bottom of the cell **g** using a digital thermometer (Type 2572, Yokogawa Electric Works Ltd.). The thermocouples of Au+0.07%Fe - Chromel is used in the temperature range of 4.2 - 273 K, while the pair of Cu - Constantan is used above 273 K. To avoid unfavorable noise from the digital thermometer we turned off the switch of the equipment during the NMR data collection periods.

Both inner and outer vessels are filled with liquid nitrogen for measurements above 77 K, while the inner vessel **H** is filled with liquid helium and the outer one **I** with liquid nitrogen for measurements between 4.2 and 77 K. The sample temperature can be kept at 4.2 K for 5 hours after a single charge, and last for 5 hours for the measurement between 4.2 K and 77 K. Among 4.2 K to 25 K, we coercively evaporate the liquid He in the inner vessel by passing a weak electric current through the resistor **K** (30 Ω).

The temperature difference between the sample and shielding can **b** is monitored by a Cu - Constantan and an Au+0.07%Fe - Chromel thermocouples. The e.m.f. corresponding to the temperature difference is amplified by a DC amplifier (AM-1001, Ohkura Electric Co. Ltd.) and is fed back to a home-built temperature controller. The controller supplies an electric current proportional to the voltage difference through the non-magnetic KARMA wire heater (100 Ω, denoted as **i** in Fig. 3-5) wound around the shield **b**. Using this set-up, the temperature fluctuation of the probe can be suppressed within ± 0.1 K during the measurements.

It was confirmed that the cryostat and the adsorption system satisfy all the requirements necessary for the NMR measurements described in section 3.2.1 and give certainly reliable T_1 values of ad-molecules *in situ* over a wide temperature range.

3.3 Measurements for ^{1}H Spin-Lattice Relaxation Times

Since the principles and experimental techniques of pulsed NMR[19-25] for T_1 measurements have widely been reviewed so far, only the necessary points for the present work will be described briefly. A little more detailed description will be given on a $\pi/2$(comb)-τ-$\pi/2$ pulse sequence used in the present study. At the end of this section, the NMR spectrometer and our operating condition will be stated.

90° ($\pi/2$) Pulse

NMR applies first a strong static magnetic field H_0 in the z-direction of the laboratory coordinate system (x, y, z) on the sample. The nuclear spin energy states are quantized in the field direction and their interval is generally $(h/2\pi)\omega_0 = (h/2\pi)\gamma H_0$. The spin system then precesses about the z-axis with ω_0, the Larmor frequency, and a macroscopic magnetization M_0 is generated along H_0. If an rf field with the frequency ω_0 is applied via an rf coil wound around the sample in the x-y plane, the resonance occurs and the magnetization of the spin system is excited to a higher energy state.

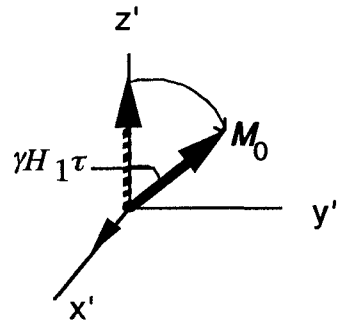

In pulse NMR experiments, a short intense rf pulse with frequency ω with an amplitude H_1 is applied to the sample in the x-y plane of the laboratory frame. At resonance, i.e., $\omega = \omega_0$, the effective field $H_e = H_1$, which is along the x'-axis of the "rotating frame" (x', y', z') which is rotating around the external field H_0 at the Larmor frequency ω_0. The magnetization will rotate about H_1 in the y'-z plane of the rotating frame with an angular velocity $\omega_1 = \gamma H_1$. When such a H_1 field is applied for a time τ, the magnetization vector will be rotated by an angle $\gamma H_1\tau$. An H_1 field which satisfies a condition $\gamma H_1\tau = \pi/2$ is called the $\pi/2$ pulse. By applying $\pi/2$ pulse the nuclear magnetization is brought down into the x-y plane (x'-y' plane) and it induces an e.m.f. in the rf coil the strength of which is proportional to the magnitude of the magnetization.

FID (Free Induction Decay)

The magnetization lies along the rotating y'-axis just after a $\pi/2$ pulse. It will decay in time as the spin system comes back to equilibrium due to two relaxation mechanisms as follows:

The first relaxation mechanism is the transverse or spin-spin relaxation process; the magnetization dephases in the x'-y' plane because the inhomogeneity of the magnetic field and/or spin-spin interactions, for example, cause the difference in the Larmor frequencies of individual nuclear spins. For a single Lorentzian line the decay of the magnetization in the x-y plane will be exponential with the time constant T_2^* and the signal intensity will decay at the rate of $\exp(-\tau/T_2^*)$. It is called free induction decay (FID). One can determine T_2^* by observing the FID just after a $\pi/2$ pulse. The second relaxation mechanism is the longitudinal or spin-lattice relaxation process. The magnetization tends to return to the z'=z direction to recover the thermal equilibrium. This process proceeds generally as

$$M_Z = M_0\,[1-\exp(-\tau/T_1)]$$

with a time constant, T_1, the so-called spin-lattice relaxation time.

$\pi/2$-τ-$\pi/2$ pulse sequence

Because the pickup coil responses only to the component of magnetization in the x-y plane, the magnetization recovery along the z-axis due to the T_1 process is not directly detectable. A second $\pi/2$ pulse is, therefore, always necessary to measure the spin-lattice relaxation time T_1. The simplest method to measure T_1 is to apply a $\pi/2$-τ-$\pi/2$ pulse sequence.

The $\pi/2$-τ-$\pi/2$ sequence[23] is also called the saturation recovery sequence, which can be illustrated as below:

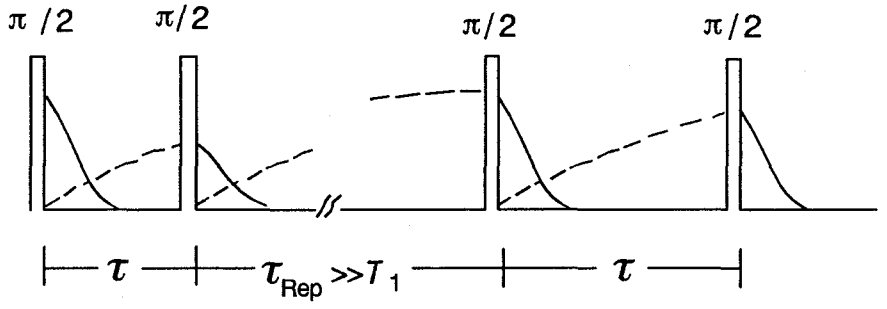

The first pulse brings the nuclear spins to the saturation which means that the magnetization is in the x-y plane. The magnetization recovers with time τ as

$$M(\tau)/M_0 = [1-\exp(-\tau/T_1)].$$

The second pulse applied after τ brings the partially recovered magnetization $M(\tau)$ to the x-y plane and so the FID signal the height of which is proportional to $M(\tau)$ is detected. Hence T_1 is obtained by measuring FID by changing the time interval τ. The repetition time τ_{Rep} between the neighboring double-pulses must be far longer than T_1 for re-establishing thermal equilibrium of the spin system.

The saturation recovery method is a popular sequence for determining T_1. However, it has two defects:

1) It is difficult to set up exactly the width of the $\pi/2$ pulse, in particular, when the S/N ratio of the FID signal is poor. Provided that the magnetization recovery is exponential, no relaxation information is lost (but S/N ratio) and the semi-log plot is still straight even if the tilt angle θ (pulse width) is slightly misset, but the line will not pass through the zero point as shown in the attached figure.

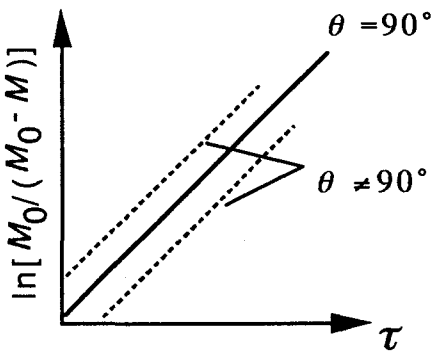

2) As described above, the repetition time τ_{Rep} between the neighboring double-pulses must be far longer than T_1 for restoring thermal equilibrium. Therefore for a sample having long T_1 as well as giving poor signal that needs many times of accumulation, it is time-consuming to use double-pulse method.

When these negative points come in the way of T_1 measurements, a $\pi/2$(comb)-τ-$\pi/2$ pulse sequence[23] described below is an advantageous method.

$\pi/2$(comb)-τ-$\pi/2$ pulse sequence

This method is principally identical to the $\pi/2$-τ-$\pi/2$ pulse sequence. It applies a series of 90° pulses just like a "comb" and brings the magnetization to completely zero (not only in the z' direct but also in the x'-y' plane), and its recovery is sampled after a time τ by using a 90° detection pulse.

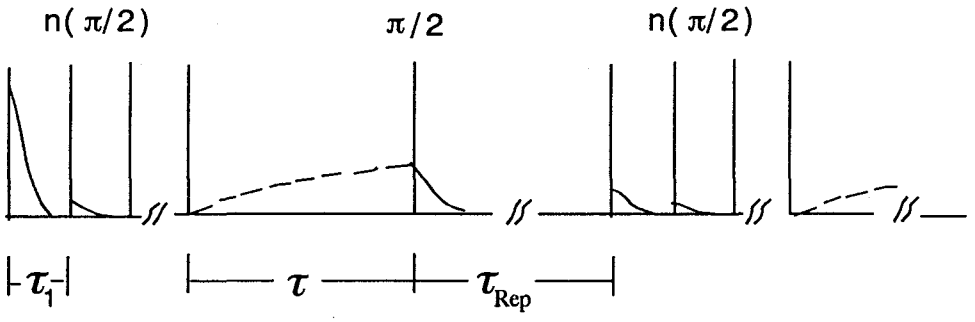

In contrast to the $\pi/2$-τ-$\pi/2$ pulse sequence, the comb sequence has an advantage that missetting of the first 90° pulses does not give any inconvenience in the T_1 measurement because the semi-log plot of the magnetization recovery vs. τ passes always the origin. Furthermore, the repetition time between the neighboring pulse cycles needs not to be long (it can be set to zero in principle) and therefore quick data collection can be realized. So this pulse sequence is suitable for measuring long T_1's of the sample with low S/N ratio.

NMR Spectrometer and Our Operating Condition

NMR measurements were carried out with a JEOL pulsed spectrometer (JNM-FSE-60SS)[26,27] at the Larmor frequencies of 20.4 and 40.4 MHz. Almost all T_1's were determined with the $\pi/2$(comb)-τ-$\pi/2$ pulse sequence (a comb consists of 31 $\pi/2$ pulses usually). It was also confirmed at times that the results obtained by the comb sequence are consistent with those by the $\pi/2$-τ-$\pi/2$ method. In the case of methane adsorbed in mordenite the proton signal is strong and its T_1 becomes as short as of the order of 100 ms at high temperatures, and so the $\pi/2$-τ-$\pi/2$ pulse sequence was used for T_1 measurements.

A $\pi/2$ pulse width was about 8 μs and the dead time of the pre-amplifier was 15 μs.

The magnetization recovery was exponential within the experimental error of ± 5% over a whole temperature range between 4.2 and 400 K in all samples adopted in the present study. As an example, Fig. 3-7 shows the exponential proton magnetization recovery for methane adsorbed in mordenite at the loading of 9.5 ml/g at 20.2 K.

The trace of FID was also recorded at the beginning of each T_1 measurement. The most of FID's were exponential, from which T_2^* was determined. As an example Fig. 3-8 shows the free induction decay for methane adsorbed in mordenite at the loading of 9.5 ml/g at 20.2 K.

The results of the relaxation time measurements will be given and discussed for the respective admolecules in the next Chapter.

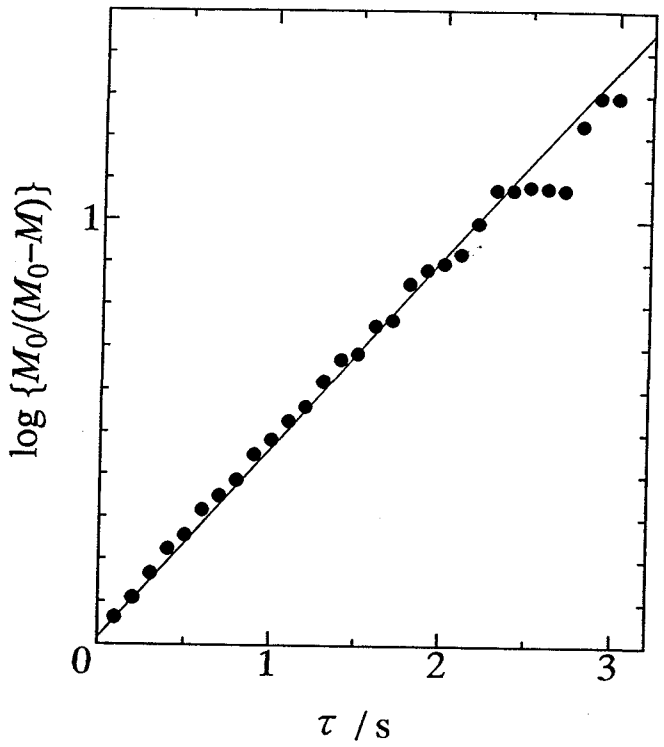

Fig. 3-7 Proton magnetization recovery for methane adsorbed in mordenite at the loading of 9.5 ml/g at 20.2 K.

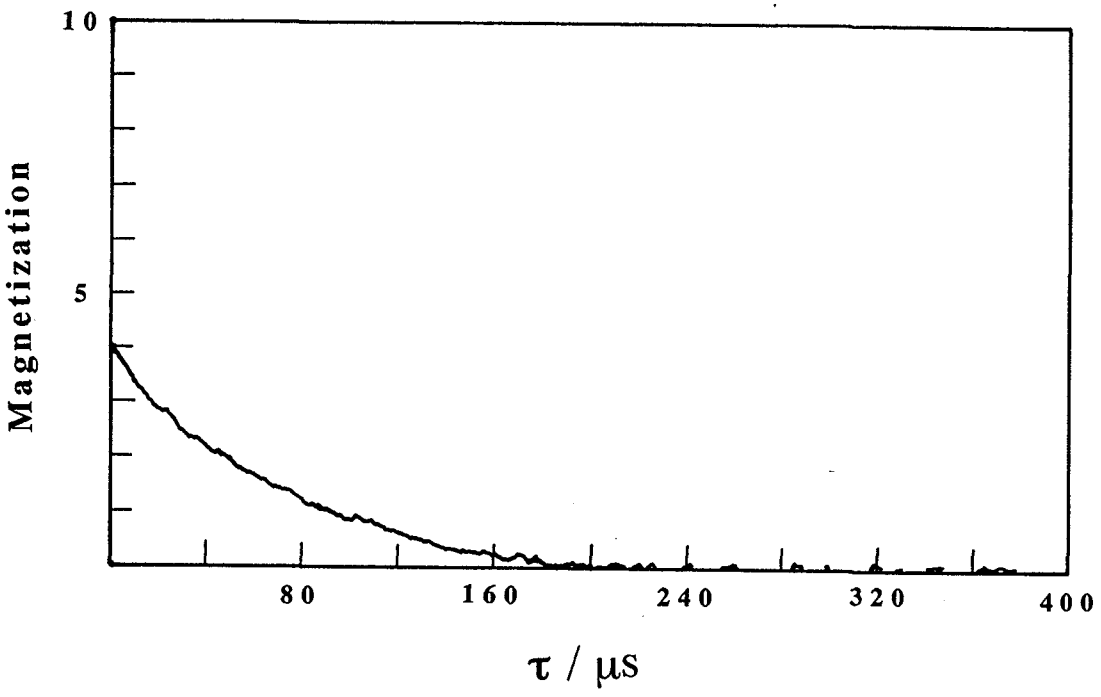

Fig. 3-8 Free induction decay for methane adsorbed in mordenite at the loading of 9.5 ml/g at 20.2 K.

References to Chapter 3

1. R. M. Barrer, *J. Chem. Soc.*, 2158 (1948)
2. D. Domine and J. Quobex, *Molecular Sieves* (ed., Society of the Chemical Industry), 78 (1968)
3. L. B. Sand, *Molecular Sieves* (ed., Society of the Chemical Industry), 71 (1968)
4. O. J. Whittemore, Jr., *Am. Mineral.*, **57**, 1146 (1972)
5. J. C. Janson, in *Stud. Surf. Sci. Catal.*, (ed. H. Van Bekkum, E. M. Flanigen, and J. C. Jansen), **58** , Elsevier, 77 (1991)
6. 上田 智, 村田寛志, 小泉光恵, *粘土化学*, **20**, 47 (1980)
7. 上田 智, 福島利久, 小泉光恵, *粘土化学*, **22**, 18 (1982)
8. S. Ueda, H. Murata, M, Koizumi and H. Nishimura, *Amer. Mineral.*, **65**, 1012 (1980)
9. W. M. Meier, *Z. Kristallogr.*, **115**, 439 (1961)
10. D.W. Breck, *Zeolite Molecular Sieves, Structure, Chemistry and Use*, John Wiley & Sons, Inc., *New York*, (1974)
11. H. Van Bekkum, E. M. Flanigen, and J. C. Jansen, *Stud. Surf. Sci. Catal.*, **58** , Elsevier, (1991)
12. 原 伸宜, 高橋 浩共編, *ゼオライト-- 基礎と応用*, 講談社サイエンティフィク (1975)
13. H. A. Resing , *Advan. Mol. Relaxation Processes*, **3**, 199 (1972)
14. H. A. Resing and J. K. Thompson, *J. Chem. Phys.*, **46**, 2876 (1967)
15. (a) B. Zibrowius, J. Caro and H. Pfeifer, *J. Chem. Soc., Faraday Trans. 1*, **84**, 2347 (1988)
    (b) I. Kustanovich, D. Fraenkel, Z. Luz, S. Vega and N. Zimmermann, *J. Phys. Chem.*, **92**, 4134 (1988)
16. (a) J. Karger and D. M. Ruthven, *Diffusion in Zeolites*, John Wiley & Sons, Inc., *New York*, (1991)
    (b) J. Karger and J. Caro, *J. Chem. Soc., Faraday Trans. 1*, **73**, 1363 (1977)
    (c) J. Karger, H. Pfeifer, M. Rauscher and A. Walter, *J. Chem. Soc., Faraday Trans. 1*, **76**, 717 (1980)
    (d) J. Karger and D. M. Ruthven, *J. Chem. Soc., Faraday Trans. 1*, **77**, 1485 (1980)
17. (a) H. Pfeifer, *Phys. Rep. C*, **26**, 293 (1976)
    (b) J. W. Riehl and K. Koch, *J. Chem. Phys.*, **57**, 2199 (1972)
18. T. Eguchi, Ph. D. Thesis, Faculty of Science, Osaka Univ., (1977)
19. G. E. Pake, *Solid State Physics*, Vol. **2**, ed. by F. Seitz and D. Turnbull, Academic Press, New York, (1956)
20. T. C. Farrar and E. D. Becker, *Pulse and Fourier Transform*, Academic Press, New

York/London, (1971)
21. C. P. Slichter, *Principles of Magnetic Resonance*, Harper and Row, New York, (1963)
22. A. Abragam, *The Principles of Nuclear Magnetism*, Oxford Univ. Press, London/New York, (1961)
23. E. Fukushima and S. B. W. Roeder, *Experimental Pulse NMR*, Addison-Wesley Publishing, Massachusetts, (1981)
24. R. Schumacher, *Magnetic Resonance*, W. A. Benjamin, New York, (1970)
25. B. C. Gerstein and C. R. Dybowski, Transient Techniques in NMR of Solids, Academic Press, New York, (1985)
26. Q. Xu, T. Eguchi, H. Nakayama, N. Nakamura and M. Kishita, *Z. Naturforsch.*, *A*, **46**, 240 (1991)
27. Q. Xu, T. Eguchi, H. Nakayama, *Bull. Chem. Soc. Jpn.*, **65**, 2264 (1992)

Chapter 4

C_nH_{2n+2} (n=1-4) ADSORBED IN MORDENITE

4.1 Introduction

Simple molecular solids have extensively been studied both experimentally and theoretically in order to understand intermolecular forces and molecular degrees of freedom. The most attractive one is crystalline methane partly because it is one of the simplest molecular solid, the molecular symmetry of which is high, and can be the most appropriate object for studying quantum effects in solid state.

Proton spin-lattice relaxation time (T_1) has been a powerful tool to investigate the molecular dynamics in solids, involving solid CH_4. Wit and Bloom[1] measured proton T_1 in bulk CH_4 and its isotopic modifications as well as in CH_4-Kr mixtures as a function of temperature between 4.2 K and 60 K. They examined the nature of low-temperature phase transitions. Analysis of their data revealed that the strong temperature dependence of T_1 is associated with molecular reorientation, but the classical theory of molecular reorientation proved to be inadequate to interpret the experimental value of T_1 obtained.

Yamamoto *et al.*[2] studied theoretically solid methane, especially phase II (the lowest-temperature phase, < 20 K). By extending the James-Keenan model and taking into account the crystal field and the octopole-octopole interaction they elucidated the mechanism of phase transitions, the molecular dynamics of methane, and the quantum effect including the temperature dependence of tunneling levels and structure of the lowest tunneling levels.

However, if the environment which methane molecules experience differs from that in the bulk solid, the behavior of molecular aggregate such as the molecular dynamics, the nature of phase transitions and the quantum effects will be largely modified. Physisorbed methane on surface corresponds to such a situation. In such an adsorption system the intermolecular interaction is greatly modified and, in addition, the molecule-surface interaction will play an important role.

Riehl[3] first measured the spin-lattice and spin-spin relaxation times of proton in a statistical monolayer of methane on graphitized carbon black at fractional coverages from 0.02 to 0.9 over the temperature range of 4.2-100 K. The results suggested that the methane molecules form an adsorbed two-dimensional gas phase at high temperatures and at low coverages, and that the 2-D gas condenses into an adsorbed "solid" at 60-65 K. They found also that adsorbed methane at high coverages also forms the same condensed phase as that at low coverages, in which the molecules behave similarly to that in solid methane; the molecules are reorienting with an activation energy of 0.4 kJ mol^{-1}.

The results obtained by Riehl suggested that the methane-methane interaction is mainly responsible for the structure and properties of the two-dimensional solid on the graphitized carbon black, and therefore the same structure as that in bulk solid methane can be found on the surface to a certain extent.

If the molecules are adsorbed in narrow pores such as in the channels or in the cages of zeolites, the dimensionality in interaction between the guest molecules will be more reduced comparing with that in monolayer as well as in solid methane. In particular, in quasi-1D pores such as the channels in mordenite, the typical porous material, the methane molecules are restricted geometrically to interact with only two nearest neighbors at most, in contrast to six in the $\sqrt{3} \times \sqrt{3}$ structure of the commensurate monolayer of methane on graphite surface or twelve in the fcc structure of the low-temperature phase of bulk solid methane. Therefore, the interactions other than direct methane-methane interactions may be expected to play a very important role in the case of pore-adsorbed methane.

Although the main channel of mordenite may be considered to be quasi- one-dimensional, there exist two different possible sites for methane to stay at low-temperature, one being the large main-channel and the other the side-pocket which can accommodate only small guest as methane molecule.[4-7]

As described in Chapter 1 the intracrystalline channel network in mordenite consists of parallel straight elliptical cylinders girthed by rings of 12 oxygen atoms (0.67 x 0.70 nm^2) and runs in the c direction (Fig. 1-1). Individual main channels are lined with subsidiary cavities (the so-called side-pocket) entered through eight-membered rings.[4] A view parallel to one of the main channels is shown in Fig. 4-1.[5]

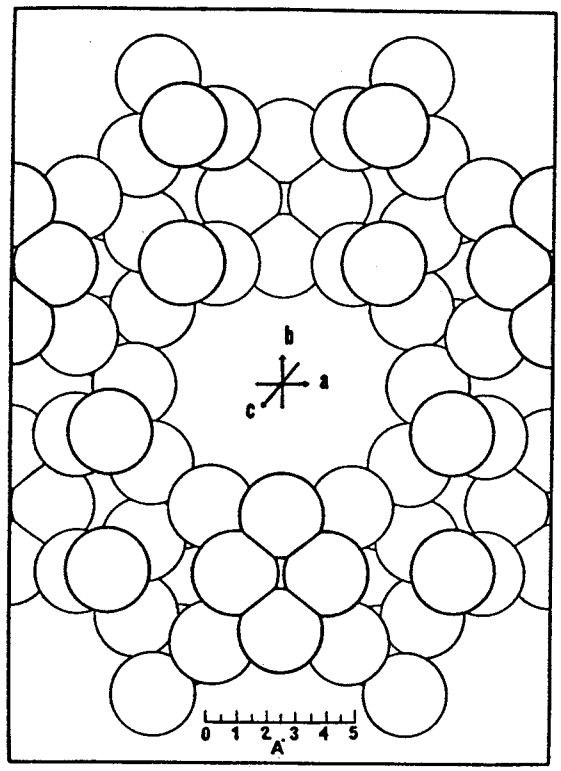

Fig. 4-1 View parallel to the c axis of the oxygen atom network in mordenite. (After G. D. Mayorga *et al.*, 1972)

Takaishi *et al.*[8] studied the motional states of various gases adsorbed in mordenite by measuring the adsorption isotherms and found that argon undergoes translational diffusion

through the channel and vibrates in the perpendicular direction to the channel. In the case of non-monoatomic molecules (O_2, N_2, and CO_2) rotations in addition to translational motion are excited. It was found that the sorbed molecules can be described by a model of one-dimensional (1D) van der Waals gas in terms of entropy, but the collision diameters obtained deviate from the values estimated by the strict one-dimensional model.

Takaishi *et al.* gave useful information on static and dynamic behavior of adsorbed molecules by the macroscopic experimental method. From the observed isotherms they concluded that the surface of the mordenite they used is highly homogeneous. They explained that the above deviation from the one-dimensionality is due to the difference between the size of the molecule and the diameter of channel pores.[8)]

However, they did not take into account of the effects of the side-pockets on the behavior of the guest molecules. Recently Itabashi[9)] revealed that the lattice structure of Na-mordenite is such that Na^+ ions are located at the channel wall and blocks the openning of the side-pockets only when the contents of Na^+ in the unit cell exceeds 5.2. Compositions of mordenite used in Takaishi's adsorption experiments are as follows[8)]: SiO_2: 79.16%; Al_2O_3; 13.45%; Na_2O: 7.39%, the SiO_2/Al_2O_3 ratio of which is 10, corresponding to the formula $Na_8Al_8Si_{40}O_{96}$ for the contents of the unit cell. Because there exist four side-pockets per unit cell, at least one side-pocket is not blocked by the Na^+ ion and open to the guest molecules and so the effect of side-pocket adsorption on the various properties of guest molecules should be taken into account in the analysis of the experimental data.

Since the macroscopic methods such as the adsorption measurements do not seem to be sensitive to the microscopic nature of guest, it is very difficult to examine the effect of pore structure on the molecular static and dynamic behaviors by the macroscopic experiments.

The first direct and detailed experiment for examining the microscopic properties of guest molecules is the ^{129}Xe NMR measurement by Ripmeester.[7)] Because it has been known that the nuclear shielding of ^{129}Xe is extremely sensitive to density of xenon and the nature of environment,[10)] the average as well as anisotropic nuclear shielding can be used to characterize various trapping sites in mordenite and the relative site occupancies of the guest xenon molecules. By observing the ^{129}Xe spectrum of xenon gas in the pore of ion exchanged and chemically modified mordenites Ripmeester examined the distribution of xenon over main-channel and side-pocket sites. He revealed that the side-pocket is open for xenon sorption in Na^+, K^+, and NH_4^+ mordenites except Cs^+ mordenite.

Thus the Xenon NMR is an useful tool for the characterization of the void space in crystals and the results of its analysis can be utilized in other experimental works. The most important result is that Na^+ mordenite can accommodate small molecules like xenon in the main-channel and the side-pocket.

The aim of the present study is to examine the static and dynamic properties of variety of small organic molecules in mordenite and, according to the above result, it is important to

distinguish the occupancy of the main-channel and the side-pocket. In the case of organic guest, however, the chemical shifts of ^{1}H and ^{13}C are not sensitive to the intermolecular interactions and therefore the spectral measurements can hardly distinguish the occupancy differences at various sites. On the other hand, the magnetic relaxation times can sensitively distinguish various kinds of molecular motions and so it can be used as a probe for occupancies of individual sites through the site-effect of motional characteristics.

The observed value of the inverse of T_1 is a sum of the relaxation rates due to molecules on different sites. If there are many different sites, the result will become very complicated and therefore difficult to analyze. In the case of mordenite, however, there are only two distinct sorts of adsorption sites, and therefore the relaxation data can be analyzed to distinguish the molecules at different sites. In favorable case one can determine the relative population of molecules at individual sites.

It seems to be in due course to mention the energetic consideration of the pores in mordenite. Mayorga *et al.* [5] carried out calculations of adsorption potential energies for nonpolar guest molecules in H-mordenite and constructed the adsorption potential energy contour maps. The contour map for methane is shown in Fig. 4-2. It can be found that guest methane molecule possesses relatively high translational freedom and can move through the eight-membered ring into the side-pocket without any activation energy but the main-channel is too narrow for methane to pass by each other.

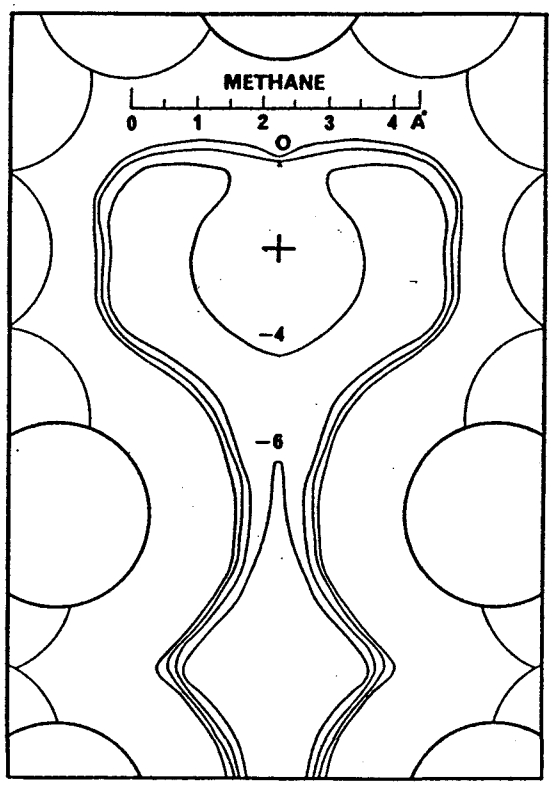

Fig. 4-2 Potential energy contour map of methane in H-mordenite. (After G. D. Mayorga *et al.*, 1972)

Mayorga *et al.* showed also that the ethane can enter the side-pockets in the H-mordenite, but the penetration needs a higher activation energy than 10 kJ mol^{-1}. For propane in H-mordenite, the potential energy in the side-pocket is 14 kJ mol^{-1} higher than that in the main channel and the penetration needs a higher activation energy than the energy for adsorption .

The potential energies in Na-mordenite may differ significantly from those in the H-type one, especially in the side-pockets, due to the presence of the Na^+ ions. There exist two sodium ions halfway between adjoining channel in the b direction, each in the center of a distorted eight-membered ring. [4,5,7,11] On calculating potential energies in H-mordenite Mayorga *et al.* assumed that the hydrogen ions corresponding to these Na^+ ions are buried in the oxygen framework. Even with such assumption, the calculation suggested that ethane and propane are difficult to be adsorbed in the side-pocket of H-mordenite. Therefore, if the volume of the Na^+ ion and the repulsion from the cation at the bottom of the side-pocket (see Fig. 4-17)[11] are taken into consideration in the energy estimation, it is probable that the largest molecule that the side-pocket in Na-mordenite can accommodate is methane.

Although it is predicted that Na-mordenite can not accommodate larger molecules than methane in its side-pocket, no experimental evidence has so far been reported on this point. Present work aims to ascertain this point by measuring magnetic relaxation, on a series of small hydrocarbons adsorbed in Na-mordenite at low temperatures.

The dynamics of molecules adsorbed in zeolites including mordenite has extensively been studied so far using the sealed specimens in glass containers (closed system). In these studies, the main interest has been the translational diffusion of guest molecules because the guest diffusion is believed to play an important role in processes for catalyzing organic reactions.[12] The coverage and temperature dependences of diffusion may in part reflect the interactions between the adsorbates and the adsorbents. However, little is known about the guest dynamics at low-temperatures, although such information must lead to very basic idea for the mechanism of adsorption and for the catalytics of the substrate.

The present work focuses on *the dynamic behavior of adsorbed molecules at low-temperature*. T_1's of methane, ethane, propane and butane adsorbed in mordenite were measured under *in situ* condition over the wide ranges of both loading coverage and temperature. Because the molecules in main-channel and in side-pocket may have different mobilities from each other, they may be distinguished by the T_1 measurements. At low temperatures where the translational diffusion may not be activated yet, the rotational motion of molecules may be the effective motion on the nuclear spin relaxation and might reflect the potential energies generated by the local environment. Therefore, the analysis of the relaxation data may bring about fruitful information on not only the molecular rotational mode and rate of admolecule on each site, but also the energy relation between the adsorption sites (main-channel or side-pocket).

4.2 Procedure for Gas Handling

Each of the gases of methane, ethane, propane and butane was purchased in a cylinder from Takachiho Chemical Industry Co., Ltd. The stated purity is shown in Table 4-1. We first introduced and stored the gas into one of the gas flasks before loading it. For propane and butane the gases are first condensed into distillation ampule and degassed by freeze-pump-thaw cycles, and then distilled into the flasks.

Table 4-1. The stated purity of gases purchased from Takachiho Co. Ltd.

	CH_4	C_2H_6	C_3H_8	n-C_4H_{10}
Purity (%)	99.999	99.9	99.99	99.9
Impurity	O_2 <0.5	CH_4 < 500	Air<20	Air<20
(ppm)	C_2H_6<0.5	C_2H_4<100	CH_4 < 10	CH_4 < 10
	H_2O< 1	C_3H_8<100	C_2H_6<10	C_2H_6<10
		C_4H_{10}<100	C_6H_6<10	C_3H_8<100

The mordenite sample was calcinated prior to the adsorption procedure. The calcination was carried out by increasing the temperature to 673 K in 12 hours or more and by keeping the temperature at 673 K for 24-36 hours in vacuo until the stationary pressure of 10^{-6} Torr was obtained. It was verified that the calcinated pure mordenite sample did not give any ^1H signal.

The specified hydrocarbon gas was introduced (see Fig. 3-4) into the NMR sample container at room temperature under precise control of the amount of guest gas. The pressure of gas was monitored using the BARATRON gauge to 0.1 Torr. After closing the valve **D** in Fig. 3-5, we cooled the NMR probe down to about 100 K with an average cooling speed of about 20 K/hr. The probe was then cooled down to 77 K by filling liquid N_2 or to 4.2 K by transferring liquid He into the inner Dewer vessel. T_1 was measured only in heating run.

For the relaxation measurements in the temperature range of 4.2-77 K the helium gas (1-5 Torr) was introduced into the sample cell at 4.2 K for heat exchange. It was found that helium gas is efficiently adsorbed into mordenite at low temperatures. A rather large amount of helium gas was necessary to realize sufficient heat exchange. Fig. 4-3 traces the proton magnetization methane without heat exchange gas as a function of time after the sample container was cooled down to 4.2 K. It indicates that the magnetization increases with time and it takes more than 6 hours to reach the thermal equilibrium. Amount of helium gas necessary for heat exchange depends on the amounts of methane already adsorbed. And so

excess amount of He was introduced and the final gas pressure was controlled to be 1-5 Torr during T_1 measurements.

The helium gas used was purchased in a cylinder from Takachiho Chemical Industry Co. Ltd, the stated purity being 99.99995% (special degree, impurities: O_2 < 50 ppb, H_2O < 500 ppb). It was introduced into and stored in one of the gas flasks prior to the measurements.

It was confirmed that the T_1 value of proton does not depend on the amount of helium gas.

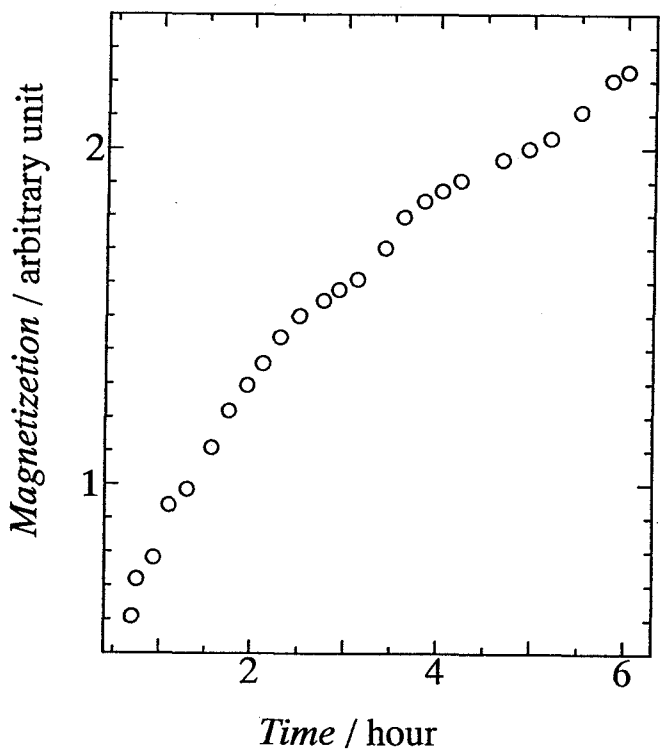

Fig. 4-3 Proton magnetization of methane in mordenite as a function of time after the sample container was cooled down to 4.2 K without heat-exchange He gas in it.

4.3 Results

The proton spin-lattice relaxation time T_1 of methane, ethane, propane and butane adsorbed in mordenite was measured between 4.2 K and room temperature at 40.4 MHz. Magnetization recoveries were exponential through almost all experiments. The results are shown in Figs. 4-4 ~ 4-7 as a function of temperature. The characteristic behavior of proton T_1 of these guest molecules are described in the following sections.

4.3.1 Methane in Mordenite

Measurements of proton T_1 of methane in mordenite were carried out at the loadings of 4.8, 9.5, 38.1, and 76.1 ml (S.T.P)/g. The unit, ml (S.T.P)/g, denotes the volume of gas adsorbed in 1 g mordenite under the standard pressure (S.T.P). Hereafter, we abbreviate the unit "ml (S.T.P)/g" to "ml/g". Because an unit cell contains 2 parallel pipes of channels, the amount, 9.5 ml/g, corresponds to 1 molecule per 2 lengths of channels.

Fig. 4-4 shows the proton T_1 data of methane in mordenite. It is clear that the T_1 behavior is largely different from that in the solid methane.[1] For example, T_1 varies discontinuously at the transition point, 20 K, in the bulk methane, while methane in mordenite does not show any discontinuous change. The behavior of T_1 of methane in mordenite is also apparently different from that of two-dimensional methane adsorbed on the surface of graphite.[3] Two T_1 minima have been observed for surface methane, which were attributed to the reorientation and the translational diffusion. The values of the T_1 minima are shorter than and the coverage dependence of T_1 is also quite different from that of methane in mordenite.

T_1 in Fig. 4-4 shows following several characteristics:

(1) At low loadings, *i.e.*, 4.8 and 9.5 ml/g, two T_1 minima are recognized at 15 K and 50 K.

(2) T_1 decreases with increase of loadings. In particular, T_1 in the vicinity of the lower-temperature minimum depends largely on the loading.

(3) At high loadings, 38.1 and 76.1 ml/g, only a broad and short T_1 minimum appears.

(4) The value of the T_1 minimum ranges between 450 ms and 1.2 s.

(5) On the high-temperature side of the minimum or minima T_1 assumes a maximum and decreases on heating.

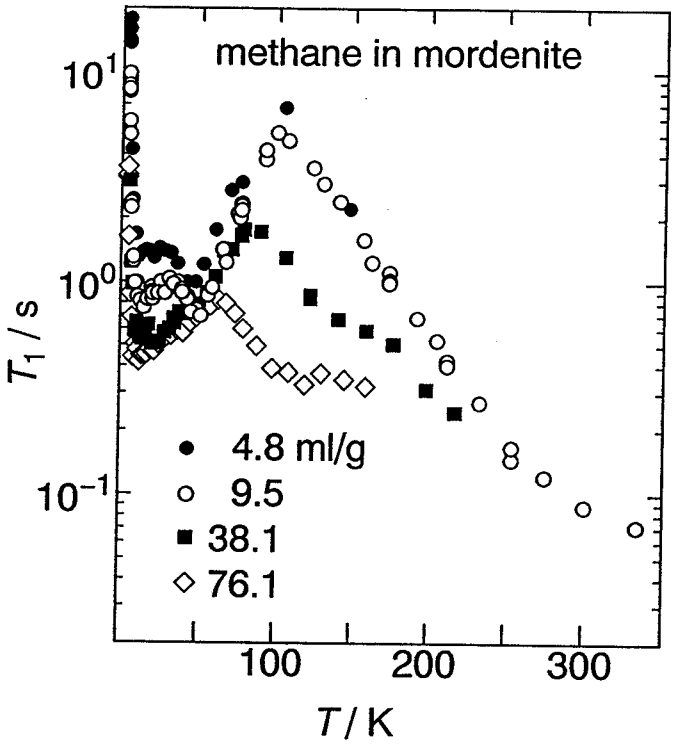

Fig. 4-4 Proton $T1$ of methane in mordenite. (40.4 MHz)

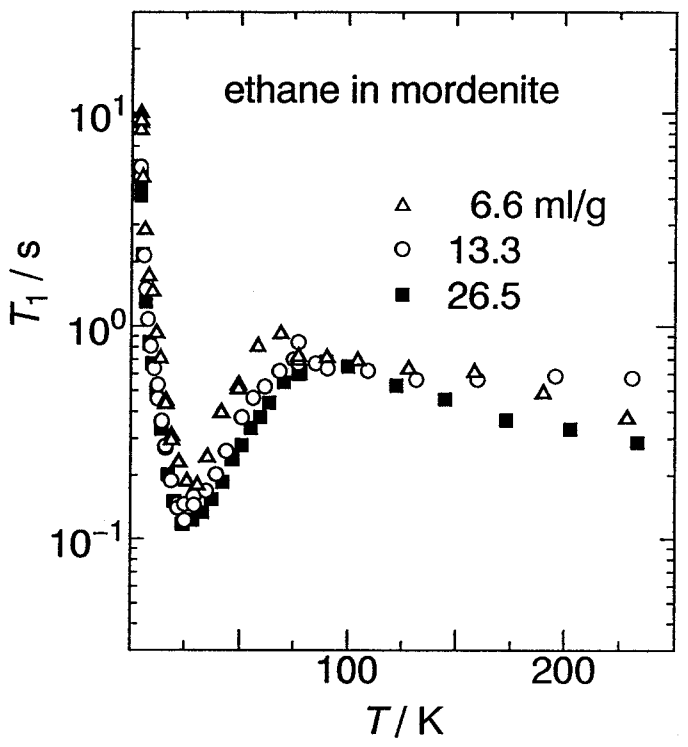

Fig. 4-5 Proton $T1$ of ethane in mordenite. (40.4 MHz)

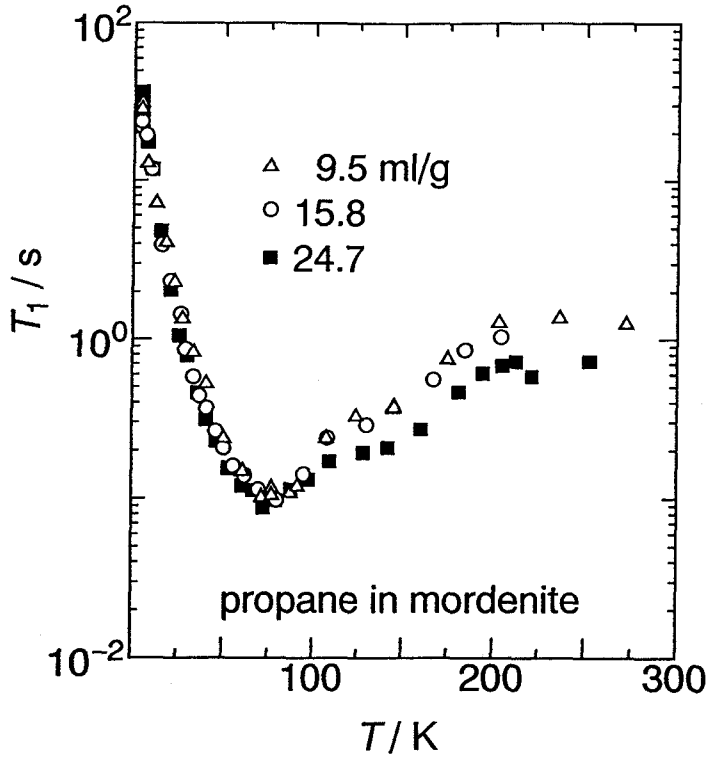

Fig. 4-6 Proton T_1 of propane in mordenite. (40.4 MHz)

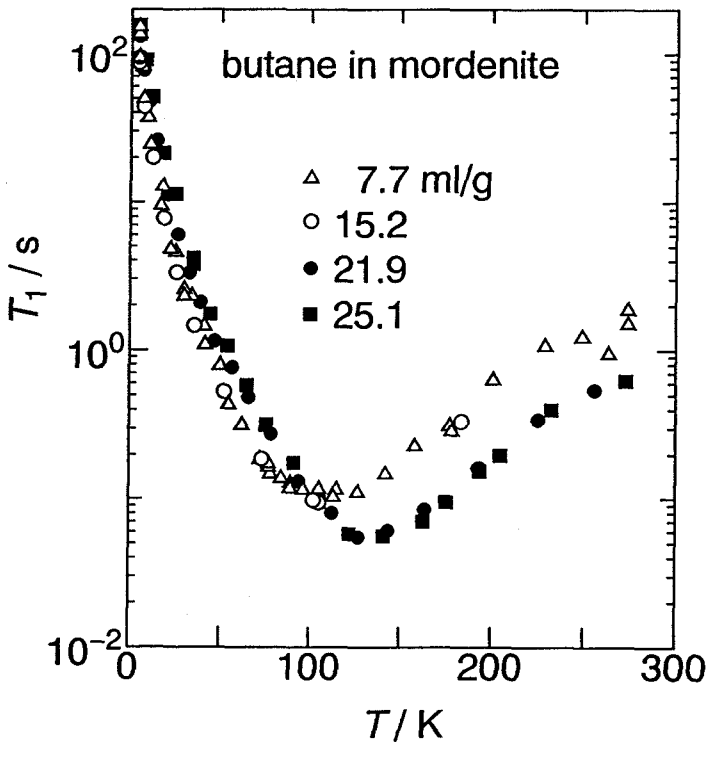

Fig. 4-7 Proton T_1 of butane in mordenite. (40.4 MHz)

4.3.2 Ethane in Mordenite

The results are shown in Fig. 4-5 as a function of temperature. Measurements were carried out at the loadings of 6.6, 13.3, and 26.5 ml/g. The conspicuous experimental facts are:

(1) Only a single T_1 minimum appears at 28 K for each loading.

(2) T_1 decreases with increasing loading.

(3) The value of T_1 minimum ranges between 120 ms and 180 ms.

(4) T_1 decreases again on heating above about 75 K.

4.3.3 Propane in Mordenite

Fig. 4-6 shows the proton T_1 for propane adsorbed in mordenite as a function of temperature. Measurements were carried out at the loadings of 9.5, 15.8 and 24.7 ml/g. Characteristic feature of T_1 is as follows:

(1) Only a single T_1 minimum appears at 75 K for each loading.

(2) T_1 is almost independent of the loadings.

(3) The value of T_1 minimum is about 100 ms.

(4) T_1 increases monotonously on heating above 75 K.

4.3.4 Butane in Mordenite

Fig. 4-7 shows the proton T_1 for butane adsorbed in mordenite as a function of temperature. Measurements were carried out at the loadings of 7.7, 15.2, 21.9 and 25.1 ml/g. Characteristic feature of T_1 is as follows:

(1) Only a single T_1 minimum appears for each loading.

(2) T_1 does not depend on loading between 7.7 and 15.2 ml/g.

(3) At these loadings, T_1 assumes a minimum value of 90 ms at 115 K.

(4) When the loading equals or exceeds 21.9 ml/g, T_1 minimum shifts to 125 K and its value equals or decreases to 70 ms.

(5) At high temperatures T_1 increases with increase in temperature.

4.4 Possible Molecular Motions in the Channel of Mordenite

What kind of motion governs the T_1? What kind of information on the molecular motion and structure adsorbed in the pores can be extracted from the temperature and loading dependence of T_1?

As described in Chapter 2 the relaxation data can be used to determine both the nature and the rate of the process that occurs at a rate comparable to the probing rf frequency.[13,14] This section will be devoted to the analysis of T_1 data to extract valuable information on the guest dynamics in mordenite pores.

In contrast to the other three samples, T_1 in methane shows very distinguishing behavior. As shown in Fig. 4-4 and mentioned in the preceding section T_1 has double minima which are loading dependent. The T_1 behavior must be attributed to at least two different modes of molecular motion. We will now specify possible motions which govern the T_1 in the methane-mordenite system.

In the pores of mordenite following possible motions may occur:

(1) translational diffusion
(2) molecular reorientation
(3) molecular rotation
(4) coupling motion of translation and reorientation
(5) rotational tumbling
(6) molecular exchange between different adsorption sites

The contribution of each motion to the relaxation will be examined theoretically below.

4.4.1 Translational Diffusion in the Main-Channel

In many zeolite-catalyzed reactions the intracrystalline diffusion of guest molecules has been believed to be the rate determining step in the overall kinetics,[12,15] and therefore studies of the translational diffusion in zeolite have built a very active research field so far.[15]

NMR pulsed field-gradient (PFG) technique has widely been used to measure directly the intracrystalline self-diffusion coefficients of guest molecules.[15-17] For example, Karger *et al.* measured the concentration dependence of the self-diffusion coefficients of methane, ethane and propane in the zeolite silicalite.[17] The result is shown in Fig. 4-8, which indicates

that in general the intracrystalline mobility decreases with increasing loading, reflecting the enhancement of mutual interferences.

The molecular mean jump length $\langle l^2 \rangle^{\frac{1}{2}}$ is given by

$$D = \langle l^2 \rangle / 6\tau_d, \tag{4-1}$$

where D is the self-diffusion coefficient and τ_d the mean residence time between two succeeding jumps.[17-19]

The mean residence time τ_d can in principle be determined by the measurement of the longitudinal relaxation time T_1. Because commercial zeolites are usually contaminated by iron impurities of hundreds to thousand ppm, there are two distinct processes which may modulate the local field which the protons in the guest experience:[20-22] true molecular transport with a mean jump time τ_d and flipping of the electronic spins in the paramagnetic impurities with a correlation time τ_e, i.e., the electron spin-lattice relaxation time. As a result the apparent correlation time τ is[20,21]

$$\tau^{-1} = \tau_d^{-1} + \tau_e^{-1}. \tag{4-2}$$

The molecular jump time depends usually much more strongly on temperature than τ_e, and so τ_d may dominate Eq. (4-2) at high temperatures but the opposite holds at lower temperatures. The observed relaxation time T_1 is then

$$T_1^{-1} = T_{1S}^{-1} + T_{1N}^{-1}, \tag{4-3}$$

where T_{1N} is the nuclear dipolar contribution and T_{1S} the contribution of interaction of proton with the electron spin.

Fig. 4-9 shows the spin-lattice relaxation time for methane, ethane and propane adsorbed in silicalite measured by Karger.[17] The T_1 minima occur at 130 -150 K for ethane and 150-360 K for propane. The values of T_1 minima at 60 MHz are of the order of ms. The T_1 minima at such high temperature are caused by the interaction between the diffusing molecules and paramagnetic impurities statistically distributed in the zeolite lattice. In such a case the correlation time τ corresponds to the residence time τ_d. According to Eq. (4-1) it was found that the mean jump distance is about 1 nm, being of the order of the distance between the adjacent channel intersections in silicalite framework.

The above work suggests strongly that the translational diffusion is activated in the high temperature region above 100 K. It is interesting to see that the presence of the paramagnetic impurity is essential for investigating the translation diffusion of molecules trapped in pores which consist of non-protonic materials.

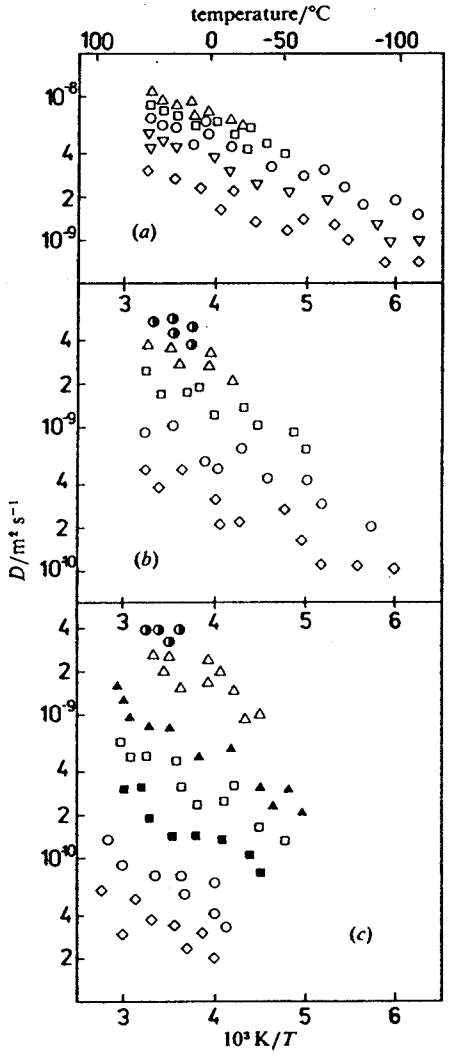

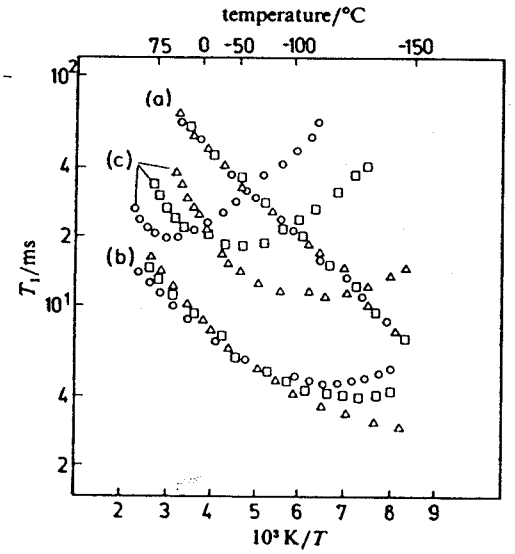

Fig. 4-8 Intracrystalline self-diffusion coefficients of (a) methane, (b) ethane and (c) propane in Silicalite. (left, after J. Caro *et al.*, 1985)

Fig. 4-9 Proton $T1$ of (a) methane, (b) ethane and (c) propane in Silicalite. (right, after J. Caro *et al.*, 1985)

The mordenite sample used in the present experiments does not contain any iron impurity (see Table 3-1). Therefore only the contribution of the proton-proton dipolar interaction to the spin-lattice relaxation should be taken into consideration.

A variety of diffusion models have been presented for the analysis of the spin-lattice relaxation caused by the fluctuation of the intermolecular dipole-dipole interactions.[23-25] For simplicity, however, we adopt a model that the intermolecular separation varies as a consequence of jumps, and each jump distance is comparable to or greater than the molecular diameter d and consider methane only, the simplest one, as an example. Suppose that the major contribution to the intermolecular dipole-dipole relaxation comes from the nearest neighbors, located at a distance d from the jumping molecule. Then, the spin-lattice relaxation time can be approximated by[3,14]

$$T_1^{-1} = 4Nc(3/10)\gamma^4(h/2\pi)^2 d^{-6} B(\tau_c). \qquad (4\text{-}4)$$

This equation holds under the weak collision limit, i.e., when $\tau_c << 1/\delta\omega = T_2$, where τ_c is the correlation time of the diffusion. N denotes the number of the nearest neighbors, c the concentration of molecules which, or the nearest neighbor of which, jumps away. The factor 4 takes into account the four proton spins per methane molecule. The function $B(\tau_c)$ is

$$B(\tau_c) = [\tau_c/(1+\omega_0^2\tau_c^2)] + [4\tau_c/(1+4\omega_0^2\tau_c^2)], \qquad (4\text{-}5)$$

where ω_0 is the Larmor frequency. When $\omega_0\tau_c = 0.6125$, T_1 assumes the minimum value

$$T_1(\min) = 0.7017\omega_0/(4Nc(3/10)\gamma^4(h/2\pi)^2 d^{-6}). \qquad (4\text{-}6)$$

In the case of 3-D closest packing (fcc) crystal such as in solid methane there exist 12 nearest neighbors. The number of molecules which interact with the jumping molecule will be $N = 11$ when one of the nearest neighbour sites is vacant. In the case of 2-D closest packing such as in the case of methane adsorbed on graphite $N = 5$. However, in the quasi-1-D channel of mordenite the jumping molecule has only one nearest molecule because one of two nearest sites should be vacant for molecule of interest to undergo a classical jump (see Fig. 4-10).

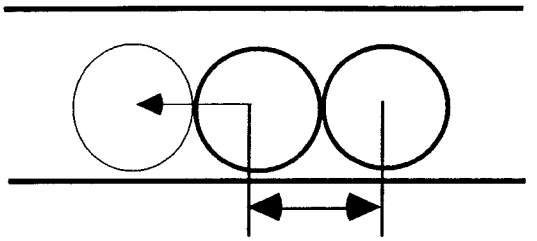

Fig. 4-10 Only one molecule can interact directly with the jumping molecule at a distance of d in the 1-D main channel of mordenite.

To estimate the contribution from the molecular diffusion to the T_1 we assume that the distance d is equal to the Lennard-Jones distance between methane molecules, 4.3 Å.[3,26] Assuming that c = 1 which means that each CH_4 has only one nearest neighbor, Eq. (4-6) leads to T_1(min) = 0.62 s at 10 MHz and T_1(min) = 2.5 s at 40 MHz.

As shown in Fig. 4-4, the experimental values of the T_1 minima for methane in mordenite at 40.4 MHz are 450 ms - 1.2 s. The value predicted with the above simple jump model is longer than the observed one. Since the model corresponds to the ideal case which gives the lowest value of T_1 and such an ideal situation cannot be expected in the actual adsorption system, the diffusion mechanism for the spin-lattice relaxation can hardly be expected to interpret the experimental relaxation data, especially the data at low temperatures. Hence we can state that the translational diffusion of methane in the main channel is certainly ruled out from the assignment of the relaxation behavior observed.

According to the above simple model, the theoretical values of T_1 minima due to the dipole-dipole interaction modulated by translational diffusion will be longer for ethane, propane and butane than that for methane because of their bulky sizes. In contrast, the experimental values of the T_1 minima observed become shorter in the order of molecular weight, as shown in Figs. 4-5 ~ 4-7. Therefore, the discrepancy between the experimental and the theoretical values of T_1 becomes larger as the molecular weight increases, and so the assumption that the molecular translational diffusion is responsible for the relaxation at low temperatures should also be ruled out for ethane, propane and butane in mordenite at least at low temperatures where the T_1 assumes the minimum or minima.

As we mentioned above some amount of paramagnetic impurities help to examine the molecular diffusion in narrow pores by NMR relaxation experiments. However, such impurities lower the relaxation time T_1 to great extent and as a result mask the effect of other motion on the T_1. In order to detect such motional effect samples should be free from

paramagnetic impurities. The present work settled this point by synthesizing impurity-free material and hence succeeded to collect much reliable relaxation data which indicate clearly the evidence of other molecular motion than diffusion, especially at low temperatures. The next section will concern further analysis of relaxation data and will prove that this new motion is the molecular rotation or reorientation in the pores of mordenite crystal.

4.4.2 Molecular Reorientation

As a possibility that the diffusion governs the T_1 was eliminated in the preceding section, it is in due course to examine the effect of molecular reorientation on the relaxation at low temperatures.

The detailed treatment of the spin-lattice relaxation due to the reorientation of methane in mordenite is given in **Appendix I.** It is noted that the theoretical calculation based on the classical molecular reorientation of methane predicts the T_1 minimum of 11 ms at 40 MHz but the values of T_1 minima observed for methane in mordenite are as long as 0.45 -1.2 s (Fig. 4-4). This fact suggests strongly that it is necessary to consider the quantum effect to interpret the experimental relaxation data. Haupt's theory[27] on spin isomerization and tunneling rotation predicts longer T_1 minimum for system with rotational tunneling than that in classical rotor. It is thus probable that methane molecules are undergoing rotational tunneling in pores of mordenite.

Classical reorientation of the methyl group of ethane contributes to the dipolar T_1 minimum by 21.2 ms. Although this value predicts the upper limit of T_1 minimum for reorientation of ethane molecules, it is still far shorter than the experimental value. In addition to this fact, as can be seen in Fig 4-11, the experimental log T_1 vs. $1/T$ plots is asymmetric with respect to the T_1 minimum, on the low-temperature side of which the slopes are very gentle, giving an activation energy as small as 0.12 kJ mol^{-1}. Therefore, it is also necessary to take into consideration the tunneling rotation to interpret the long experimental T_1 minimum values of 120 - 180 ms for ethane in mordenite.

Propane and butane may have various motional degrees of freedom, i.e., the axial rotation of whole-molecule about its long axis, rotations of the CH_3- groups about the C-C axes and the molecular tumbling. The theoretical T_1 minimum value caused by composite rotational modes was calculated for butane in **Appendix II.** Experimentally, propane and butane in mordenite exhibit T_1 minima of about 100 ms. The observed T_1 behavior for propane and butane in mordenite may therefore be attributed to the reorientation about the long axes of these molecules.

4.4.3 Molecular Rotation

Provided that we are only concerning the spin-lattice relaxation the molecular rotation and reorientation cannot be distinguished. Hereafter the terms "rotation" and "reorientation" are assumed to have the same meaning.

4.4.4 Coupling Motion of Translation and Reorientation

Since the molecules of interest are confined in a narrow pore in the present case and each moving molecule cannot pass other molecules, the intermolecular dipolar interaction is week enough, and the translational-rotational coupling can, if any, be regarded as simple rotation in the analysis of T_1 data.

4.4.5 Rotational Tumbling

When the potential energy barrier for a specified motion of "light" atoms as hydrogen is very low, quantum mechanical tunneling takes place and this coherent motion affects significantly the proton spin-lattice relaxation via dipole-dipole interaction. In the present work this effect should be considered only when the internal rotation of methyl groups is discussed. This point will be examined in the next section.

4.4.6 Molecular Exchange between Different Adsorption Sites

Possibility that the guest molecules at various adsorption sites undergo mutual exchange and this exchange contributes to the proton spin-lattice relaxation will be examined in Section 4.6.1.

Returning to methane in mordenite, the following problems must be solved:

(1) What causes the two T_1 minima at low loadings?

(2) Why does T_1 decrease with increasing loading? Why does the value of T_1 minimum at 15 K show strong dependence than that at 50 K on the loading? And finally why does only one broad T_1 minimum appear at high loadings, 38.1 and 76.1 ml/g?

In addition to the above problems, there arise other interesting questions for all systems in the present study as follows:

(3) How homogeneously are the molecules dispersed? Is there a possibility of formation of domains (clusters) in the pore?

(4) Can any specific adsorption sites be characterized in the channel?

As described in section 4.1, methane can enter not only the main-channel but also the side-pocket. In contrast, ethane, propane and butane can hardly gain access to the side-pocket. The difference of T_1 behavior between methane and the other three kinds of molecules is closely related to the possibility for guest molecule to gain access to the side-pocket. Therfore, the two experimental T_1 minima in Fig. 4-4 are attributable to the reorientation of methane molecules in the main-channel and the side-pocket.

It is, however, profitable to give more detailed discussion on ethane, propane and butane, before going to the more quantitative treatment of methane. Inaccessibility to the side-pocket and less quantum effects of the large molecules will cause the discussion simpler and clearer.

4.5 Discussion on Ethane, Propane and Butane in Mordenite

We give quantitative analyses of the spin-lattice relaxation data for ethane, propane and butane, which can be considered to reorient in the main-channel of mordenite.

4.5.1 Ethane in Mordenite

As shown in Fig. 4-5, the proton spin-lattice relaxation time T_1 of ethane in mordenite gives only a single minimum at about 28 K for each loading. T_1 decreases slightly with increasing loading. As briefly described in section 4.4, such a T_1 minimum is attributable to the reorientation and, in part, rotational tunneling about the C-C axis. For more detailed discussion the T_1 data were plotted against the reciprocal temperature in Fig. 4-11.

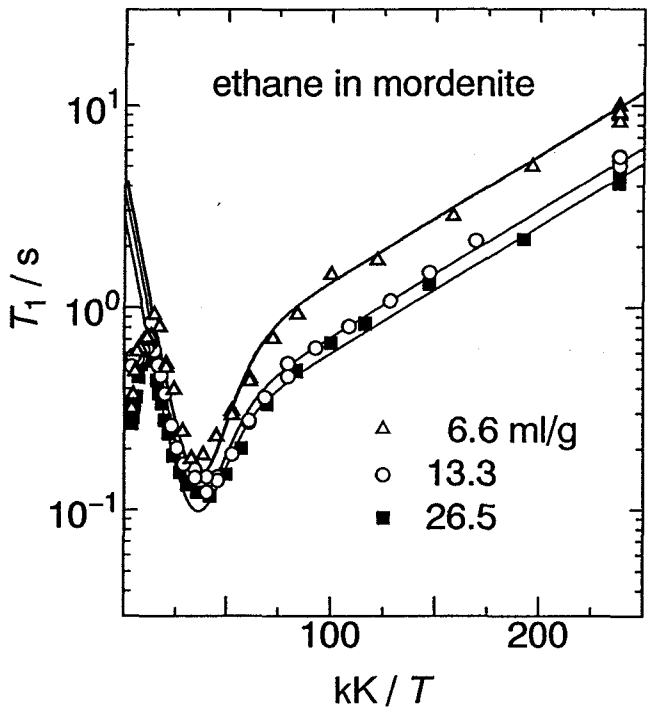

Fig. 4-11 The logT_1 vs $1/T$ plots for ethane adsorbed in mordenite. (40.4 MHz)

Although the T_1 minimum at each loading can be considered to originate from the reorientation about the C-C axis, the well-known BPP[20] theory for methyl groups which undergo the thermally activated classical reorientation of ethane yields a T_1 minimum of 21.2 ms at 40 MHz[28] and therefore it cannot interpret the absolute values of the experimental T_1 minimum (120 - 180 ms). The experimental value of the minimum is about 6-9 times longer than the theoretical value. The BPP theory predicts that the plot of logT_1 against $1/T$ gives V shape graph and the slopes on the both sides of the T_1 minimum are equal to each other in the case that the relaxation is governed by a single activation process. However, the experimental

logT_1 vs. $1/T$ plots (Fig. 4-11) are not symmetric, suggesting that the relaxation cannot be interpreted by a single activation process. It is also noted that the slope of the logT_1 vs. $1/T$ plots gives very small value, 0.12 kJ mol^{-1}, on the low-temperature side of the T_1 minimum. These discrepancies between the experimental and the theoretical T_1's can be ascribed to the influence of the tunneling rotation of the CH_3 groups on the dipolar relaxation in the lowest temperature region.[27,29-34] In the case of ethane the presence of two CH_3 groups in each ethane molecule makes the situation complex in dealing with the rotational tunneling phenomenon, but the effects of tunneling rotation can qualitatively be comprehended in a similar way to the case of methane (**Appendix I**) if one pays no attention to the details of the tunneling system.

In the presence of the tunneling rotation with a far larger frequency than the Larmor frequency, i.e., $\omega_t >> \omega_0$, the spin-lattice relaxation time T_1 can be approximated by

$$\frac{1}{T_1} \sim C\left(\frac{\tau_c}{1+\omega_0^2\tau_c^2} + \frac{4\tau_c}{1+4\omega_0^2\tau_c^2}\right). \tag{4-7}$$

In the low temperature limit τ_c corresponds to the lifetime of the tunneling level,[27,29-34] which is approximated by

$$\tau_c = \tau'_0 \exp(E_{01}/RT), \tag{4-8}$$

where E_{01} is the energy difference between the two lowest torsional states (see Eq. (A.I-16)). At the intermediate temperatures the contribution from the higher torsional states becomes progressively important, and the stochastic activation over the barrier becomes dominant at high temperatures. In the first approximation we take account of both tunneling in Eq. (4-8) and the activated process to represent the effective correlation time over the whole temperature region[32,34] as

$$\tau_c^{-1} = \tau'^{-1}_0 \exp(-E_{01}/RT) + \tau_0^{-1}\exp(-E_a/RT). \tag{4-9}$$

We analyzed the T_1 at each loading using Eqs. (4-7, 9), and obtained the solid curves in Fig. 4-11. It is clear that the calculated curves agree well with the experimental data. The parameters used for the fitting are listed in Table 4-2.

Table 4-2 indicates that the T_1 data can be reproduced by a single activation energy for reorientation. Its value, 1.0 kJ mol^{-1}, is much smaller than the value of 6.6 kJ mol^{-1} in solid ethane,[28] and the temperature of T_1 minimum, 28 K, is also much lower than the value of about 60 K in solid ethane. These facts imply that ethane molecules interact only weakly with each other and the ethane-channel interaction is also weak in the main-channel of mordenite.

Table 4-2 Parameters for ethane adsorbed in mordenite.

Loading / ml g^{-1}	6.6	13.3	26.5
E_a / kJ mol^{-1}	1.0	1.0	1.0
τ_0 / 10^{-11} s	3.5	3.5	4.0
E_{01}/ kJ mol^{-1}	0.12	0.12	0.12
τ'_0 / 10^{-8} s	1.2	0.8	0.8
C / 10^9 s^{-2}	1.2	1.5	1.8

The rotational tunneling effect at the three different loadings can be evaluated using a single value of E_{01}, the energy difference between the two lowest torsional states. The small value of E_{01}, 0.12 kJ mol^{-1}, is consistent with the presence of the small barrier for reorientation (E_a).[27,29]

The coupling constant C increases with increasing loading, suggesting that the intermolecular dipole-dipole interaction increases due obviously to the decrease of the intermolecular distance with increasing loading.

4.5.2 Propane in Mordenite

As shown in Fig. 4-6, only a single T_1 minimum appears at about 75 K for propane in mordenite. In comparison with that of ethane in mordenite, the temperature of T_1 minimum shifts to a higher temperature. T_1 below about 100 K is almost independent of loading in contrast to the case of ethane. The T_1 minimum has a value of about 100 ms. As described in section 4.4, it is attributable to the classical reorientation of a whole-molecule about its long axis. For more quantitative analysis, we plot the T_1 data against a reciprocal temperature in Fig. 4-12.

The slope of the plot of $\log T_1$ against $1/T$ on the high-temperature side of the T_1 minimum is higher than that for ethane in mordenite, indicating that propane, the molecule with a larger size than ethane, is more strongly hindered to reorient in the main-channel of mordenite.

The slopes of the $\log T_1$ vs. $1/T$ are asymmetric with respect to the T_1 minimum and the slope is gentle on the low-temperature side. This fact implies that the internal rotation of the CH_3 groups about the C-C axis is excited and governs predominantly the relaxation in low temperature region.

However, the thermally activated reorientation of CH_3 groups should theoretically give the T_1 minimum of about 20 ms at 40 MHz. On the other hand the experimental value is

near 500 ms. It is therefore necessary to take account of the effects of rotational tunneling of CH_3 group.

In the lower temperature region (< 10 K) T_1 depends only weakly on temperature, implying another unknown relaxation mechanism. There may be a possibility, that a trace of paramagnetic impurities (less than 20 ppm) influences such long relaxation time at very low temperatures.

Now we try to fit the experimental T_1 data by taking account of the three relaxation mechanism described above, providing that these mechanisms are independent of each other. We calculate the contribution of the reorientation about the long axis of a whole-molecule using BPP equation. Eq. (4-7) and Eq. (4-9) are applied to the T_1 calculation due to the internal rotation and the rotational tunneling of CH_3 groups as in the case of ethane.

The results are shown in Fig. 4-12 by the solid curves. The broken line represents the contribution of the molecular overall reorientation about the long axis of the molecule. The dotted line corresponds to the contribution of both the rotation and the rotational tunneling of CH_3 group. The broken-dotted line means the probable influence of a very small quantity of paramagnetic impurities. The calculated curves agree well with the experimental data. The parameters used for fitting are listed in Table 4-3.

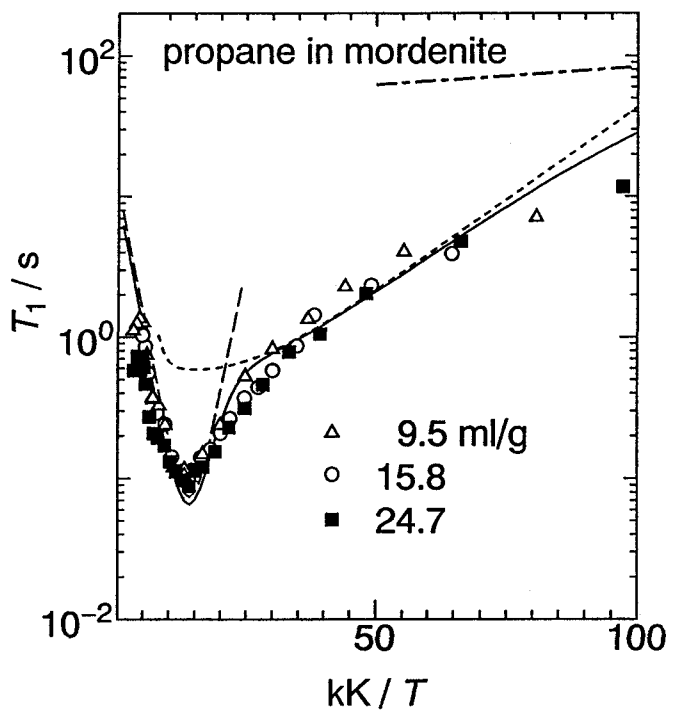

Fig. 4-12 The logT_1 vs $1/T$ plots for propane adsorbed in mordenite. (40.4 MHz)

Table 4-3 Parameters for propane adsorbed in mordenite.

Mode	I[a)]	II[b)]
E_a / kJ mol^{-1}	3.5	6.0
τ_0 / 10^{-11} s	0.7	0.4
E_{01}/ kJ mol^{-1}	-	0.5
τ_0 / 10^{-8} s	-	0.1
C / 10^9 s^{-2}	2.4	0.3

a) Mode I represents the molecular reorientation about the long axis.
b) Mode II represents the contribution of both internal rotation and rotational tunneling of CH_3 groups.

The activation energy E_a of 3.5 kJ mol^{-1} for the molecular reorientation about its long axis are much larger than the value of 1.0 kJ mol^{-1} for the reorientation of ethane about the C-C axis. E_a of 6.0 kJ mol^{-1} for the CH_3 group rotation is comparable with average E_a for methyl rotation [35] and is close to the value of 7.5 kJ mol^{-1}, the intramolecular barrier obtained for $CH_3NH_3^+$.[36]

In order to verify the assignment of the motional modes, we measured also the frequency-dependence of T_1 at the loading of 15.8 ml/g. Fig. 4-13 shows the results at 40.4 and 20.4 MHz. We fitted the experimental data with the same parameters in Table 4-3, and obtained the solid curve at 40.4 MHz, and broken-dotted line at 20.4 MHz. Each of the calculated curve agrees with the experimental data at each frequency, supporting the results of the above analyses.

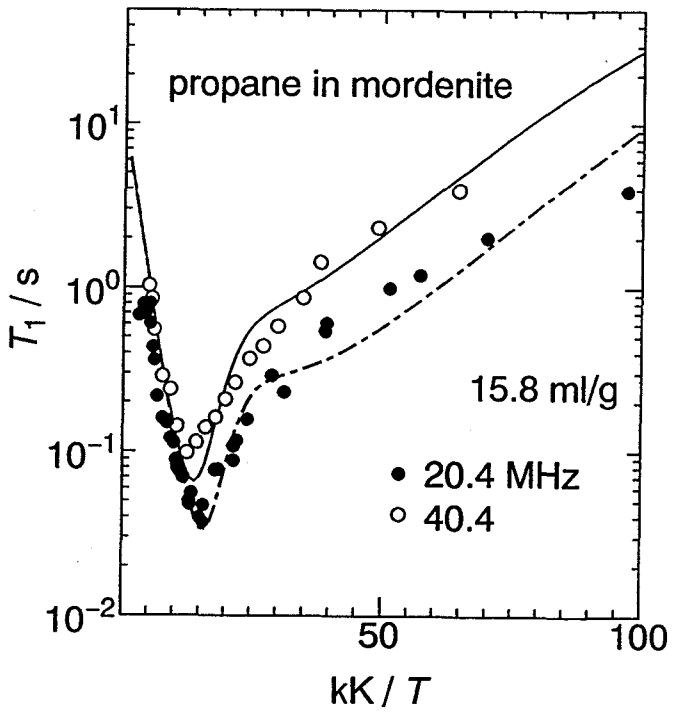

Fig. 4-13 Frequency dependence of T_1 for propane adsorbed in mordenite at the loading of 15.8 ml/g.

4.5.3 Butane in Mordenite

The T_1 behavior of butane in mordenite is similar to that of propane in mordenite except for the loading dependence. As shown in Figs. 4-7 and 4-14, only a single T_1 minimum appears at each loading. The T_1 minimum in butane appears at higher temperature than in propane. At loadings of 7.7 and 15.2 ml/g T_1 minima are 90 ms and locate at 115 K. However, when the loading equals to and exceeds 21.9 ml/g, T_1 minimum shifts to 125 K and its value lowers to 70 ms. In low-temperature region, T_1 at loadings of 21.9 and 25.1 ml/g is longer than at loadings of 7.7 and 15.2 ml/g.

As described in section 4.4 the T_1 minimum is attributable to the reorientation about the long axis of the molecule. For more quantitative analysis we plot the T_1 data against a reciprocal temperature in Fig. 4-14.

Similarly to the case of propane, the slopes of the logT_1 vs. $1/T$ plots are asymmetric with respect to the T_1 minimum, on the low-temperature side of which the slope seems gentle, which can also be considered to be due to both the internal rotation and rotational tunneling of the CH_3 groups.

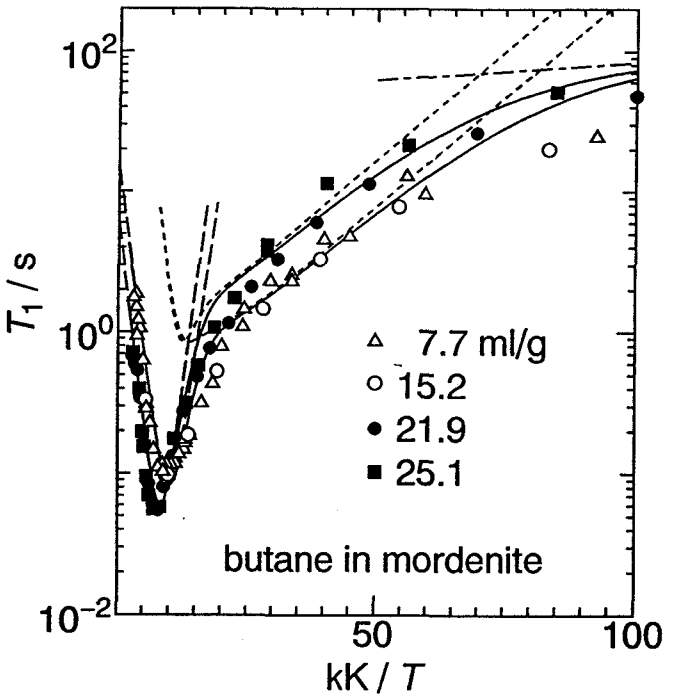

Fig. 4-14 The logT_1 vs $1/T$ plots for butane adsorbed in mordenite. (40.4 MHz)

In the lower temperature region (< 10 K), the T_1 tends to become independent of temperature as in the case of propane.

We analyzed the T_1 of butane by the same method as in the case of propane and fitted the theoretical model to the experimental data at loadings of 7.7 and 15.2 ml/g and of 21.9 and 25.1 ml/g. The results are shown in Fig. 4-14 by the solid curves. The broken line represents the contribution of the overall reorientation about the long axis of the molecule. The dotted line corresponds to the contribution of both the classical reorientation and the rotational tunneling of CH_3 groups about the C-C axis. The broken-dotted line means possible

influence of a very small quantity of paramagnetic impurities. The calculated curves agree well with the experimental data. The parameters used for fitting are listed in Table 4-4.

Table 4-4 Parameters for butane adsorbed in mordenite.

Loading / ml g^{-1}	7.7 , 15.2		21.9 , 25.1	
Mode	I[a)]	II[b)]	I[a)]	II[b)]
E_a / kJ mol^{-1}	5.0	6.0	5.5	6.0
τ_0 / 10^{-11} s	0.6	0.04	1.0	0.04
E_{01}/ kJ mol^{-1}	-	0.6	-	0.6
τ_0 / 10^{-8} s	-	0.14	-	0.3
C / 10^9 s^{-2}	2.1	0.21	3.0	0.21

a) Mode I represents the molecular reorientation about the long axis.
b) Mode II represents the contribution of both internal rotation and rotational tunneling of CH_3 groups.

When the loading increases from 7.7 and 15.2 ml/g to 21.9 and 25.1 ml/g, the activation energy for the overall reorientation about the molecular long axis increases from 5.0 to 5.5 kJ mol^{-1}.

Mordenite possesses two parallel pipes of channels running along the c direction in each unit cell[4,37-39] (see Fig. 1-1). Because the length of butane is nearly equal to the unit cell parameter c, a simple calculation indicates that the loading of 15 ml/g corresponds to two molecules per unit cell. The whole pore space in mordenite is principally filled by butane molecules just at this loading. Hence the butane molecules can align with their long axes parallel to the pore axis until the loading reaches 15 ml/g, but when the loading exceeds the amount they have to rearrange themselves to attain closer packing. As a result intermolecular interaction becomes stronger and increases the barrier for molecular reorientation. The intermolecular distance also become shorter, working to lower the T_1(min) value.

The activation energy E_a of 5.0-5.5 kJ mol^{-1} for the reorientation about the long molecular axis is much larger than the value of 3.5 kJ mol^{-1} for propane, indicating that the longer the size of hydrocarbon the larger the potential barrier for molecular reorientation in the main-channel of mordenite. The activation energy E_a for internal rotation of CH_3 groups, 6.0 kJ mol^{-1} coincides with that for propane, suggesting that the potential barrier for the methyl rotation is originated from purely intramolecular interaction.

The frequency dependence of T_1 at the loading of 21.9 ml/g was also determined. Fig. 4-15 shows the results at 40.4 and 20.4 MHz. We fitted the experimental data with the same parameters in Table 4-4, and obtained the solid curve at 40.4 MHz, and broken-dotted line at 20.4 MHz. The calculated curves agree well with the experimental data, supporting our assignment and analysis of the relaxation mechanisms.

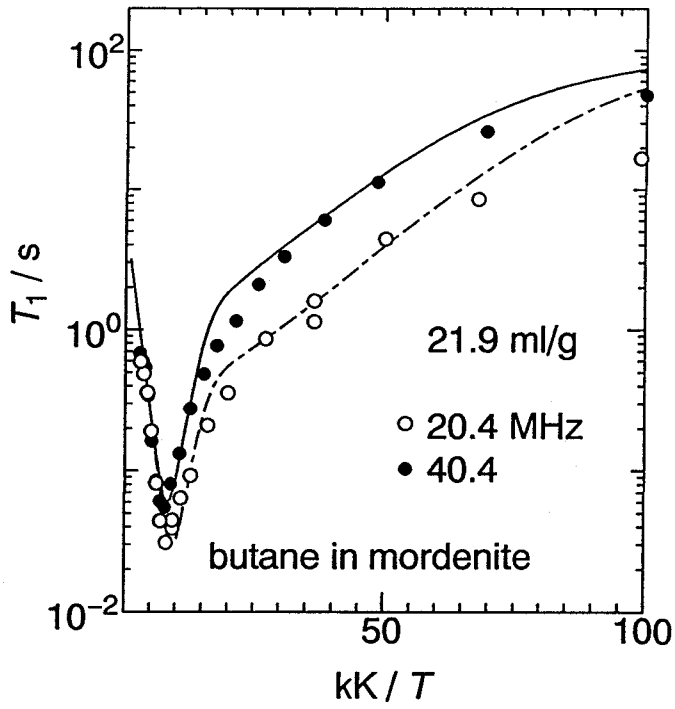

Fig. 4-15 Frequency dependence of T_1 for butane adsorbed in mordenite at the loading of 21.9 ml/g.

The results for ethane, propane and butane adsorbed in mordenite can briefly be summarized as follows:

(1) The activation energies for molecular overall reorientation of ethane, propane, and butane in the main-channel of mordenite are 1.0, 3.5, and 5.0-5.5 kJ mol^{-1}, respectively.

(2) The temperatures of T_1 minima for ethane, propane and butane are 28, 75, and 115-125 K, respectively, each of which is mainly determined by the overall reorientation of individual molecule about its long axis.

The orderly behavior of the guest molecules can be considered as a kind of corresponding state. It is obvious that all the three kinds of molecules are located and reorienting about their molecular long axes in the main-channel of mordenite. This conclusion will be useful for analyzing the behavior of methane in mordenite as described in the next section.

4.6 Discussion of Methane in Mordenite

4.6.1 Introduction

As described in the previous section, ethane, propane and butane exhibit orderly behavior in the pore of mordenite. Each of the T_1 in these systems assumes a single minimum the temperature of which is mainly determined by the molecular axial reorientation. In the case of methane in mordenite, two T_1 minima appear at low loadings at 15 K and 50 K. T_1 decreases with increasing loading, especially, in the vicinity of the minimum at 15 K. At high loadings, i.e., 38.1 or 76.1 ml/g, only one broad but a significantly short T_1 minimum appears.

What causes the different T_1 behavior of methane from that of the other three kinds of molecules? What are the two T_1 minima attributed to? What does the loading dependence of T_1 mean?

As described in §4.4.1, the translational diffusion in the main-channel of mordenite should yield so long T_1 minimum that it can be ruled out in the assignment of the observed relaxation data. Because the side-pocket as well as the main-channel is available for methane molecule, it is quite natural to assign the two T_1 minima to the reorientation in both the main-channel and the side-pocket of mordenite pores.

Another molecular motion which may contribute to the proton relaxation is the exchange of molecules between the sites in main-channel and side-pocket. This motion contributes to T_1 only when the exchange causes the large fluctuation of dipole-interaction between protons and such a situation occurs only when the exchange is accompanied by rotation of methane. However, the rate of molecular rotation is usually much higher than site exchange rate and so the site exchange does not practically contribute to the spin-lattice relaxation.

4.6.2 Methane in Side-Pocket and Main-Channel

It has been difficult to obtain certain evidence for the adsorption in the side-pocket by any direct experiment. To our knowledge few experimental studies have been reported on this point so far, except the xenon NMR measurements by Ripmeester.[7)]

Some theoretical calculations have been carried out concerning this problem. Smit *et al.* performed *Monte Carlo* computer simulations on the behavior of a single methane molecule in mordenite.[11)] Their simulations predicted that the heat of adsorption of methane in Na-mordenite should increase steeply with decreasing Al/Si ratio below 0.15 (Fig. 4-16). They analyzed the distribution of CH_4 in Na-mordenite and gave a simple interpretation to this peculiar effect, which is related to the presence of the side-pocket. The calculations were

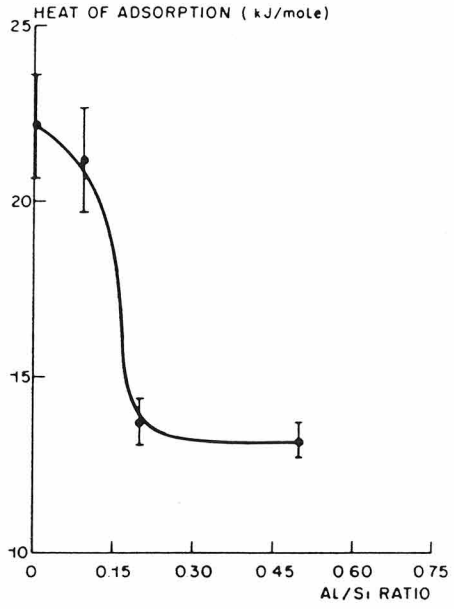

Fig. 4-16 Heat of adsorption of methane in Na-mordenite as a function of the Al/Si ratio as obtained by *Monte Carlo* calculations. (After B. Smit *et al.*, 1988)

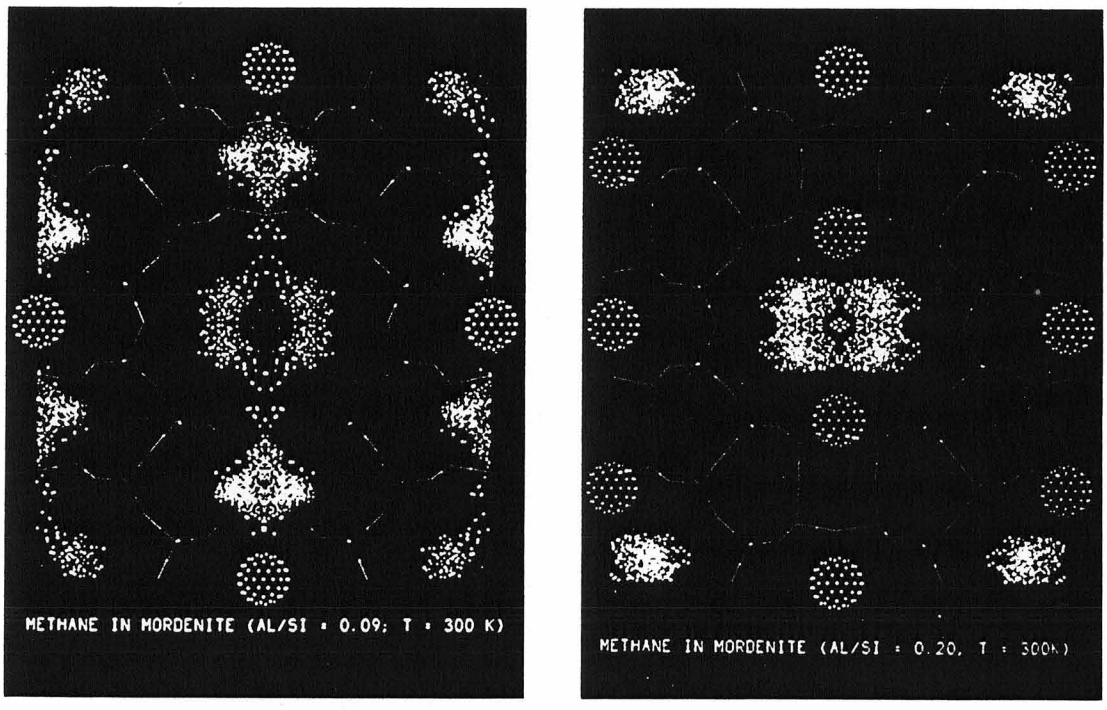

Fig. 4-17 Distribution of a single methane adsorbed in Na-mordenite at 300 K and Al/Si = 0.09 (a, left) and Al/Si = 0.2 (b, right) as obtained by *Monte Carlo* calculations. (After B. Smit *et al.*, 1988)

carried out on a methane molecule in mordenites with different Al/Si ratios at 300 K. As shown in Fig. 4-17a, at a low Al/Si ratio one can see that the methane molecule is distributed in the straight channels and in the side-pockets. A molecule trapped in a pocket has a lower energy than in the central channel. As the Al/Si ratio is increased, these side pockets become seriously blocked by the sodium ions (Fig. 4-17b). Methane can not enter the blocked side-pockets. They stated that the effective blocking by the sodium ions relates closely the decrease of the heat of adsorption at increasing Al/Si ratios (Fig. 4-16).

Thus, the experimental information on the two types of adsorption sites, in particular, on the energies of adsorption potentials, is valuable and desirable.

Hereafter, we would like to determine which T_1 minimum observed for methane can be assigned to the reorientation in the main-channel, and which minimum to that in the side-pocket. Using the relaxation data, we would like to evaluate the activation energies of reorientation and, if possible, the energy difference of the two adsorption sites as well as the occupation number on each site.

4.6.3 Activation Energies of Reorientation and Difference of Potential Energies between Side-Pocket and Main-Channel

Fig. 4-18 shows the plot of the temperatures of T_1 minima observed for ethane, propane and butane against the number of carbons in the guest molecule. It is obvious that the T_1 minimum at 15 K for methane is on the line that passes the three points for ethane, propane and butane, satisfying the law of corresponding state. On the other hand, the point representing another T_1 minimum, 50 K, for methane locates at an unrelated position to other points. This fact implies that the low-temperature T_1 minimum must be attributed to the reorientation of methane in the main-channel, and the high-temperature one to that in the side-pocket.

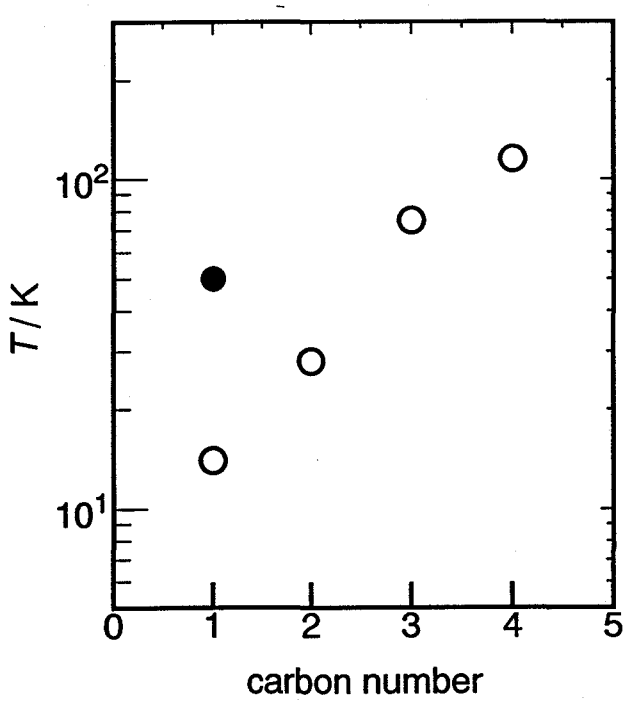

Fig. 4-18 Plot of the temperature of T_1 minimum against the carbon number of guest molecule in mordenite.

The above assignment can lead to an appropriate interpretation of the loading dependence of the T_1 shown in Fig. 4-4. The following would be assumed:

(1) The potential energy for the adsorption of methane is lower in the side-pocket and higher in the main-channel as suggested by Smit *et al.*[11]

(2) Under thermal equilibrium the distribution of methane molecules follows Boltzmann's distribution.

For quantitative discussion the T_1 data of methane is plotted against a reciprocal temperature in Fig. 4-19. As described above the two T_1 minima at 15 K and 50 K can be attributed to the reorientation of the methane molecules in the main-channel and in the side-pocket, respectively. Since both of the observed FID and the magnetization recovery behave exponentially, the spin-temperature concept holds and therefore the observed spin-lattice relaxation rate T_1^{-1} can be represented by the sum of the two contributions from the molecules in the main-channel and the side-pocket. It follows that

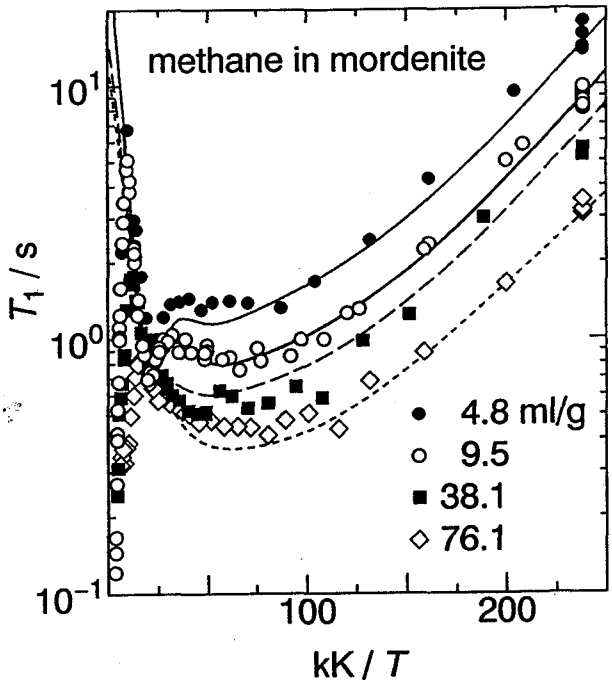

Fig. 4-19 The logT_1 vs $1/T$ plots for methane in mordenite. (40.4 MHz)

$$T_1^{-1}(\text{obs}) = n_p T_1^{-1}(\text{pocket}) + n_c T_1^{-1}(\text{channel}), \qquad (4\text{-}10)$$

where T_1(obs), T_1(pocket) and T_1(channel) denote observed T_1 , T_1 in the side-pocket, and T_1 in the main-channel , respectively. n_p and n_c denote the proportions of molecules in the side-pocket and in the main-channel, respectively, and therefore the relation

$$n_p + n_c = 1 \qquad (4\text{-}11)$$

holds. It is assumed that the distribution of methane molecules follows the Boltzmann's distribution, until all of the side-pockets are occupied. As described later the saturation of side-pockets occurs at the loading of 76.1 ml/g. We have then the following relation for the ratio of the molecules in the side-pockets to those in the main-channels:

$$n_p/n_c = \exp(-\Delta E / RT), \tag{4-12}$$

where ΔE denotes the potential energy difference for adsorbed methane molecule between the side-pocket (E_p) and the main-channel (E_c), that is,

$$\Delta E = E_p - E_c \tag{4-13}$$

The observed T_1 minima exhibit longer values than the calculated values for classical reorientation, as described in **Appendix I.** Each of the minima is influenced by the rotational tunneling of the methane molecule. As in the case of ethane (§4.5.1) in the presence of the rotational tunneling and when the tunneling frequency ω_t is much greater than the Larmor frequency ω_0 the spin-lattice relaxation time T_1 can be approximated by [34]

$$\frac{1}{T_1} \sim C\left(\frac{\tau_c}{1+\omega_0^2\tau_c^2} + \frac{4\tau_c}{1+4\omega_0^2\tau_c^2}\right). \tag{4-14}$$

In the low temperature limit τ_c corresponds to the lifetime of the tunneling level, and is approximated by

$$\tau_c = \tau'_0 \exp(E_{01}/RT), \tag{4-15}$$

where E_{01} is the energy difference between the two lowest torsional states. At the intermediate temperatures, the contribution from the higher torsional states becomes progressively important, and at high temperatures, the stochastic activation over the barrier becomes dominant. In the first approximation, we combine the tunneling process and the thermally activated process to represent the averaged relaxation rate by Eq. (4-14) over the whole temperature region. In such a case the effective correlation time τ_c can be expressed by

$$\tau_c^{-1} = \tau'_0{}^{-1}\exp(-E_{01}/RT) + \tau_0^{-1}\exp(-E_a/RT). \tag{4-16}$$

As described in the previous section T_1 decreases with increasing loading, and in particular in the low-temperature region including the lower-temperature T_1 minimum. Such loading dependence arises from two mutually related origins. The first one is the reinforcement of the intermolecular dipole-dipole interactions in the main-channel with increase in loading, which causes the coupling constant C in Eq.(4-14) larger. The second one is the decrease of ΔE with increasing loading, which leads to the decrease of the ratio n_p/n_c. It is difficult to determine the accurate weight of each contribution, but the former seems more important. To the first approximation, we assume that ΔE is independent of temperature and loading, and the lowering of T_1 in the low-temperature region with increasing loading originates mainly from the reinforcement of the intermolecular dipole-dipole interactions, which results in the increase of the coupling constant C for reorientation in the main-channel.

Therefore, Eqs. (4-10~13) can be applied at each loading with the exception that Eq. (4-12) is not applicable at the loading of 76.1 ml/g and to the lowest temperature region at the loading of 38.1 ml/g due to saturation of the side-pocket. Since one unit cell contains two pipes of channels and each pipe has two side-pockets on its two sides (see Fig. 1-1),[4, 37-39] 1 gram mordenite will accommodate methane gas of 29.72 ml (S.T.P) in the side-pocket providing that every side-pocket traps one molecule. Therefore, for example, at the loading of 76.1 ml/g molecules with an amount of 46.4 ml/g must be adsorbed in the main-channels even at the lowest temperature. This situation corresponds to a constant value of n_C, 0.61, and Boltzmann's principle is not applied to this case of saturation.

The depth of the T_1 minimum at 50 K is almost independent of the loading, and the coupling constant C is considered to be constant for the reorientation in the side-pocket. The activation energy E_a and the energy difference between the two lowest torsional states, E_{01}, in the side-pocket can also be considered to be independent of the loading. We also assume that E_a and E_{01} are approximately independent of the loading for molecule in the main-channel. By applying Eqs. (4-14~16) to each T_1 minimum, and adjusting the values of n_C and n_P at each loading, we attempted to fit the theoretical T_1 to the experimental relaxation data. The obtained curves are shown in Fig. 4-19. The parameters for the fitting are listed in Table 4-5.

Table 4-5 Parameters of the reorientation of methane in the side-pocket and main-channel.

Loading / ml g^{-1}	4.8		9.5		38.1		76.1	
Site	Channel	Pocket	Channel	Pocket	Channel	Pocket	Channel	Pocket
E_a / kJ mol^{-1}	1.0	2.0	1.0	2.0	1.0	2.0	1.0	2.0
τ_0 / 10^{-11} s	1.0	1.8	1.0	1.8	2.5	1.8	3.0	1.8
E_{01} / kJ mol^{-1}	0.11	0.3	0.11	0.3	0.11	0.3	0.14	0.3
τ'_0 / 10^{-9} s	0.75	4.0	0.75	4.0	0.75	4.0	0.8	4.0
C / 10^9 s^{-2}	0.33	0.39	0.54	0.39	0.72	0.39	0.75	0.39
ΔE / J mol^{-1}	- 70		- 70		- 70		-	

Fig. 4-19 indicates that the calculated curves agree well with the experimental data. It can be found in Table 4-5 that the activation energy for reorientation in the side-pocket, 2.0 kJ mol^{-1}, is larger than the value in the main-channel, 1.0 kJ mol^{-1}, indicating the reorientation in the side-pocket is more hindered than in the main-channel. We also plot τ_C at loading of 9.5 ml/g vs $1/T$ in Fig. 4-20 in order to see the difference between the reorientations at both sites.

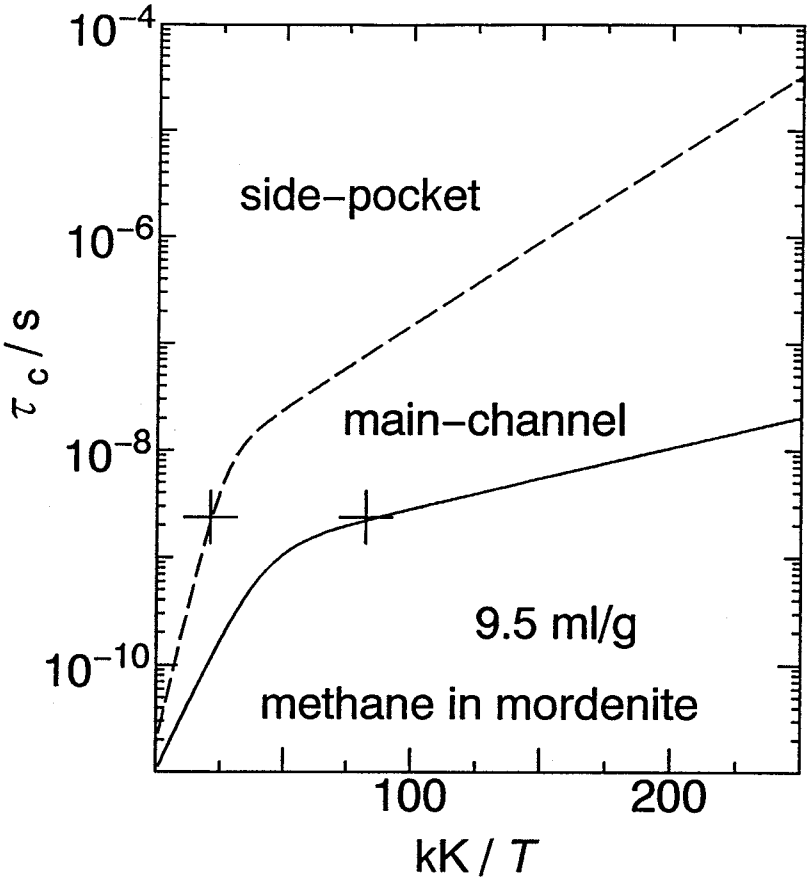

Fig. 4-20 Temperature dependence of τ_C for molecular rotation of methane in the side-pocket and the main-channel of mordenite at the loading of 9.5 ml/g.

We plot the activation energies, E_a, for reorientation in the side-pocket and main-channel for methane, together with the values for ethane, propane and butane in Fig. 4-21. It is found that E_a for methane in the main-channel is nearly the same as the value for ethane, suggesting that ethane molecule lies along the channel and rotates about the molecular axis in the channel direction. It is also found that E_a for reorientation of the four kinds of molecules in the main-channel satisfies the law of corresponding state. As to methane in the side-pocket, it experiences an activation energy twice as large as that in the main-channel. Since the potential energy in the side-pocket is lower than that in the main-channel, the curvature of potential energy surface is sharper in the former than in the latter and so the molecule in the side-pocket should overcome a higher activation energy.

The coupling constant, C, for the reorientation in the side-pocket was kept constant in the above analyses of T_1 data. On the other hand, C for the reorientation in the main-channel increases with increasing loading, indicating reinforcement of the intermolecular dipole-dipole interactions, as a result of the decrease of the intermolecular distance of the molecules in the main-channel.

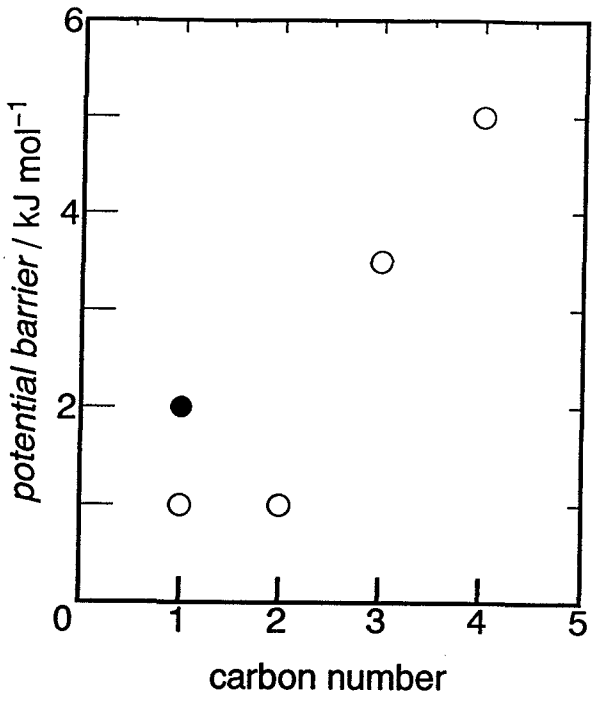

Fig. 4-21 Plot of activation energy for reorientation against the carbon number of guest molecule in mordenite.

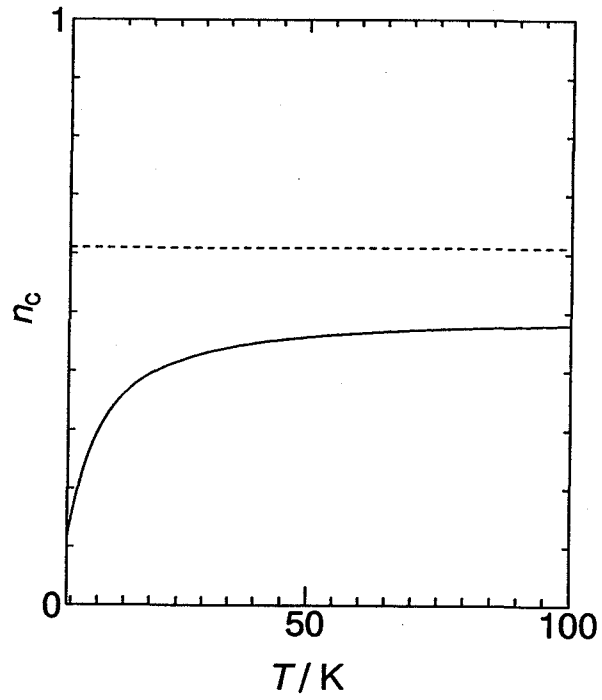

Fig. 4-22 Temperature dependence of n_C. dotted line: at the loading of 76.1 ml/g; solid line: at the loadings of 4.8, 9.5 and 38.1 ml/g.

The above data analysis succeeded in estimating the potential energy difference between the two adsorption sites, ΔE, to be about - 70 J mol^{-1} ($\approx$ 8.4 K). Although this value cannot be evaluated by any other experimental method at present, it will be very important for the future work on the catalytic activity of mordenite.

As shown in Fig. 4-16, a sudden decrease of the heat of adsorption of about 5 kJ mol^{-1} can be observed as the Al/Si ratio exceeds 0.15 from the calculation by Smit.[11] Smit suggested that the observed decrease of the heat of adsorption at high Al/Si ratios can be explained with the reason that the lower-energy side-pocket was effectively blocked by the sodium ions. In addition to such a reason, it is to be noted that the sodium ion itself can cause the adsorption potential in the main-channel higher at high Al/Si ratio than that at low Al/Si ratio, because the counter ion has opposite charge to the wall of the channel consisting of oxygen network, and has lower polarizability than O^{2+}(the polarizabilities of Na^{+} and O^{2+} are 0.24 and 3.0×10^{-24} cm^3, respectively.)

In relation to ΔE which was determined for the first time in the present work, Mayorga[5] suggested significantly high potential energy difference between the main-channel and the side-pocket, i.e., of the order of several kJ mol^{-1} for H-mordenite. In H-mordenite it was considered that the proton is buried in the oxygen framework whereas there is an Na^{+} ion located in the bottom of the side-pocket in the case of Na-mordenite. The Na^{+} ion of Na-mordenite works to raise significantly the total potential energy in the side-pocket.

By substituting the value of ΔE into Eq. (4-12) we obtain the temperature dependence of n_C in the low-temperature region, as shown in Fig. 4-22. It is obvious that at low loadings the number of molecules in the main-channels is considerably less than in the side-pockets at low temperatures, but n_C tends to be equal to n_P on heating, and both the fractions approach the limiting value of 0.5. At the loading of 76.1 ml/g, however, because the side-pockets can accommodate methane gas of only 29.72 ml/g, n_C exhibits a value of 0.61, which does not depend on the temperature below the temperature at which the desorption begins to occur.

In this section, we gave a quantitative discussion of the relaxation behavior for methane adsorbed in mordenite at low temperatures. The results revealed that the methane molecules distribute in the main-channels and the side-pockets approximately according to Boltzmann's distribution. The difference of adsorption potential energies between the side-pocket and the main-channel was estimated to be - 70 J mol^{-1}. It is worth noting that we can detect such a small potential energy difference by using NMR relaxation measurements. The molecules reorient in each site, the activation energy of which is higher in the side-pocket than in the main-channel.

4.7 Argon-Methane Mixture in Mordenite

4.7.1 Introductory Remarks

We have studied the dynamic behavior of methane adsorbed in mordenite and found that the methane molecules are Boltzmann distributed in the main-channels and the side-pockets. The potential energy difference between the side-pocket and the main-channel has been estimated to be - 70 J mol^{-1}. In order to shed light on the effect of this energy difference on the adsorption equilibrium in more detail, we measured the proton spin-lattice relaxation time on mixture of methane and argon, the molecules with similar shapes and sizes, in mordenite and expect to extract information about possible selective or preferential adsorption mechanism.

The equilibrium solid phases of argon and methane are both face-centered cubic in crystal structure.[40,41] Both argon and methane can essentially be regarded as spherical molecules, the diameters of which are 3.4 and 3.8 Å, respectively. Greer determined the argon-methane phase diagram between 15 and 65 K by X-ray diffraction,[41] as shown in Fig. 4-23. It can be found that above about 60 K, solid solution is formed over a wide range of concentration, but in the low-temperature regime solid solution is formed only at the Ar-rich or CH_4-rich region.

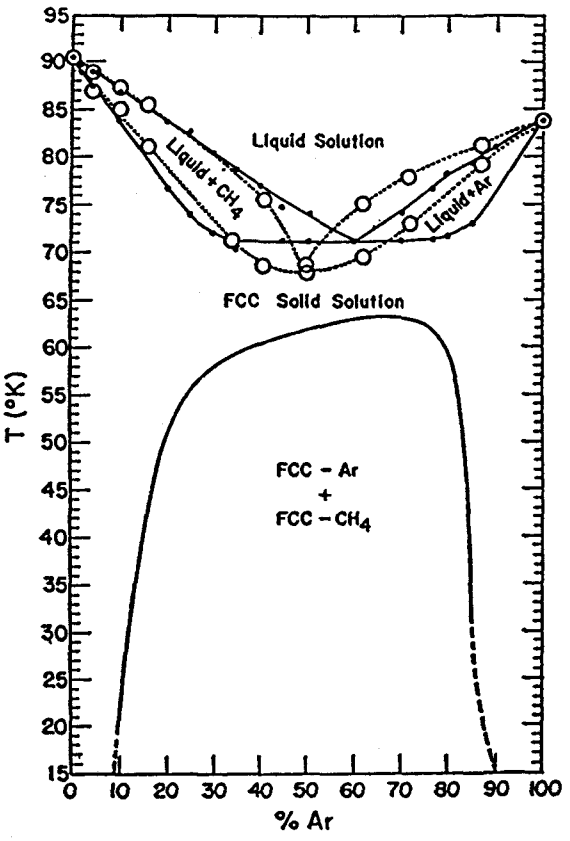

Fig. 4-23 The bulk argon-methane phase diagram. (After S. C. Greer, *et al.*, 1969)

Two-component adsorption system in usual zeolite is also of another interest. In zeolite the adsorbent-adsorbate interactions play a more important role than the adsorbate-adsorbate interactions. It is expected that the "phase diagram" will exhibit considerably different behavior from that in the bulk states when argon and methane are co-adsorbed. Because there exist two components in addition to the substrate, the system becomes complicated and therefore the Boltzmann distribution in the main channels and the side pockets, Eq.(4-12), can not be simply applied to each component. The theoretical treatment may be difficult, but the information on the adsorption states and the intermolecular interactions is perhaps included in and can be experimentally extracted from such a "phase diagram".

Few studies have been reported on the subject of two-component adsorption. Forste *et al.* measured molecular translational mobility of methane adsorbed on ZSM-5 by the use of PFG NMR and found that the mobility lowers significantly by co-adsorbing benzene molecules (Fig. 4-24).[42] The result suggested that benzene molecules are predominantly trapped in the channel intersections, and in this way they work a hindrance to the intracrystalline translational diffusion of the methane molecules.

However, argon has the diameter close to that of methane, and both of them are essentially spherical. Argon is more mobile in zeolite.[15,43] Therefore, the situation is expected to be significantly different from that in the benzene-methane mixture. Furthermore, in contrast to the measurement of translational mobility as examined by Forste, low-temperature experiments will lead to local information on the equilibrium adsorption states.

Such considerations led us to study the argon-methane system co-adsorbed in mordenite at low temperatures.

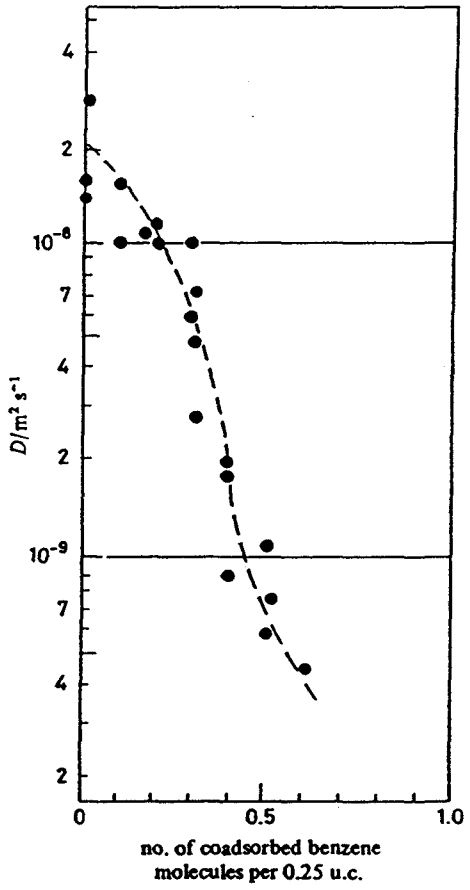

Fig. 4-24 Self-diffusion coefficiet of methane adsorbed in ZSM-5 at 293 K vs the amount of co-adsorbed benzene. (After C. Forste, *et al.*, 1987)

4.7.2 Results and Discussion

The argon gas was obtained in a cylinder from Takachiho Chemical Industry Co. Ltd. The stated purity is 99.9999% (special degree, impurities: O_2 < 0.1 ppm, N_2 < 1 ppm, H_2 < 0.3 ppm, H_2O < 1 ppm).

Methane is first loaded into the sample container. Then the sample is kept at 77 K and argon is loaded. The temperature was raised up to room temperature to speed up mixing and then cooled down slowly. Three co-adsorption systems were prepared: The loading of methane was fixed to be 9.5 ml/g, while argon were loaded by 0, 9.5, 19.0 and 42.9 ml/g.

Proton spin-lattice relaxation time T_1 for the argon-methane system in mordenite was measured at 40.4 MHz over a wide temperature range from 4.2 K to room temperature. The results are plotted in Fig. 4-25 against the reciprocal temperature.

It was found that T_1 is approximately independent argon's loading up to 19.0 ml/g. When the loading of argon was increased up to 42.9 ml/g, the value of the T_1 minimum at 50 K lowered significantly, while that below 15 K rose slightly.

In order to understand such an argon-loading dependence of T_1 of methane, we must examine what types of adsorption states exist in the argon-methane system co-adsorbed in mordenite, and how T_1 behaves in each of the states. Hereafter we define the ratios $R_{ar} = n_p(Ar)/n_c(Ar)$ and $R_{me} = n_p(Me)/n_c(Me)$, where $n_p(Ar)$ and $n_c(Ar)$ represent the composition of argon adsorbed in the side-pocket and the main-channel, respectively, and so on.

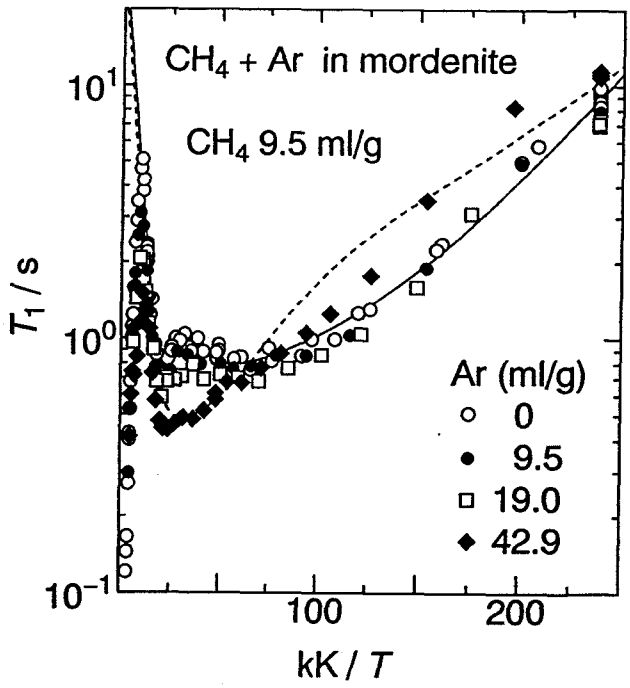

Fig. 4-25 ProtonT_1 for argon-methane co-adsorbed in mordenite. (40.4 MHz)

First we assume that the ratio of molecules in the side-pocket to those in the main-channel for methane is the same as the ratio for argon, that is, $R_{ar} = R_{me}$. In such a case, it is expected that the distribution of methane molecules in the side-pockets and the main-channels will be the same as that in the absence of argon. If it is assumed that the reorientation of methane in the main-channel is not affected by the presence of argon, T_1 in the vicinity of low-temperature T_1 minimum will not change. From Fig. 4-25, it is found that when the loading of argon is less than 19.0 ml/g, T_1 is almost independent of the loading of argon, indicating that the adsorption state may be concluded to belong to the case described above, suggesting that the guest-host interaction energy differs only slightly between methane and argon and the entropy of mixing of two gases dominates the adsorption characteristic.

Second, we assume that ratio of methane molecules in the side-pocket to those in the main-channel is not equal to the ratio for argon, that is, $R_{ar} \neq R_{me}$. There are two possibilities: (I) $R_{ar} > R_{me}$, argon is adsorbed preferentially in the side-pocket; (II) $R_{ar} <$

R_{me}, methane is adsorbed preferentially in the side-pocket. In case **I**, because the main-channel is rich but the side-pocket is poor in methane molecules, the value of the T_1 minimum at 15 K is expected to be lowered, but that of the minimum at 50 K to be raised as the composition of argon increases. In case **II**, because the main-channel is poor but the side-pocket is rich in methane molecules, the value of the T_1 minimum at 15 K is expected to be raised, but that of the minimum at 50 K to be lowered. From Fig. 4-25 it can be recognized that the adsorption state at the argon loading of 42.9 ml/g corresponds to case **II**, that is, $R_{ar} < R_{me}$. In comparison with the situation that only methane is adsorbed in mordenite, relatively large number of methane molecules are adsorbed preferentially in the side-pockets when large amount of argon is co-adsorbed.

For quantitative analysis of the T_1 data along with the above consideration, we assume that the parameters for methane reorientation deduced in the previous section (Table 4-5) for pure methane can be applied to the co-adsorbed system. In addition, we assume that n_C and n_P are approximately independent of temperature. Then we reproduced the T_1 data by using Eqs. (4-10, 11, 14~16) with the parameters corresponding to the loading of 9.5 ml/g in Table 4-5 and obtained the broken line in Fig. 4-25. For the best fitting, the relation

$$T_1^{-1}(\text{obs}) = 0.9T_1^{-1}(\text{pocket}) + 0.1T_1^{-1}(\text{channel})$$

that is, n_C=0.1 and n_P=0.9 had to be used. The calculated T_1 agrees fairly well with the experimental ones. It can be concluded, therefore, that about 90% methane molecules are adsorbed in the side-pockets and 10% in the main-channels.

The results of the above analysis of the temperature and the loading dependence of T_1 bring about a gross idea for the "phase diagram" of the methane-argon co-adsorption system in mordenite:

(1) When argon of 9.5 or 19.0 ml/g is co-adsorbed with methane of 9.5 ml/g in mordenite, the ratio of methane molecules between the side-pocket and the main-channel is equal to the ratio for argon.

(2) When argon of 42.9 ml/g is co-adsorbed with methane of 9.5 ml/g in mordenite, about 90% methane molecules are preferentially located in the side-pockets and 10% in the main-channels. This phenomenon indicates that, when mordenite has accommodated excess of adsorbate, the degree of molecular motional freedom is lost and hence the side-pocket accommodates preferentially its favorite molecular species, that is, methane, to other species, argon. In this case the concept of "mixing" does not hold. This phenomenon is just the "molecular recognition". Such a system may be employed for enrichment and purification of specified molecules.

Appendix I. Molecular Reorientation of Methane in Mordenite

Here we consider the spin-lattice relaxation caused by the reorientation of methane.

Let us assume that the barrier to reorientation of the molecules is sufficiently high so that the protons can be treated as distinguishable particles. However, the correlation time, τ_c, of the reorientation is short enough to satisfy the relation $\tau_c << T_2$ and so the weak-collision condition holds. We assume also that the spin-temperature concept can be applied to the adsorption system. According to the BPP theory,[20] the proton spin-lattice relaxation occurs due to the modulation of the proton intramolecular dipolar interaction by the molecular reorientation with a single correlation time τ_c (isotropic reorientation). In such a case the proton dipolar spin-lattice relaxation rate can be given by

$$T_1^{-1} = (9/10)\gamma^4(h/2\pi)^2 r^{-6} B(\tau_c), \qquad \text{(A.I-1)}$$

where r is the inter-proton distance and γ the proton gyromagnetic ratio.

T_1 assumes a minimum value at $\omega_0\tau_c = 0.6125$, the value of which is given by

$$T_1(\text{min}) = 0.7017\omega_0/(9/10)\gamma^4(h/2\pi)^2 r^{-6}. \qquad \text{(A.I-2)}$$

The value of T_1 minimum is, therefore, 11 ms at $\omega_0 = 2\pi \times 40.4$ MHz, when the proton-proton distance is taken to be $r = 1.78 \times 10^{-8}$ cm.[1,3]

As shown in Fig. 4-4 for methane in mordenite, the values of T_1 minima at 15 and 50 K are as long as 0.45 - 1.2 s, each of which is tens times longer than the calculated value (0.011 s). Therefore, we can not interpret the relaxation behavior observed for methane adsorbed in mordenite by assuming only the classical molecular reorientation of methane molecule.

In order to analyze the T_1 data, it is necessary to find a means whereby some protons do not participate directly in the relaxation. It has been shown by de Wit and Bloom that spin isomerization provides such a mechanism, which successfully interpreted the relaxation behavior of solid methane. [1]

Assume hindered rotation of CH_4 molecule which is located at the tetrahedral symmetry site. The symmetry states of the spatial part of the wave function consist of $A + E + 3T$ where A, E, and T are the one-, two-, and three-dimensional irreducible representations of the tetrahedral group when the potential barrier to rotation is very high, statistical mechanics applies and the torsional ground states degenerate. For a low barrier to rotation this spatial degeneracy is lifted (see Fig. A.I-1): If the crystal field has tetrahedral or higher symmetry, the three T symmetry species remain degenerate. In physical terms, the difference between a high and a low barrier is that in the former case the protons may be treated as distinguishable particles whereas in the latter case, because of the overlap of the individual proton wave

functions and the resultant quantum mechanical rotational tunneling, the protons must be treated as indistinguishable particles.

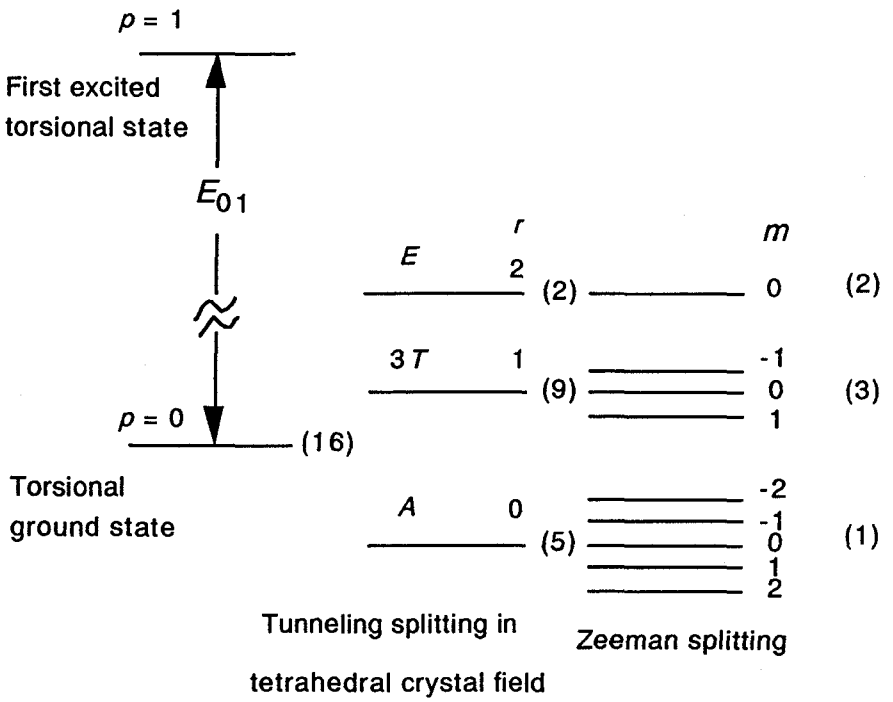

Fig. A.I-1 The energy scheme for the tunneling split torsional ground state. In a finite tetrahedral crystal field the torsional ground state of CH_4 splits into three states with symmetry A, E, and T. The degeneracy of the $3T$ levels is lifted by a crystal field with lower symmetries. However, we assume for simplicity the crystal field in the present material to be tetrahedral. In an external static magnetic field the Zeeman splitting of each level occurs. m denotes the magnetic quantum number of the corresponding nuclear spin energy level. The number in the parenthesis means the degeneracy of the respective state.

The protons belonging to the E species have total spin $I = 0$ and play no role. The protons belonging to the T species have total spin $I = 1$; they relax at a rate R_T ($=T_{1T}^{-1}$) as determined by the intramolecular interactions. The protons belonging to the A species have total spin $I = 2$. It has been shown that within the $I = 2$ manifold the matrix elements of the intramolecular dipolar Hamiltonian are identically zero. Therefore the A spins can relax only through a spin exchange process with the T spins; the time constant for this intermolecular process is expected to be much less than T_1. It follows that the relaxation rate for the entire spin system is given by

$$\begin{aligned} R &= R_T\,[C_T/(C_T + C_A)] \\ &= R_T\,[2N_T/(2N_T + 6N_A)], \end{aligned} \qquad \text{(A.I-3)}$$

where C_A and C_T are the heat capacities and N_A and N_T the number of spins belonging to the A and T species, respectively. R_T is given by[1)]

$$R_T = (3/10)\, R_{\text{classical}}, \tag{A.I-4}$$

which predicts a T_1 minimum value of

$$T_1(\text{min}) = [(2N_T + 6N_A)/2N_T\,]\,(10/3)\,[T_1(\text{min})]_{\text{classical}}, \tag{A.I-5}$$

where $R_{\text{classical}}$ is the spin-lattice relaxation rate due to classical molecular reorientation and $[T_1(\text{min})]_{\text{classical}}$ is given by Eq. (A.I-2). In the high-temperature limit N_T/N_A = 9/5, while the ratio of N_T/N_A = 6/5 was reported by nuclear magnetic susceptibility studies on solid methane at 4.2 K (Wong *et al.*).[44)] Therefore, on the basis of the above symmetry consideration, the only effect of the spin isomerization may increase the values of the T_1 minima. The estimated minimum at 40 MHz is given in Table A.I-1 together with the experimental and the classical values.

Table A.I-1 Calculated value of the T_1 minimum based on the spin isomerization together with the experimental and classical values at 40 MHz.

	T_1(min) / s
Classical	0.011
Spin isomerization	0.1 [a)]
	0.14 [b)]
Experimental	0.4-1.2

a) In the high temperature limit
b) At 4.2 K (Wong *et al.*)

The effect of spin isomerization improves the agreement between the theoretical and experimental T_1 minimum values to some extent but a significant discrepancy still remains. This discrepancy can be improved a little more by taking into account the existence of different sites. The symmetry of crystal field in the pore may be lower than the tetrahedral, and taking account of this point leads probably to a little longer relaxation time, but it will not result in any satisfactory value. It is remarked in Fig 4-19 that the experimental log T_1 vs. $1/T$ plot gives a very gentle slope on the low-temperature side of the T_1 minimum at 15 K, which gives an activation energy as small as 0.11 kJ mol^{-1}. This fact suggests strongly that a different relaxation mechanism from the quantum spin isomerization works. It must be, by our experience, the rotational tunneling of methane molecule.

Haupt[27)] has developed a detailed theory for spin-lattice relaxation in the presence of tunneling of CH_3 groups through hindering barriers. His theory is a kind of extension of the theory of de Wit and Bloom discussed above.

Haupt's approach was successfully extended to the four-proton case of NH_4^+ by Armstrong *et al.*[29] It is then expected to provide a semi-quantitative interpretation of the proton relaxation of methane in mordenite at low temperatures. The main ideas in this theory are summarized below. Only the first-order approximation will be considered.

The assumptions are:

(1) the CH_4 molecule is rigid so that proton pair exchange is neglected;

(2) only intramolecular dipolar interaction is considered so that other interaction such as spin rotational effect on the relaxation is excluded;

(3) modulation of the potential barrier by phonons can be treated as a perturbation and lattice accommodation is not considered;

(4) the potential barrier is of sinusoidal form and independent of the rotational state of the molecule;

(5) the thermal energy, kT, is far lower than the barrier height.

In addition, although the crystal field in the present case may have a symmetry lower than the tetrahedral symmetry, we assume, for simplicity, that the methane molecule in mordenite experiences a tetrahedral crystal field.

The Hamiltonian is written in the form,

$$H = H_Z + H_R + H_P + H_{DD} + H_{RP}, \tag{A.I-6}$$

where H_Z, H_R, and H_P are the Zeeman, hindered rotor, and phonon contributions, respectively. The eigenstates are labeled m, m' ... r, r'... p,p' .... The dipolar Hamiltonian is H_{DD} and H_{RP} describes the interaction between the hindered rotor and the vibrational degrees of freedom of the lattice. For the case of high magnetic fields $H_Z >> H_{DD}$ so that H_{DD} can be treated as a perturbation. The eigenstates of $H_Z + H_R$ are shown schematically in Fig. A.I-1.

The transition probability between spin states $|m>$ and $|m'>$ is

$$W_{m\to m'} = \sum_{rp} \sum_{r'p'} P_r P_p W_{mrp\to m'r'p'}, \tag{A.I-7}$$

where P_r and P_p are the Boltzmann factors for the states $|r>$ and $|p>$. Assuming the existence of a spin temperature, the following formula of Habel and Slichter[45] applies:

$$\frac{1}{T_1} = \frac{1}{2} \sum_{mm'} \frac{W_{m\to m'}(E_m - E_{m'})^2}{\sum_m E_m^2}. \tag{A.I-8}$$

Using first-order perturbation theory one obtains

$$W_{mrp\rightarrow m'r'p'} = \int_{-\infty}^{\infty} \langle mrp \,|\, H_{DD} + H_{RP} \,|\, m'r'p' \rangle \langle m'r'p' \,|\, H_{DD} + H_{RP} \,|\, mrp \rangle \times \exp\left[-\frac{2\pi i}{h}(E_{m'r'p'} - E_{mrp})(t'-t)\right] dt' \,. \quad \text{(A.I-9)}$$

To first order the relation,

$$\langle mrp \,|\, H_{DD} + H_{RP} \,|\, m'r'p' \rangle = \langle mr \,|\, H_{DD} \,|\, m'r' \rangle_{p=p} + \langle rp \,|\, H_{RP} \,|\, rp \rangle_{m=m'}, \quad \text{(A.I-10)}$$

holds. In this equation the second term on the right does not contribute to magnetic relaxation. Therefore, it follows that

$$W_{mr\rightarrow m'r'} = \int_{-\infty}^{\infty} \overline{\langle mr \,|\, H_{DD} \,|\, m'r' \rangle \langle m'r' \,|\, H_{DD} \,|\, mr \rangle} \times \overline{\exp\left[-\frac{2\pi i}{h}(E_{m'r'p'} - E_{mrp})(t'-t)\right]} dt' \quad \text{(A.I-11)}$$

where the bar indicates a average over the time t. It is now assumed that the torsional states have a time dependence which can be represented by a stationary random function, but that the magnetic spin states are independent of time. That is,

$$E_{m'r'} - E_{mr} = E_{m'r'}(t) - E_{mr}(t) = \bar{E}_{m'r'} - \bar{E}_{mr} + \Delta_{rr'}(t), \quad \text{(A.I-12)}$$

where $\bar{E}_{m'r'}$ and $\bar{E}_{mr}$ are mean values of the energy eigenvalues. It follows that

$$\overline{\exp\left[-\frac{2\pi i}{h}(E_{m'r'} - E_{mr})(t'-t)\right]} = \exp\left[-\frac{2\pi i}{h}(\bar{E}_{m'r'} - \bar{E}_{mr})\tau\right] + \overline{\exp\left[-\frac{2\pi i}{h}\Delta_{rr'}(t)\tau\right]}. \quad \text{(A.I-13)}$$

It is assumed that the correlation function varies exponentially with time as

$$\overline{\exp\left[-\frac{2\pi i}{h}\Delta_{rr'}(t)\tau\right]} = \exp\left[-\tau/\tau_{rr'}\right]. \quad \text{(A.I-14)}$$

Hence

$$W_{m\rightarrow m'} = \sum_{r'} P_r \langle mr \,|\, H_{DD} \,|\, m'r' \rangle \langle m'r' \,|\, H_{DD} \,|\, mr \rangle \times \int_{-\infty}^{\infty} \exp\left[-\frac{2\pi i}{h}(\bar{E}_{m'r'} - \bar{E}_{mr})\tau\right] \exp\left[-\tau/\tau_{rr'}\right] d\tau. \quad \text{(A.I-15)}$$

The integral denotes the spectral density at a frequency $2\pi(E_{mr} - E_{m'r'})/h$ and the correlation time $\tau_{rr'}$ is related to the lifetime of either state $|r\rangle$ or $|r'\rangle$. A detailed calculation, taking into account the modulation of the potential barrier by phonons, shows that at low temperatures where tunneling provides the dominant relaxation mechanism the correlation time is given by

$$1/\tau_{rr'} \sim 1/\tau_{01} \propto \exp[-E_{01}/RT], \tag{A.I-16}$$

where E_{01} is the energy separation between the ground and first excited torsional states.

Next let us consider the matrix elements of H_{DD}. The dipole-dipole Hamiltonian can be written symbolically as the product of a spatial and a spin part. That is,

$$\langle mr \,|\, H_{DD} \,|\, m'r' \rangle = \langle m \,|\, F(I) \,|\, m' \rangle \, \langle r \,|\, f(\theta,\phi) \,|\, r \rangle, \tag{A.I-17}$$

where I is a spin operator and (θ, ϕ) specifies the orientation of the CH_4 molecule relative to the external magnetic field. The factor $\langle m \,|\, F(I) \,|\, m' \rangle$ is a constant. However, the factor $\langle r \,|\, f(\theta,\phi) \,|\, r \rangle$ is largely dependent on the wave functions of the torsional oscillator. Following the reasoning of Haupt[27], this matrix element becomes smaller as barrier becomes lower. We can therefore write

$$\langle mr \,|\, H_{DD} \,|\, m'r' \rangle = D_{rr'} \, \langle m \,|\, F(I) \,|\, m' \rangle, \tag{A.I-18}$$

where $D_{rr'}$ is almost constant for high barriers but decreases as the barrier height lowers.

The spin-lattice relaxation time may be written as

$$\frac{1}{T_1} = \sum_{\substack{m m' \\ r r'}} P_r \, |\langle m \,|\, F(I) \,|\, m' \rangle D_{rr'}|^2 \frac{\tau_{rr'}}{1 + \tau_{rr'}^2 \, [2\pi(E_{mr} - E_{m'r'})/h]^2}. \tag{A.I-19}$$

The above formalism predicts the following behavior of T_1. At high temperatures where classical reorientation occurs, the activation energy for molecular group is determined by the barrier height. At low temperatures, where tunneling provides the dominant relaxation mechanism, E_{01} determines the slope of the plot of $\log T_1$ vs. $1/T$. At intermediate temperatures, the slope will be a complicated function of temperature as the two processes take place simultaneously. The presence of the factor $|D_{rr'}|^2$ leads to a reduced relaxation efficiency and hence a longer value of the T_1 minimum than in the classical case is expected.

By such treatment, the long T_1 minima observed for methane in mordenite can be interpreted by the molecular reorientation which is accompanied by quantum rotational tunneling at low temperatures.

Appendix II. Molecular Reorientation of Butane in Mordenite

There exist various cases of reorientation that must be considered for butane:

(1) internal rotation of CH_3- group;

(2) *a.* overall rotation about the long axis of the molecule;

b. 180° flip motion about the long axis;

(3) reorientation of the long axis.

It is noted that the molecular overall reorientation about the molecular long axis is distinguished from the 180° flipping. Because of the narrowness of channel of mordenite, the reorientation of the long axis (case 3) can be ruled out for butane.

The spin lattice relaxation time T_1 due to the intramolecular contribution can also be expressed by[46]

$$T_1^{-1} = \frac{2}{3} \Delta M_2 \gamma^2 B(\tau_c), \qquad \text{(A.II-1)}$$

where ΔM_2 is the part of the second moment that is reduced by the fluctuation of the dipole interaction caused by the molecular motion.

Hoch calculated the theoretical second moment for the individual type of molecular reorientation as listed below. [47] Use was made of the known molecular parameters and the Van Vleck formula[48] together with the appropriate reduction factors for the various motions, and the results of the intramolecular contribution are shown in Table A. II-1.

By assuming the reorientation of the CH_3- group is sufficiently rapid and by ignoring the intermolecular contribution, we estimate the $T_1(\mathrm{min})$ values for the two types of the reorientation about the long axis, respectively, by the use of the intramolecular contribution to M_2 calculated by Hoch[47] and of the relation

$$T_1(\mathrm{min}) = 0.7017\omega_0 / (2/3)\, \Delta M_2 \gamma^2. \qquad \text{(A.II-2)}$$

Table A.II-1 lists the $T_1(\mathrm{min})$ values attained by various molecular motions altogether with the reduction of M_2 data.

Table A. II-1 Calculated values of T_1 minima (40 MHz) due to the reorientations about the long axis of the molecule by the use of the M_2 data calculated by Hoch. [47]

Type of reorientation	M_2 / gauss^2	T_1(min) / ms
CH_3 reorientation	11	-
Free rotation about long axis of molecule with CH_3 reorientation	3	46.2
180° flip motion about long axis with CH_3 reorientation	8	123.2

As shown in Fig. 4-7, butane adsorbed in mordenite exhibits T_1 minima of 70-90 ms, which is between free rotation (46 ms) and 180° flip motion (123.2 ms) about the long axis. It turned out, therefore, that the reorientation about the long axis of the butane molecule occurs with simultaneous rapid rotation of CH_3- group in mordenite.

References to Chapter 4

1. G. A. de Wit and M. Bloom, *Can. J. Phys.*, **47**, 1195 (1969)
2. (a) 山本常信, 岡田謙吉, 片岡洋右, 安田秀雄 : *物性*, **14**, 311 (1973)
   (b) 片岡洋右, *化学の領域*, **29**(7), 36 (1975)
   (c) T. Yamamoto, Y. kataoka and K. Okada, *J. Phys. Chem.*, **66**. 2701 (1977)
3. J. W. Riehl and K. Koch, *J. Chem. Phys.*, **57**, 2199 (1972)
4. W. M. Meier, *Z. Kristallogr.*, **115**, 439 (1961)
5. G. D. Mayorga and D. L. Peterson, *J. Phys. Chem.*, **76**, 1641 (1972)
6. T. Ohgushi and H. Yokoyama, *J. Chem. Soc., Faraday Trans. 1*, **88**, 3095 (1992)
7. J. A. Ripmeester, *J. Magn. Reson.*, **56**, 247 (1984)
8. (a) T. Takaishi, A. Yusa, and F. Amakasu, *Trans. Faraday Soc.*, **647**, 3565 (1971)
   (b) T. Takaishi, A. Yusa,Y. Ogino and S. Ozawa, *J. Chem. Soc., Faraday Trans. 1*, **70**, 671 (1974)
   (c) T. Takaishi, A. Yusa,Y. Ogino and S. Ozawa, *Jpn. J. Appl. Phys., Suppl., v2, pt2,* 279 (1974)
   (d) T. Takaishi, *Pure & Appl. Chem.*, **58**, 1375 (1986)
9. K. Itabashi, T. Fukushima and K. Igawa, *Zeolites*, **6**, 30 (1986)
10. (a) D. Brinkman and H. Y. Carr, *Phys. Rev.*, **150**, 174 (1966)
    (b) C. J. Jamesom, A. K. Jameson, and S. M. Cohen, *J. Chem. Phys.*, **62**, 4224 (1975)
    (c) J. A. Ripmeester, *Annu. Rev. Phys. Chem.*, **42**, 433 (1991)
11. B. Smith and C. J. J. den Ouden, *J. Phys. Chem.*, **92**, 7169 (1988)
12. (a) H-J. Doelle, J. Heering, L. Riekert and L. Marosi, *J. Catal.*, **71**, 27 (1981)
    (b) J. Wei, *J. Catal.*, **76**, 433 (1982)
13. A. Abragam, *The Principles of Nuclear Magnetism*, Oxford Univ. Press, London/New York, (1961)
14. C. P. Slichter, *Principles of Magnetic Resonance*, Harper and Row, New York, (1963)
15. J. Karger and D. M. Ruthven, *Diffusion in Zeolites*, JohnWiley & Sons, Inc., *New York*, (1991)
16. (a) J. Karger and J. Caro, *J. Chem. Soc., Faraday Trans. 1*, **73**, 1363 (1977)
    (b) J. Karger, H. Pfeifer, M. Rauscher and A. Walter, *J. Chem. Soc., Faraday Trans. 1*, **76**, 717 (1980)
    (c) J. Karger and D. M. Ruthven, *J. Chem. Soc., Faraday Trans. 1*, **77**, 1485 (1980)
17. J. Caro, M. Bulow, W. Schirmer, J. Karger, W. Heink, H. Pfeifer and S. P. Zdanov, *J. Chem. Soc., Faraday Trans. 1*, **81**, 2541 (1985)
18. H. Pfeifer, in *NMR - Basic Principles and Progress,* (ed. P. Diehl, E. Fluck and R. Kosfeld), Springer - Verlag, *Berlin*, **7**, 53 (1972)

19. H. Pfeifer, *Phys. Rep. C*, **26**, 293 (1976)
20. N. Bloembergen, E. M. Purcell, and R. V. Pound, *Phys. Rev.*, **73**, 679, (1948)
21. H. A. Resing and J. K. Thompson, *J. Chem. Phys.*, **46**, 2876 (1967)
22. H. A. Resing , *Advan. Mol. Relaxation Processes*, **3**, 199 (1972)
23. H. C. Torrey, *Phys. Rev.*, **92**, 962, (1953)
24. (a) C. A. Sholl, *J. Phys., C*, **7**, 3378 (1974)
    (b) W. A. Barton and C. A. Sholl, *J. Phys., C*, **9**, 4315 (1976)
    (c) I R MacGillivray and C. A. Sholl, *J. Phys., C*, **18**, 1691 (1985)
25. L. D. Bustard, *Phys. Rev., B*, **22**, 1 (1980)
26. J. O. Hirschfelder, C. F. Curtiss and R. B. Bird, *Molecular Theory of Gases and Liquids*, Wiley, New York, (1964)
27. J. Haupt, *Z. Natureforsch.*, **A**, 26, 1578 (1971)
28. L. J. Burnett and B, H, Muller, *J. Magn. Reson.*, **23**, 343 (1976)
29. R. L. Armstrong, H. M. V. Driel and A. R. Sharp, *Can. J. Phys.*, **52**, 369 (1974)
30. W. Muller-Warmuth, R. Schuler, M. Prager and A. Kollmar, *J. Chem. Phys.*, **69**, 2382 (1978)
31. S. Takeda and H. Chihara, *J. Magn. Reson.*, **54**, 285 (1983)
32. S. Takeda and H. Chihara, *J. Magn. Reson.*, **56**, 48 (1984)
33. D. J. Ligthelm, R. A. Wind and J. Smidt, *Physica B*, **100**, 175 (1980)
34. T. Eguchi and H. Chihara, *J. Magn. Reson.*, **76**, 143 (1988)
35. R. J. Abraham and K. Parry, *J. Chem. Soc.*, **B**, 539 (1970)
36. Q. Xu, T. Eguchi, H. Nakayama, N. Nakamura and M. Kishita, *Z. Naturforsch.*, *A*, **46**, 240 (1991)
37. H. Van Bekkum, E. M. Flanigen, and J. C. Jansen, *Stud. Surf. Sci. Catal.*, **58** , Elsevier, (1991)
38. 原伸宜, 高橋浩共編, *ゼオライト -- 基礎と応用*, 講談社サイエンティフィク (1975)
39. 富永博夫編, *ゼオライト -- 科学と応用*, 講談社サイエンティフィク (1987)
40. C. S. Barrett and L. Meyer, *J. Chem. Phys.*, **41**, 1078 (1964)
41. S. C. Greer, L. Meyer and C. S. Barrett, *J. Chem. Phys.*, **50**, 4299 (1969)
42. C. Forste, A. Germanus, J. Karger, H. Pfeifer, J. Caro, W. Pilz and A. Zikanova, *J. Chem. Soc., Faraday Trans. 1*, **83**, 2301 (1987)
43. A. Tsujs, G. Peeters, E. F. Vansant, I. Verhaet and P. de Bievre, *J. Chem. Soc., Faraday Trans. 1*, **79**, 2821 (1983)
44. K. P. Wong, J. D. Noble, M. Bloom and S. Alexander, *J. Magn. Reson.*, **1**, 55 (1969)
45. L. C. Habel and C. P. Slichter, *Phys. Rev.*, **113**, 1504 (1959)
46. G. Soda and H. Chihara, *J. Phys. Soc. Jpn.*, **36**, 954, (1974)
47. M. J. R. Hoch, *J. Chem. Phys.*, **65**, 2522 (1976)
48. J. H. Van Vleck, *Phys. Rev.*, **74**, 1168 (1948)

Chapter 5

HIGH-TEMPERATURE REGION OF METHANE IN MORDENITE

In this chapter, we focus upon the high temperature region where it is thought that the guest molecules translate quickly ($\tau_d \leq 10^{-10}$ s) in the pores of mordenite.

In addition to the rotational motion of the guest molecules, which is dealt with in the previous chapter, the translational motion through the pore as well as the vibration in the cross-sectional plane of the pore of mordenite are activated with increasing temperature. If the translational motion is sufficiently fast, the exchange between molecules in the gas and the adsorbed phases at equilibrium occurs. The pressure of the gas phase will increase with increasing temperature.

In order to investigate the behavior of methane molecules in mordenite in high temperature region, its adsorption isotherm was measured at several temperatures. The results will be exhibited in the first section.

Another purpose of the adsorption isotherm measurement is to understand the proton magnetic relaxation data in high-temperature region. Thus with the adsorption isotherm, one can determine precisely the pressure of the gas at equilibrium with the adsorbed phase in the NMR sample container at arbitrary temperature. Referring to the adsorption isotherm, the proton relaxation data in the high temperature region will be analyzed in the final section of this chapter.

5.1 Adsorption of Methane in Mordenite

Takaishi *et al.* studied the motional states of gases adsorbed in mordenite and found that argon has three degrees of freedom; one is the translation through the channel and two the vibrations against the wall. In the case of di- or polyatomic molecules (oxygen, nitrogen and carbon dioxide) rotational degrees of freedom join them.[1] They concluded that these molecules in mordenite behave as one-dimensional (1D) gas, but some deviations from strict one-dimensionality occur with respect to collision diameters, owing to a difference between the size of molecule and the diameter of the channel pore. Ohgushi also observed the one-dimensional behavior of rare gases in the pores of mordenite.[2]

Because methane has a diameter close to those of N_2, O_2 and Ar and has the spherical shape like the rare gas molecule, it is expected that one-dimensional gas behavior may also be observed for methane in mordenite.

In the present work the behavior of methane in the high-temperature region is studied and compared with that of the other gases.

5.1.1 Statistical Mechanical Theory for One-Dimensional Gas Model

Takaishi has developed statistical mechanical theory of 1-D gas in the zeolitic pore. The gas was assumed to consist of monoatomic molecules or diatomic molecules such as N_2 and O_2.[1,3] Here we extend his theory to the case of polyatomic molecules such as methane.

The one-dimensional fluid has extensively been studied by many workers.[4] They gave exact formulation, which contains integrations concerning the potential energy function between molecules. Those expressions are, however, complicated and scarcely of practical use. A very simple model of the one-dimensional van der Waals gas used by Takaishi,[1] is adopted here. The equation of state of 1-D gas is given by

$$(\phi^{(1)} + \frac{N^2_{ads}\alpha^{(1)}}{L^2})(L - N_{ads}\beta^{(1)}) = N_{ads}RT\,, \tag{5-1}$$

where $\phi(1)$ denotes the one-dimensional pressure, N_{ads} the number of adsorbed molecules, L the length of the pore, and $\alpha(1)$ and $\beta(1)$ the constants analogous to the van der Waals' parameters a and b of three-dimensional gas, respectively. When T = constant, the Helmholtz free energy F can be given by

$$-F = \int \phi^{(1)} dL\,. \tag{5-2}$$

Substituting Eq. (5-1) into Eq. (5-2) we get

$$F = F_{ideal} - N_{ads}RT\ \ln[1-\frac{N_{ads}\beta^{(1)}}{L}] - \frac{N^2_{ads}\alpha^{(1)}}{L} \tag{5-3}$$

$$= F_{ideal} - N_{ads}RT\ \ln[1-\theta] - \frac{N_{ads}\alpha^{(1)}\theta}{\beta^{(1)}}, \tag{5-4}$$

where F_{ideal} is the Helmholtz free energy of the ideal one-dimensional gas and θ is the coverage ($\theta = N_{ads}\beta^{(1)}/L$). Thus, the chemical potential is given by

$$\mu_{ads} = f(T) - RT\ \ln\beta^{(1)} + RT\ \ln(\frac{\theta}{1-\theta}) + RT\frac{\theta}{1-\theta} - \frac{2\alpha^{(1)}}{\beta^{(1)}}\theta, \tag{5-5}$$

where $f(T)$ corresponds to the internal energy and is given by

$$\frac{f(T)}{RT} = \frac{1}{2}\ln\left(\frac{h^2}{2\pi mkT}\right) - \ln[j'(T)] - \frac{\chi}{RT}. \qquad (5\text{-}6)$$

The first term of the right-hand side of Eq. (5-6) comes from the degree of freedom of translation along the pore axis. $j'(T)$ in the second term is the partition function of the admolecules referred to the degrees of freedom other than the translation. χ in the third term denotes the energy required to evaporate one mole of admolecules from the lowest energy level on the surface to the lowest state in the gas phase. By differentiating Eq.(5-5) with respect to T, we have

$$\begin{aligned}\bar{s}_{ads} &= \bar{s}_{conf} + \bar{s}_{therm} \\ &= -R\left[\ln\left(\frac{\theta}{1-\theta}\right) + \frac{\theta}{1-\theta}\right] + R\left[\ln\left(\frac{\beta^{(1)}\sqrt{2\pi mkT}}{h}\right) + \frac{1}{2} + \frac{\partial}{\partial T}\{T\ln j'(T)\}\right], \qquad (5\text{-}7)\end{aligned}$$

where $\bar{s}_{ads}$ denotes the differential molar entropy of the adsorbate, and is divided into two terms; namely, the configurational entropy, $\bar{s}_{conf}$, and the thermal (non-configurational) entropy, $\bar{s}_{therm}$.

The adsorption isotherm can be obtained as

$$\frac{P}{P_0} = \frac{\theta}{1-\theta}\exp\left[\frac{\theta}{1-\theta} - \frac{2\alpha^{(1)}}{RT\beta^{(1)}}\theta\right], \qquad (5\text{-}8)$$

with

$$P_0 = \frac{2\pi mkT}{h^2}\frac{kT}{\beta^{(1)}}\frac{j(\text{gas})}{j'(T)}\exp(-\chi/RT), \qquad (5\text{-}9)$$

where j(gas) is the partition function of gaseous molecules with respect to the internal degrees of freedom. The isosteric heat of adsorption, q_{iso}, becomes

$$q_{iso} = RT^2\left(\frac{\partial \ln P}{\partial T}\right)_{N_{ads}} = q_{iso}^{\circ} + \frac{2\alpha^{(1)}}{\beta^{(1)}}\theta\ , \qquad (5\text{-}10)$$

where q_{iso}° is the initial heat of adsorption. The value of $\alpha^{(1)}/k\beta^{(1)}$ for methane is estimated in **Appendix III** to be 128.96 K. Thus, the dependence of q_{iso} on θ may be negligibly small in lower coverage region.

In order to have an explicit functional form of $\bar{s}_{therm}$, let us examine the term $j'(T)$. We first consider the rotational freedom of methane. The partition function of the methane with respect to the rotational freedom can be expressed as,

$$j'_{\mathrm{rot}}(T) = \frac{\pi^{1/2}}{\sigma}\left(\frac{kT}{B}\right)^{3/2}, \tag{5-11}$$

where B denotes the rotational constant, σ the symmetry number which is 12 for methane. If the distance of C-H bond is taken to be 1.09 Å,[5] we obtain the partition function for rotational freedom as

$$j'_{\mathrm{rot}}(T) = 7.05 \times 10^{-3} T^{3/2}, \tag{5-12}$$

and therefore, the rotational entropy, s_{rot}, is

$$s_{\mathrm{rot}}/R = 1.5 \ln T - 3.45. \tag{5-13}$$

In addition to the rotational freedom, adsorbed methane may vibrate against the channel wall in the cross-sectional plane of the pore of mordenite.[1,3] Theses vibrations may be approximated by a two-dimensional anisotropic oscillator with characteristic frequencies ν_1 and ν_2. When the conditions that $h\nu_1$, $h\nu_2 < 2kT$, are satisfied, the entropy of oscillation is given by

$$s_{\mathrm{osc}}/R = \{1 + \ln(kT/h\nu_1)\} + \{1 + \ln(kT/h\nu_2)\}. \tag{5-14}$$

By substituting Eqs. (5-13, 14) into (5-7), the thermal entropy of adsorbed methane is represented by

$$\bar{s}_{\mathrm{therm}}/R = 4 \ln T + \frac{1}{2}\ln\frac{2\pi mk}{h^2} - 0.95 + \ln\left(\beta^{(1)}\frac{k}{h\nu_1}\frac{k}{h\nu_2}\right)$$

$$= 4 \ln T + 46.4 - 2.303 \log(\nu_1\nu_2), \tag{5-15}$$

where the relation,

$$m = 16/N_0 \ (N_0 = \text{Avogadro constant}),$$

and the value $\beta^{(1)} = 3.59$ Å (see **Appendix III**) were used. Therefore, if the methane in the pore of mordenite can be approximated by a one-dimensional rigid body gas, its thermal entropy is given by the form of Eq. (5-15).

5.1.2 Experimental

Mordenite sample and its amount used for adsorption experiments are the same as those used in the NMR measurements. The pre-treatment was also carried out in an analogous way.

The apparatus for the volumetric measurements is connected to the NMR probe in which the mordenite sample is contained. This system was already described in detail in Chapter 3.

Adsorption isotherm was measured in the temperature range of 150-320 K. At temperatures lower than 200 K, it needs several hours for the sample to attain the adsorption equilibrium. The temperature is controlled by the same device as in the NMR measurements.

5.1.3 Results and Discussion

Adsorption isotherms of methane are shown in Fig. 5-1. The obvious feature is that the plot of $\log V_{ads}$ against $\log P$ gives nearly straight lines at low loadings, similarly to the case of Ar, O_2 and N_2 observed by Takaishi.[1] When only a small fraction of one kind of site participates in adsorption, such linear relation is expected. The observed isotherms, therefore, suggest that the present specimen has highly homogeneous surface, in spite of the uneven potential along the channel pore. It is supposed that the adsorbed molecule translates freely through the channel and experiences averaged even potential, similarly to the quasi-free electron in a one-dimensional periodic potential field.

If adsorption behavior can be approximated as,

$$V_{ads} = aV_m P/(1+aP), \tag{5-16}$$

or

$$\frac{\theta}{1-\theta} = aP, \tag{5-17}$$

it is called "Langmuir-type adsorption". Here V_m designates the monolayer capacity, and the parameter a depends only on temperature.[6,7] By rewriting Eq. (5-16), it follows that

$$P/V_{ads} = 1/aV_m + P/V_m. \tag{5-18}$$

By plotting P/V_{ads} against P, which is called "Langmuir plot", straight lines should be obtained.

In the present work, the Langmuir plots gave straight lines above 250 K indicating that the system obeys the ideal Langmuir adsorption mechanism. Figure 5-2 shows an example

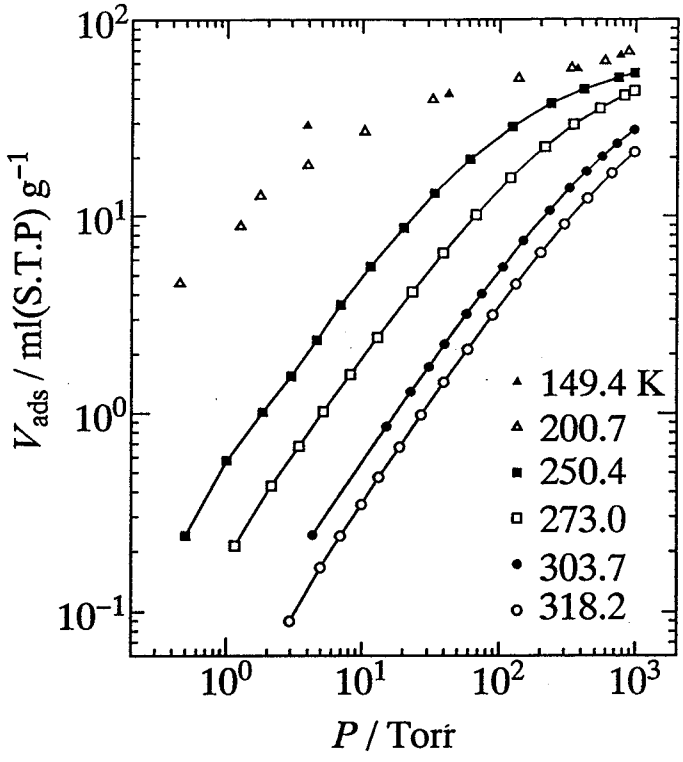

Fig. 5-1 Adsorption isotherms of methane in mordenite.

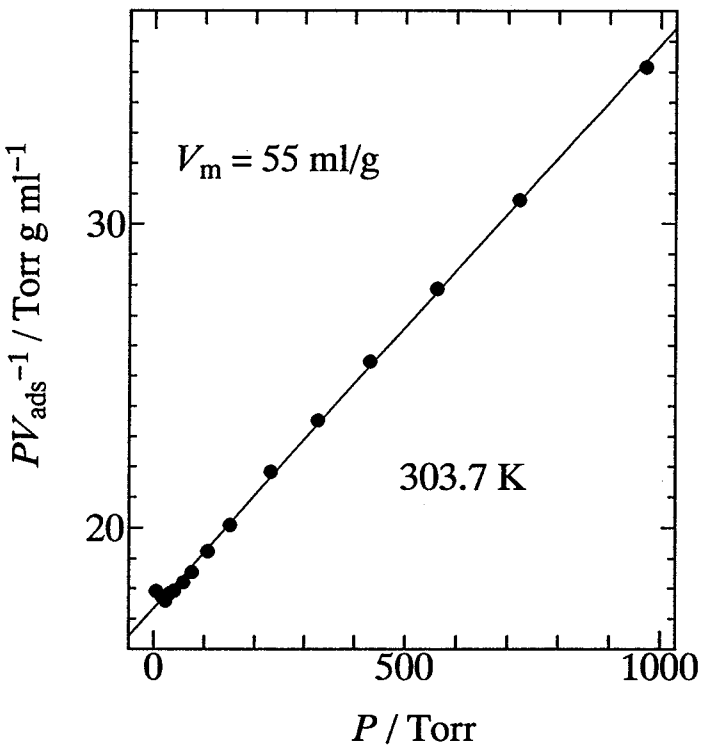

Fig. 5-2 Langmuir plots of adsorption isotherm of methane in mordenite at 303.7 K.

of such plot at 303.7 K. From the slope the monolayer capacity was evaluated to be 55 ml/g. Takaishi determined the values for N_2, O_2, and Ar to be 38, 47.6 and 52.6 ml, respectively, per gram of hydrated mordenite,[1] which correspond to 43.4, 54.4 and 60 ml per gram of dehydrated sample, respectively. The V_m value obtained for methane can be compared with these values. Using the Clapeyron-Clausius equation,

$$q_{iso} = -RT^2(\partial \ln P/\partial T)\theta \ , \tag{5-19}$$

where θ is the coverage, i.e., $\theta = V_{ads}/V_m$, the differential isosteric heat of adsorption, q_{iso} is determined, as is shown in Fig 5-3 which gives q_{iso} = 26.2 kJ mol^{-1} at the coverage of 0.037. The value of q_{iso} is plotted as a function of coverage in Fig. 5-4. It follows that q_{iso} is almost independent of coverage up to θ = 0.4, in agreement with the theoretical prediction in Eq. (5-10).

The differential molar entropy of adsorbate, $\bar{s}_{ads}$, can be calculated by the relation,

$$-q_{iso}/T = \bar{s}_{ads} - s_{gas}, \tag{5-20}$$

where S_{gas} designates the entropy of gas in equilibrium with the adsorbed phase. As described in the previous section, the differential molar entropy of the adsorbate consists of the configurational and the thermal terms, that is,

$$\bar{s}_{ads} = \bar{s}_{conf} + \bar{s}_{therm}. \tag{5-21}$$

If the present system is described as a one-dimensional van der Waals gas, $\bar{s}_{conf}$ is given by

$$\bar{s}_{conf} = -R[\ln(\frac{\theta}{1-\theta}) + \frac{\theta}{1-\theta}]. \tag{5-22}$$

Combining Eqs. (5-21) and (5-22), we obtain $\bar{s}_{therm}$ as a function of coverage θ. As the adapted model predicts, $\bar{s}_{therm}$ is independent of coverage as can be seen in Fig. 5-5. $\bar{s}_{ads}$ was calculated using Eq. (5-20) with q_{iso} = 26 kJ mol^{-1}, and using S_{gas} calculated from the pressure at each coverage on the basis of the standard state. The dependence of $\bar{s}_{therm}$ upon temperature is shown in Fig. 5-6, from which the relation,

$$\bar{s}_{therm} = 4.07 \ln T - 11.43, \tag{5-23}$$

is deduced. This result agrees with the statistical mechanical relation in Eq. (5-15). Therefore, it is concluded that the motional behavior of methane in mordenite in the high temperature region can be described by the one-dimensional gas model.

Combining Eqs. (5-15) and (5-23), we get

$$\nu_1\nu_2 = 1.3 \times 10^{25} \text{ Hz}^2. \tag{5-24}$$

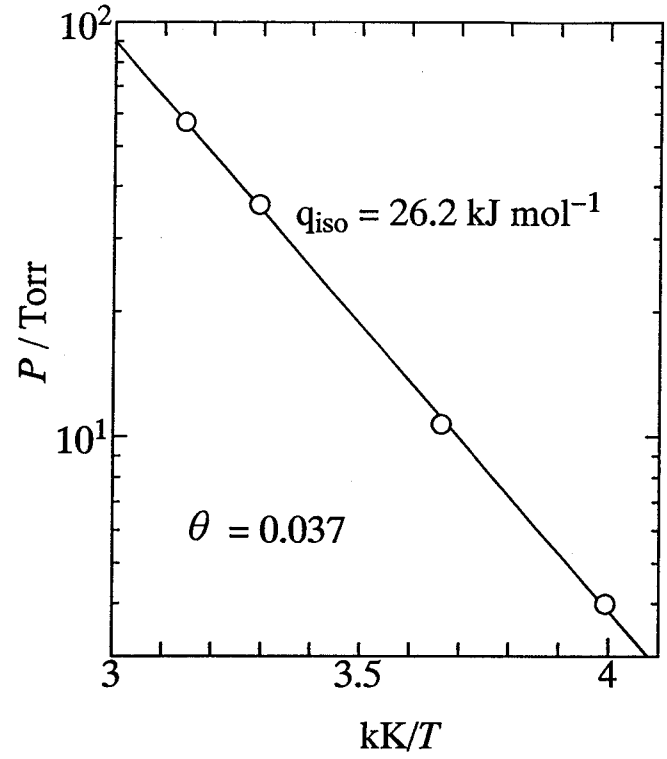

Fig. 5-3 Plot of log$P$ against $1/T$ for methane adsorbed in mordenite at the coverage of 0.037.

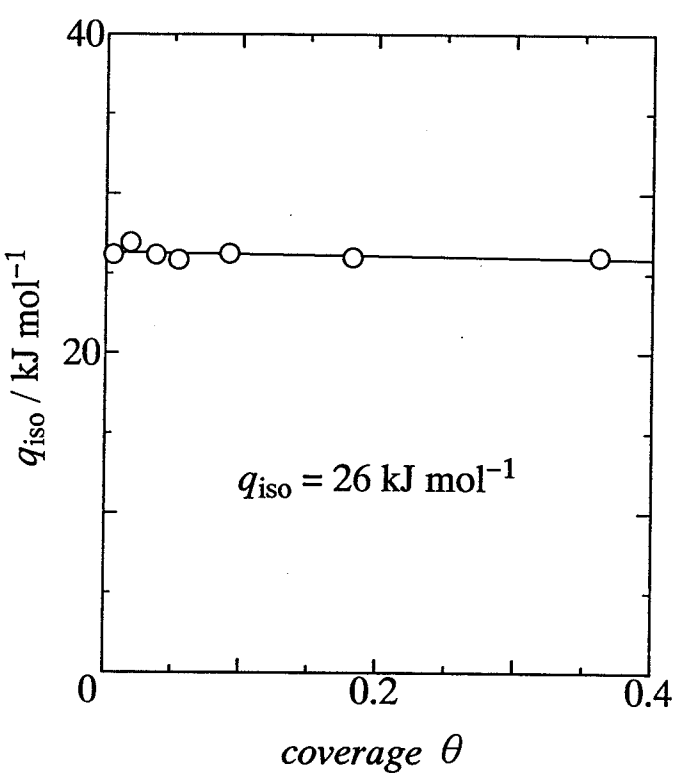

Fig. 5-4 Isosteric heat of adsorption of methane in mordenite against coverage.

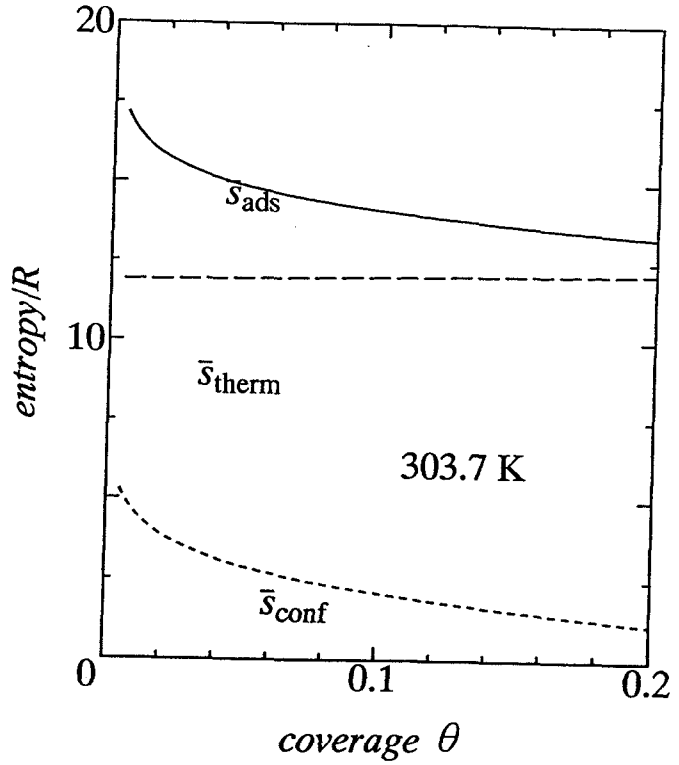

Fig. 5-5 Differential molar entropy of adsorbate, differential molar configurational and thermal entropies for methane adsorbed in mordenite at 303.7 K.

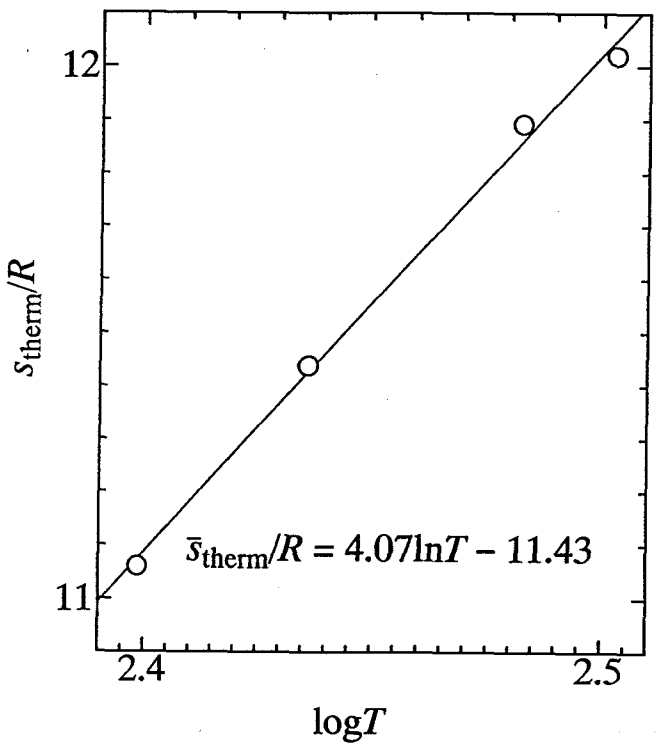

Fig. 5-6 Temperature dependence of differential molar thermal entropy for methane adsorbed in mordenite.

At this stage the determination of individual frequencies is impossible, but this equation tells that ν_1 and ν_2 assume values of the order of 10^{12} Hz.

The value of $\beta^{(1)}$ corresponds to molecular diameter and is calculated in **Appendix III.**[8] The obtained value is considerably smaller than that from other sources.[9] The experimental value of $\beta^{(1)}$ is obtained as follows. There is the general relation,

$$(\text{no. of unit cells / g of mordenite} \times 2) \times c = \beta^{(1)} \times V_m,$$

where the factor 2 means the existence of two pores in the unit cell,[10,11] c is the dimension of the unit cell in the pore direction (7.6×10^{-10} m), and V_m is expressed in the unit of number of molecules. The value of V_m is obtained from Langmuir plots as 55 ml/g or 14.8×10^{-21} molecules/g. If we assume that the formula of the unit cell of the dehydrate mordenite used in the present study is $Na_{5.68}Al_{5.68}Si_{42.3}O_{96}$, the number of the unit cells per gram of mordenite is estimated as 2.0×10^{20}. Thus, we have the value of $\beta^{(1)}$ as 2.05 Å. The value is surprisingly small in comparison with the values above mentioned. Small $\beta^{(1)}$ values were also observed for N_2, O_2, and Ar by Takaishi.[1]

The relation between $\beta^{(1)}$ and the collision diameter, σ, is given by

$$\beta^{(1)} = \sigma \cos\Delta , \qquad (5\text{-}25)$$

where Δ is the collision angle. If the gas behaves as an ideal one-dimensional gas, a collision should occur in a way shown in Fig. 5-7(a), in which Δ is 0, and $\beta^{(1)}$ is equal to σ. In the real system, the diameter of the channel pore is larger than that of methane, and so a collision shown in Fig. 5-7(b) may happen. In this case, $\Delta > 0$, and the effective value of $\beta^{(1)}$ is smaller than σ. This is the reason why the small $\beta^{(1)}$ values was observed.

In addition, the effect of the side-pocket on $\beta^{(1)}$ should also be noted. As shown in Fig. 5-7(c), a methane molecule can enter the side-pocket. There will exist a certain possibility that a molecule pass through the other with such a configuration, in which $\Delta = 90°$, and $\beta^{(1)} = 0$, and therefore, the average value of $\beta^{(1)}$ may be much smaller.

It may be concluded, from the present data, that adsorbed methane is well described by an one-dimensional van der Waals gas model. Adsorbed methane has one translational, two vibrational, and three rotational degrees of freedom. The apparent small value of $\beta^{(1)}$ can be interpreted in terms of the difference of the sizes of methane and the pores, and the effect of the presence of the side-pocket on the mutual collision between methane molecules.

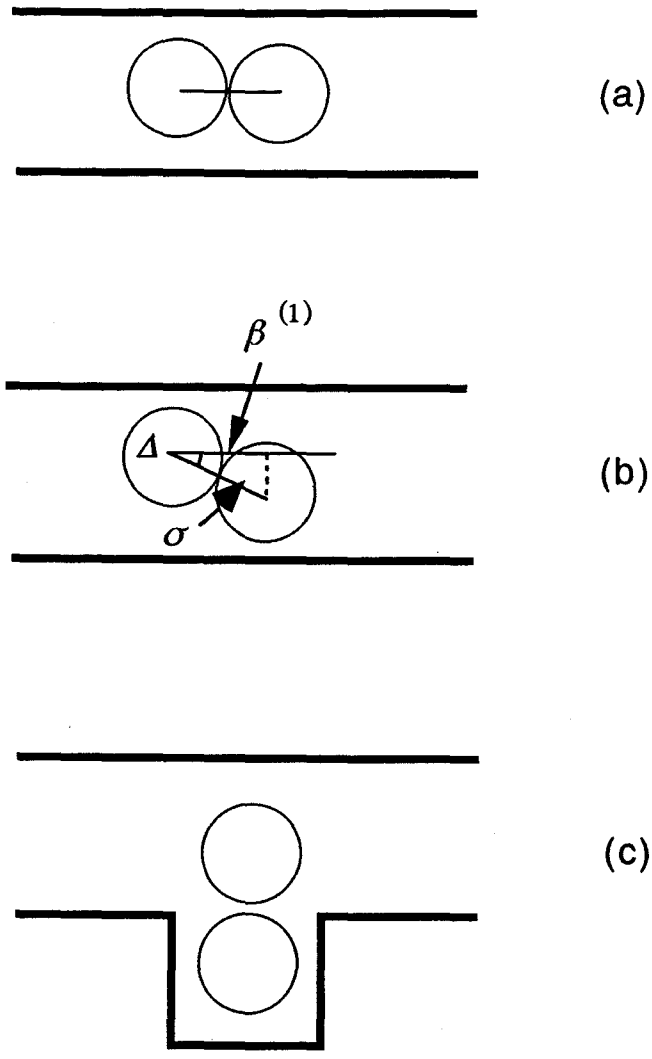

Fig. 5-7 Geometry of the collisional state of a pair of methane molecules in the channel pore of mordenite, (a) ideal one-dimensional gas, (b) real situation which deviates from the ideal one-dimensionality, (c) effect of the side-pocket.

5.2 Spin-Lattice Relaxation of Methane in Mordenite in High-Temperature Region

As shown in Fig. 4-4, T_1 of ^1H in methane in mordenite decreases on heating at higher temperatures than about 100 K. In this temperature region the rate of the reorientation of methane molecules is too high ($\tau_r < 10^{-10}$ s) to contribute to T_1 as described in Chapter 4, and hence the translational motion is expected to govern the T_1. The results of adsorption isotherm measurement in the previous section suggest strongly that the methane in mordenite is described by a one-dimensional gas model. As described in Chapter 4, however, translational motion contributes only weakly to the proton relaxation, and therefore, the remarkable inflection of the T_1 curve at about 100 K must be interpreted by other relaxation mechanism(s). The spin-rotation interaction may be a candidate for the relaxation mechanism. [12-15]

5.2.1 Relaxation Due to Spin-Rotation Interaction

Spin-lattice relaxation due to the coupling between nuclear magnetic moments and the rotational levels has been observed in liquids,[16-18] solids,[19] gases,[13,14] and in adsorption systems such as sulfur hexafluoride in zeolite 13-X. [15,20]

Nuclear spins in molecules are coupled to the molecular rotation through the intra- and the inter- molecular dipolar interaction, as well as the spin-rotation interaction. For dilute gases or adsorption systems the intermolecular interaction is usually much weaker than the other two. Collision between molecules gives rise to transitions between the rotational states (J) of the molecules. The transition between different rotational states causes a fluctuation of the intramolecular spin-dependent interactions. The fluctuation enables the nuclear spin system to exchange energy with the rotational and translational degrees of freedom of the molecules (cf. Chapter 2). Since the translational and rotational degrees of freedom correspond to a heat reservoir or "lattice" at a constant external temperature T, the nuclear spin system thereby approaches to the thermal equilibrium at a rate that is governed by the strength of the intramolecular interactions and the power spectrum of the frequency associated with the fluctuations of these interactions.

The relaxation time due to the spin-rotation interaction depends on a correlation time τ_{sr} for molecular angular velocity. To a good approximation τ_{sr} is regarded as the time between molecular collisions in gases.[14] For associated liquids (such as water) in which molecules undergo rotational diffusion, τ_{sr} is related to the dipolar correlation time, τ, by[16,21]

$$\tau_{sr}\tau = I_0/(6kT), \tag{5-26}$$

where I_0 is the moment of inertia of the molecule. However, for solid as well as for adsorbed system, there has been no clear theoretical description available so far.

It has been considered that in the case of neat gas of methane, spin-lattice relaxation is brought about by spin-rotation interaction.[13,14] In the system where the molecular reorientation is described using a single correlation time, T_1 due to spin-rotation interaction can be expressed in the form,[14]

$$\frac{1}{T_1} = \frac{4\pi^2}{\alpha} C_{\mathrm{eff}}^2 \frac{\tau_{\mathrm{sr}}}{1+(\omega_0-\omega_J)^2\tau_{\mathrm{sr}}^2} \quad , \tag{5-27}$$

where α is defined as

$$\alpha = (\frac{h}{2\pi})^2/(2I_0kT), \tag{5-28}$$

and C_{eff}, the "effective spin-rotation coupling constant", is given for the spherical-top molecule by

$$C_{\mathrm{eff}}^2 = C_{\mathrm{a}}^2 + \frac{4}{45}C_{\mathrm{d}}^2, \tag{5-29}$$

with

$$C_{\mathrm{a}} = \frac{1}{3}(C_{\parallel} + 2C_{\perp}), \tag{5-30}$$

and

$$C_{\mathrm{d}} = (C_{\perp} - C_{\parallel}), \tag{5-31}$$

where $C_{\parallel}$ and $C_{\perp}$ represent the spin-rotation interaction tensor components.

Since τ_{sr}^{-1} is proportional to density ρ in dilute gas, the T_1 vs. ρ curve in the vicinity of the T_1 minimum can be used to estimate C_{eff}. The C_{eff}^2 value for methane is 137.60 $(\mathrm{kHz})^2$ and an experimental result obtained by Bloom exhibits the T_1 minimum of about 2 ms (at 30 MHz) as shown in Fig. 5-8.[14] Furthermore, it was found that T_1 decreases with increasing temperature at a constant density, and a linear relation between $\log(T_1/\rho)$ and $\log T$ (see Fig. 5-9) has been observed.[13]

5.2.2 Discussion of Methane in High-Temperature Region

As described in Chapter 4, the two proton T_1 minima appearing in the low-temperature region are attributed to the reorientation of guest methane molecules in the side-pocket and the

main-channel of mordenite. The maximum in T_1 observed at about 100 K suggests the onset of the relaxation due to the spin-rotation interaction.

In order to analyze the relaxation data collected under *in situ* condition we must take into account the dead volume between the sample cell and the top of the probe (17.2 ml) and the amount of mordenite used in the NMR measurements (2.1 g). The word "loading" means the amount which occupies the whole volume of probe. In the low-temperature region, it corresponds to the actual amount adsorbed in the mordenite crystals. However, because the pressure of the gas phase at equilibrium with the adsorbed phase increases with increasing temperature, the amount of methane actually adsorbed in mordenite crystal decreases. Fig. 5-10 shows the actual amount of methane adsorbed in crystals at the loadings for NMR measurements. The actual amount of adsorbed gas decreases only a little (about 1 ml/g) up to 318 K at the loading of 4.8 or 9.5 ml/g, but the actual amount of adsorbed gas in the case of 76.1 ml/g is reduced to about a half and the pressure in the sample cell goes up to several atmospheres (about 5 atm) at room temperature.

Let us consider the temperature dependence of T_1 at the loading of 9.5 ml/g, for which the actual amount of adsorbed gas is approximately constant below 320 K. In gaseous methane, T_1 decreases with increasing temperature at a constant density, and there is a linear relation between $\log(T_1/\rho)$ and $\log T$ (Fig. 5-9). The present adsorption system is different from the pure gaseous one, but it also shows a similar tendency. Fig. 5-11 is the plot of $\log T_1$ against $\log T$ after subtraction of the contribution from the reorientation. Solid line shows almost linear behavior. When Eq. (5-27) is applied to this data with C_{eff}^2 =137.60 $(\mathrm{kHz})^2$ as employed by Bloom,[14] one obtains $\tau_{\mathrm{sr}} \sim 4.7 \times 10^{-11}$ s at 300 K (as compared with $\sim 2.36 \times 10^{-10}$ s in the gas of methane of 1 atm at 300 K[14]).

In the present adsorption system, T_1 decreases with increasing loading. If we regard the loading as the density of gas, such behavior is opposite to that in the neat gas as described above. Because no detailed theory for spin-rotation in the adsorption system is available, the reason is not clear at this stage, but we can derive an idea for it by examining the mobility data in the adsorption systems in porous materials.

For gases, T_1 increases with increasing density. On the other hand, it is found in most of the adsorption system in porous materials, that mobility decreases with increasing loading, and the correlation time τ, (or the time between two jumps), increases with increasing loading. The increase of the time between two jumps may correspond to the increase of the time between collisions, which may lead to the lowering of T_1. As shown in Fig. 5-11, T_1 at high loadings approaches to that at lower ones at higher temperatures due to the fact that the actual amount of adsorption approaches the latter (Fig. 5-10), although the upper temperature of the measurement at 76.1 or 38.1 ml/g was limited by the inner pressure of our sample cell.

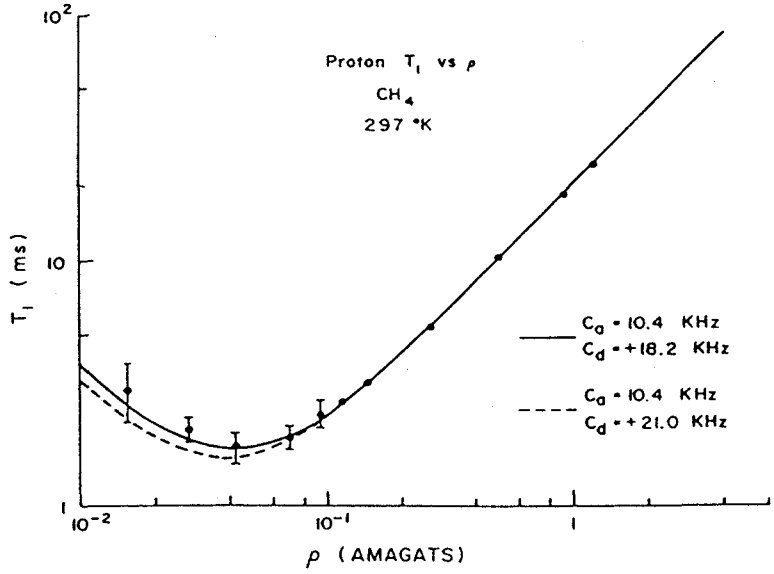

Fig. 5-8 Plot of $T1$ as a function of density in CH4 gas at 297 K. (After R. Y. Dong and M. Bloom, 1969)

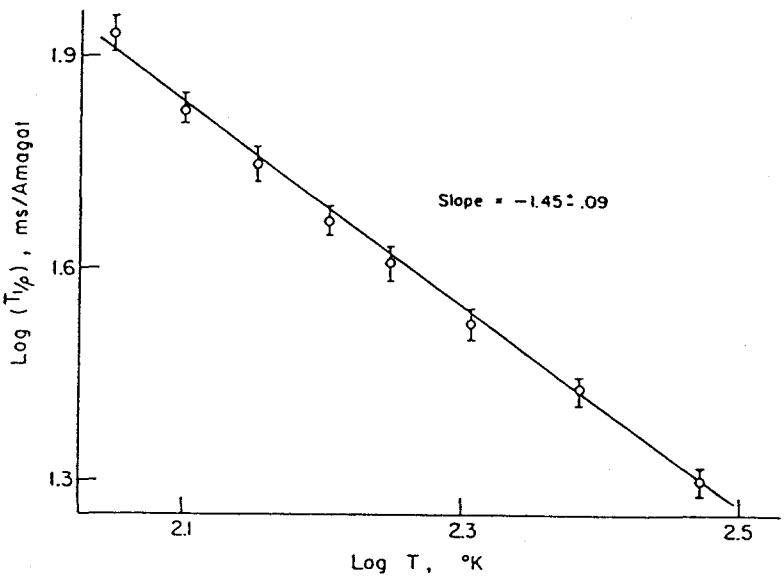

Fig. 5-9 Plot of $\log(T1/\rho)$ against $\log T$ for CH4 gas. (After M. Bloom *et al.*, 1967)

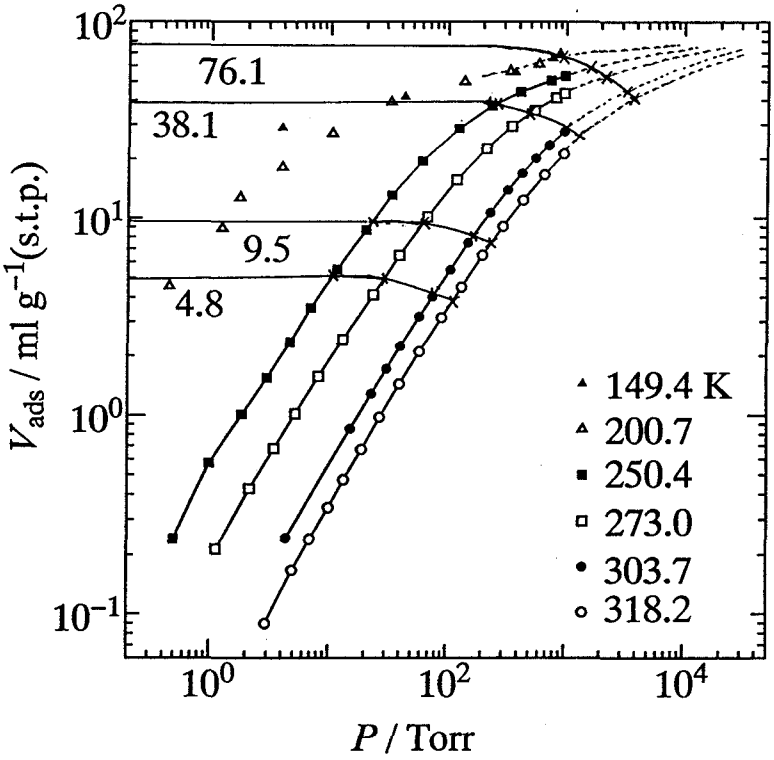

Fig. 5-10 Actual amount of methane adsorbed in mordenite at the loadings of 4.8, 9.5, 38.1 and 76.1 ml/g.

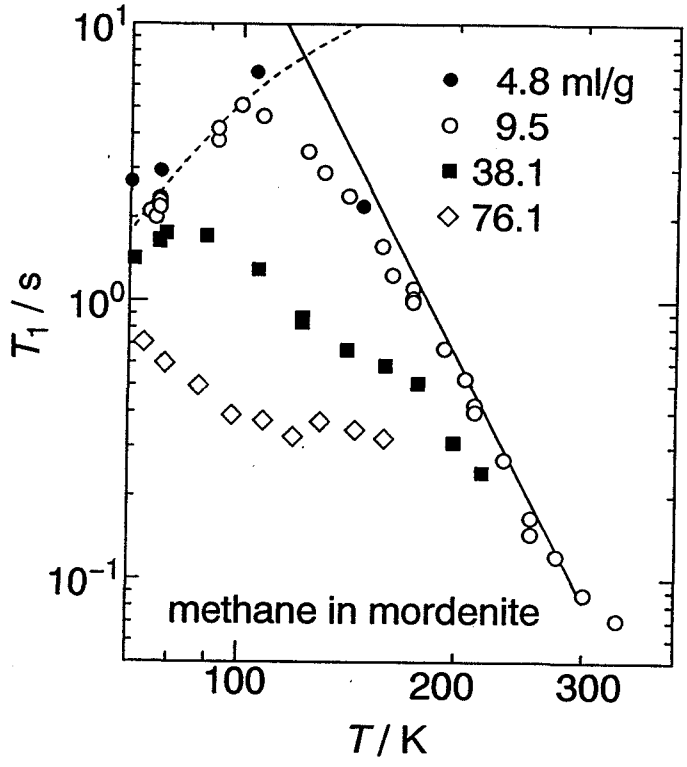

Fig. 5-11 Plot of logT_1 against log$T$ for methane adsorbed in modenite.

Appendix III. Calculation of the Values of $\alpha^{(1)}$ and $\beta^{(1)}$

The values of $\alpha^{(1)}$ and $\beta^{(1)}$ can be easily calculated from the values of the critical temperature $T_c^{(3)}$ and the critical pressure $P_c^{(3)}$, of the 3D gas in a way used by Takaishi,[1] which is quite analogous to that developed by Hill[8] for the two-dimensional van der Waals gas. Let $B^{(3)}$ and $B^{(1)}$ be the second virial coefficients of the three- and one-dimensional van der Waals gas, respectively, then we have the relations,

$$B^{(3)} = b-(a/kT), \tag{AIII-1}$$

and

$$B^{(1)} = \beta^{(1)}-(\alpha^{(1)}/kT), \tag{AIII-2}$$

where a and b are the van der Waals' parameters of the three-dimensional gas. If the interaction potential between two molecules, $u(r)$, is expressed by

$$u(r) = \infty \quad \text{for } r < 2r_0, \tag{AIII-3}$$

and

$$u(r) = -A/r^6 \quad \text{for } r \geq 2r_0, \tag{AIII-4}$$

where r is the distance between molecules and A a constant, we have the relations,

$$B^{(3)} = \frac{1}{2}\int_0^{\infty} r^2\,dr \int_0^{2\pi} d\theta \int_0^{\pi} \sin\phi\, d\phi\, [1-\exp(-u/kT)]$$

$$= \frac{16\pi}{3}r_0^3 - \frac{\pi}{12kT}\frac{A}{r_0^3}, \tag{AIII-5}$$

and

$$B^{(1)} = \frac{1}{2}\int_0^{\infty} 2\,dr\, [1-\exp(-u/kT)]$$

$$= 2r_0 - \frac{1}{5kT}\frac{A}{(2r_0)^5}. \tag{AIII-6}$$

In the derivation of the above equations, the condition $|-u/kT| << 1$ is assumed. Solving Eqs. (AIII-1~6), we have the relations,

$$\alpha^{(1)} = \frac{3a}{10\pi}\left(\frac{2\pi}{3b}\right)^{\frac{2}{3}}, \tag{AIII-7}$$

and

$$\beta^{(1)} = \left(\frac{3b}{2\pi}\right)^{\frac{1}{3}}. \tag{AIII-8}$$

Furthermore, by virtue of the relations

$$b = \frac{kT_c^{(3)}}{8P_c^{(3)}} \tag{AIII-9}$$

and

$$a = \frac{27kT_c^{(3)}}{64P_c^{(3)}}, \tag{AIII-10}$$

we obtain

$$\frac{\alpha^{(1)}}{k\beta^{(1)}} = \frac{27}{40}T_c^{(3)} \tag{AIII-11}$$

and

$$\beta^{(1)} = \left[\frac{3kT_c^{(3)}}{16\pi P_c^{(3)}}\right]^{\frac{1}{3}}, \tag{AIII-12}$$

where $T_c^{(3)}$ and $P_c^{(3)}$ are the critical temperature and the critical pressure, respectively, of the three-dimensional gas. Using experimental values of $T_c^{(3)}$ and $P_c^{(3)}$,[22] the values of $\alpha^{(1)}/k\beta^{(1)}$ and $\beta^{(1)}$ are obtained as shown in Table AIII-1.

Table AIII-1 Constants of 1-dimensional van der Waals gas and critical temperature and pressure[22] of methane.

$T_c^{(3)}$ / K	191.05
$P_c^{(3)}$ / atm	45.8
$\alpha^{(1)}/k\beta^{(1)}$ / K	128.96
$\beta^{(1)}$ / 10^{-10} m	3.59

References to Chapter 5

1. T. Takaishi, A. Yusa, and F. Amakasu, *Trans. Faraday Soc.*, **647**, 3565 (1971)
2. T. Ohgushi and H. Yokoyama, *J. Chem. Soc., Faraday Trans. 1*, **88**, 3095 (1992)
3. T. Takaishi, *Pure & Appl. Chem.*, **58**, 1375 (1986)
4. I. Prigogine, *The Molecular Theory of Solutions*, North-Holland Pub. Co., (1957)
5. P. W. Atkins, *Physical Chemistry*, Oxford Univ. Press, (1978)
6. 近藤精一, 石川達雄, 安部郁夫, *吸着の科学*, 丸善, (1991)
7. 慶伊富長, *吸着*, 共立全書, (1965)
8. T. L. Hill, *J. Chem. Phys.*, **14**, 441, (1946)
9. Jacob N Iaraelachvili, *Intermolecular and Surface Forces,* Academic Press Limited (1985)
10. H. Van Bekkum, E. M. Flanigen, and J. C. Jansen, *Stud. Surf. Sci. Catal.*, **58** , Elsevier, (1991)
11. W. M. Meier, *Z. Kristallogr.*, **115**, 439 (1961)
12. A. Abragam, *The Principles of Nuclear Magnetism*, Oxford Univ. Press, London/New York, (1961)
13. M.Bloom, F. Bridges and W. N. Hardy, *Can. J. Phys.*, **45**, 793 (1967)
14. R. Y. Dong and M. Bloom, *Can. J. Phys.*, **48**, 793 (1970)
15. H. A. Resing , *Advan. Mol. Relaxation Processes,* **3**, 199 (1972)
16. W. R. Hackleman and P.S. Habbard, *J. Chem. Phys.*, **39**, 2688 (1963)
17. J. H. Rugheimer and P.S. Habbard, *J. Chem. Phys.*, **39**, 552 (1963)
18. H. S. Gutowsky, I. J. Lawrenson and K. Shimomura, *Phys. Rev. Lett.*, **6**, 349 (1961)
19. R. Blinc and G. Lahagnar, *Phys. Rev. Lett.*, **18**, 685 (1967)
20. H. A. Resing and J. K. Thompson, *J. Chem. Phys.*, **46**, 2876 (1967)
21. P.S. Habbard, *Phys. Rev.*, **131**, 1155 (1961)
22. 日本化学会編, *化学便覧*, 丸善, (1966)

Chapter 6

SUMMARY

In the present study the dynamic behavior of the small paraffins C_nH_{2n+2} (n = 1-4) adsorbed in mordenite was investigated by proton spin-lattice relaxation time and adsorption measurements.

As far as the dynamics of molecules adsorbed in zeolite is concerned, the translational motion (diffusion) in the vicinity of room temperature has mainly been studied so far. We focused upon another dynamic behavior, especially the *reorientational* motion of adsorbed molecules at *low-temperature*.

First of all, a new NMR probe was designed and constructed, whose specimen chamber is directly connected to a vacuum line. This system enables one to introduce gases into the sample container under precise control of the surface coverage and therefore to determine the temperature, frequency and coverage dependence of ^1H spin-lattice relaxation time T_1 between 4.2 and 400 K under *in situ* conditions.

Commercial mordenite sample is usually contaminated by about 200 ppm of iron, which causes undesirable spin-lattice relaxation and prevent one from determining accurate values of T_1. In the present work the high-purity mordenite sample was synthesized, in which the amount of iron impurity was less than 20 ppm. With this mordenite sample the reliable values of T_1 of ^1H in adsorbed materials were obtained.

T_1 of ^1H for methane, ethane, propane and butane adsorbed in mordenite was measured over the wide ranges of both loading coverage (e.g., θ = 0.09 ~1.4 for methane; θ: monolayer coverage) and temperature (4.2 K ~ room temperature). The results are summarized in turn as follows.

In the case of ethane adsorbed in mordenite, the plot of logT_1 vs. $1/T$ indicates that T_1 assumes a single minimum at 28 K. The slopes on both the sides of the T_1 minimum are not identical, suggesting that the proton relaxation is governed by both the reorientation of ethane molecule about its C-C axis and at low temperatures rotational tunneling. The correlation time for such composite motion is represented by

$$\tau_c^{-1} = \tau'_0{}^{-1}\exp(-E_{01}/RT) + \tau_0^{-1}\exp(-E_a/RT). \quad (1)$$

where E_{01} is the excitation energy from the ground torsional state of CH_3 group and E_a the activation energy for the axial reorientation of the ethane molecule in the main-channel of the mordenite. E_{01} and E_a were evaluated to be 0.12 and 1.0 kJ mol^{-1}, respectively. T_1 decreases slightly with increasing loading, which is probably due to the reinforcement of the intermolecular dipole-dipole interactions.

For propane adsorbed in mordenite, a single T_1 minimum appears at 75 K. The slopes of the $\log T_1$ vs. $1/T$ are asymmetric with respect to the T_1 minimum. The intramolecular reorientation of the CH_3 group about the C-C axis as well as the tunneling rotation govern the relaxation on the low temperature side of T_1 minimum. The correlation time can be represented by Eq. (1), in which E_{01} was evaluated to be 0.5 kJ mol^{-1}, and E_a, the barrier for internal rotation, was estimated to be about 6 kJ mol^{-1}, in agreement with the value of the internal barrier in $CH_3NH_3^+$ ion obtained in our previous study. The variation of T_1 on the high-temperature side of the T_1 minimum is attributable to the reorientation of the whole-molecule about its long axis, the correlation time of which is expressed by the usual Arrhenius' equation,

$$\tau_c = \tau_0 \exp(E_a/RT). \qquad (2)$$

The activation energy was estimated to be 3.5 kJ mol^{-1}. For propane, T_1 is almost independent of the loading.

In general, butane exhibits the similar T_1 behavior to that for propane. Only a single T_1 minimum appears in 115-125 K region. In the lowest temperature region the proton relaxation is governed by both the internal reorientation and the tunneling rotation of CH_3 group about the C-C axis. The correlation time is again represented by Eq. (1), in which E_{01} was evaluated to be 0.6 kJ mol^{-1} and E_a to be about 6 kJ mol^{-1}. The relaxation on the high-temperature side of the T_1 minimum is attributable to the reorientation of whole-molecule about its long axis. However, butane shows the loading dependence differently from propane. When the loading increases from 7.7 or 15.2 ml/g to 21.9 or 25.1 ml/g, the activation energy for the overall reorientation increases slightly from 5.0 to 5.5 kJ mol^{-1}. In addition, the temperature of the T_1 minimum goes up from 115 to 125 K, and the T_1(min) value lowers from 90 to 70 ms. Such loading dependence of T_1 is brought about by the rearrangement of the admolecules in the main-channel to accommodate excess butane molecules.

Methane shows the relaxation behavior very different from the other three. In contrast to the other alkanes, two T_1 minima were observed at 15 and 50 K. Analysis of the T_1 data, referring to the activation energies of the other alkanes in mordenite, assigned the former minimum to the reorientation of CH_4 in the main-channel and the latter to that in the side-pocket of mordenite.

By further analysis of the loading dependence of the values of the T_1 minima the difference of potential energies between these two adsorption sites was estimated to be about 70 J mol^{-1} ($\approx$ 8.4 K). The potential energy for methane is lower in the side-pocket than in the main-channel. Thus at low temperatures (T < 30 K), the molecules occupy predominantly the side-pockets, but with increasing temperature and/or loading proportion of methane molecules in the main-channels increases and approaches to 50 % above 40 K or at greater loading than about 60 ml/g.

The activation energies E_a for the reorientation of methane in the main-channel obey a kind of law of the corresponding state; the magnitude of E_a varies with the number of carbons of the guest molecules as 1.0, 1.0, 3.5, and 5.0-5.5 kJ mol^{-1}, and the temperature at which T_1 minimum appears increases as 14, 28, 75, and 115-125 K in the order of increase of the number of carbons of the guest alkane. It is noted that methane and ethane experience almost the same potential energy barrier for reorientation but the T_1 minimum for ethane appears at twice as high temperature as that for methane. These findings suggest strongly that ethane molecule is locating in the channel by turning its molecular axis along the channel axis. When it undergoes reorientation about its axis, the energy barrier it experiences is almost the same as that for methane but, because its moment of inertia is 6/4 times that of methane, its correlation time reaches the value $\tau_c \sim 1/\omega_0$ at a higher temperature than the correlation time for methane does.

The guest dynamics in co-adsorbed system of methane and argon in mordenite was also examined by ^1H spin-lattice relaxation time measurements to obtain some microscopic information about the guest-guest interaction and about possible selectivity between two different sites. The results are summarized as follows:

(1) When argon of 9.5 ($\theta \approx 0.17$) or 19.0 ml/g ($\theta \approx 0.34$) is co-adsorbed with methane of 9.5 ml/g in mordenite, the proportion of methane to argon does not differ between in the side-pocket and in the main-channel, suggesting that the guest-host interaction energy differs only slightly between methane and argon and the entropy of mixing of two gases dominates the adsorption characteristic.

(2) When argon of 42.9 ml/g ($\theta \approx 0.78$) is co-adsorbed with methane of 9.5 ml/g in mordenite, about 90% methane molecules are located in the side-pockets and 10% in the main-channels. This phenomenon indicates that, when mordenite has accommodated excess of adsorbate, the degree of molecular motional freedom is lost and hence the side-pocket accommodates preferentially its favorite molecular species, that is, methane, to other species, argon. In this case the concept of "mixing" does not hold. This phenomenon is just the "molecular recognition".

In order to investigate the behavior of methane molecules adsorbed in mordenite in high temperature region the adsorption isotherm was measured between 150 and 320 K. It was found that the Langmuir adsorption applies at low coverages above 250 K and the monolayer capacity was estimated to be 55 ml/g. The differential isosteric heat of adsorption was estimated to be 26 kJ mol^{-1}, which is almost independent of coverage at lower coverage than 0.4. The isotherm of adsorbed phase was analyzed by a model of the one-dimensional van der Waals gas and it was found that the thermal (nonconfigurational) entropy of the adsorbed methane, $\bar{s}_{therm}$, is independent of the coverage, and that $\bar{s}_{therm}$ is expressed by

$$\bar{s}_{therm} = 4.07 \ln T - 11.43, \qquad (3)$$

showing the validity of the one-dimensional model for methane in mordenite. It was also found that the adsorbed methane has one translational, two vibrational and three free rotational degrees of freedom. Examination of the collision diameters between methane molecules clarified that the real adsorption system deviates to some extent from the ideal one-dimensionality due probably to the misfitting of the size of methane molecule to the channel pore, and also due to the existence of the side pockets.

T_1 of proton in methane in mordenite decreases with increasing temperature at high temperatures, which is due to the spin-rotation interaction.